SELECTIVE CATALYTIC REDUCTION OF NITRIC OXIDE OVER CERIUM-DOPED ACTIVATED CARBONS

by

ANNAPRABHA ATHAPPAN

Presented to the Faculty of the Graduate School of

The University of Texas at Arlington in Partial Fulfillment

of the Requirements

for the Degree of

DOCTOR OF PHILOSOPHY

THE UNIVERSITY OF TEXAS AT ARLINGTON

December 2012

ACKNOWLEDGEMENTS

Working on this research was a wonderful opportunity and a great experience in catalysis development and material analysis that may have significant impact. I am deeply grateful to my supervising professor, Dr. Melanie L. Sattler, for letting me choose this topic and helping me financially throughout the research work. I would like to express my great appreciation to her and it is my honor to work under her. I would like to thank my committee members, Dr. Andrew Hunt, Dr. Chien-Pai Han, Dr. Hyeok Choi, and Dr. Laureano R. Hoyos, for their support and guidance in this research work.

I owe my deepest gratitude to Dr. Jiechao Jiang, Dr. Muhammed Yousufuddin, and Mr. David Yan for training and helping me in material analysis. I owe my sincere and earnest thankfulness to Dr. Purnendu K. Dasgupta, Dr. Brian Edwards, Mr. Phillip Shelor, Mrs. Ruchika Bhawal, Mr. Paul Shover, Mr. Lewis Crow, Mr. Charles Savage, and Ms. Helen Hough for their timely help.

I would like to acknowledge the assistance provided by Dr. Sumathi Sethuraman, assistant professor at Universiti Tunku Abdul Rahman, Malaysia; Dr. R. Ramakrishnan, founder of A & B Environmental Services, Inc., USA; my father Dr. PR. Athappan, retired head of the chemistry department at Madurai Kamaraj University, India and Mr. Tom McKarns, Principal at Eco Physics, Inc., USA.

My heartfelt thanks go to my husband, Saravanan Nachimuthiah, for his immense support and encouragement throughout my career. I would like to thank my in-laws, Mr. and Mrs. Nachimuthiah, and my wonderful children, Sanjiv and Sanjana, for their continual understanding. I would like to thank all of my friends for their encouragement, care and support.

Thank you all!

November 20, 2012

ABSTRACT

SELECTIVE CATALYTIC REDUCTION OF NITRIC OXIDE

OVER CERIUM-DOPED ACTIVATED CARBONS

Annaprabha Athappan, Ph.D.

The University of Texas at Arlington, 2012

Supervising Professor: Melanie L. Sattler

Selective catalytic reduction (SCR) with ammonia for diesel engine NOx reduction using activated carbon (AC) was studied. Comparisons of unmodified and cerium-doped Granular Activated Carbon (GAC), Activated Carbon Fiber (ACF), and Multiwall Carbon Nanotubes (MWCNTs) were conducted. Physical and chemical properties and durability of the catalysts were examined using Scanning Electron Microscope (SEM), Energy Dispersive Spectroscopy (EDS), carbon hydrogen and nitrogen (CHN) analysis, X-ray Diffraction (XRD) analysis, Raman spectroscopy, X-ray Photoelectron spectroscopy (XPS), Thermo gravimetric analysis (TGA), Brunauer-Emmett-Teller (BET) surface area analysis and density analysis.

Experiments were carried in a fixed bed column at various temperatures from 100º to 400º C for low concentration NOx (150 ppm) and high concentration NOx (500ppm) at a total flow rate of 200ml/min, NOx/NH3 ratio of 1:1 and oxygen concentration of 5.6%. The stability of the cerium-doped GAC (CeGAC) was studied by conducting a 12-hour steady-state run.

It was found that CeGAC has a high reduction efficiency of about 80% at 300ºC for low concentration NOx. CeMWCNTs have a high reduction of 85% at 300ºC for high concentration NOx. However, the NO oxidation and ammonia slip emission in the exhaust is higher for CeMWCNTs than for other types of catalyst. CeGAC with high space velocity of 30,000 h-1 shows a stable reduction percentage for various temperatures. The 12 hour stability test for CeGAC shows steady-state reduction percentage throughout the test. Reducing the NOx/NH_3 ratio to 1:0.9 maintains the reduction percentage and lowers NO oxidation and ammonia slip significantly. This study indicates that CeGAC could be applicable in onboard engines with computerized ammonia injection control systems.

TABLE OF CONTENTS

LIST OF ILLUSTRATIONS

Figure Page

LIST OF TABLES

LIST OF ACRONYMS

GAC – Granular Activated Carbon

ACF – Activated Carbon Fiber

MWCNTs – Multiwall Carbon Nano Tubes

SEM - Scanning Electron Microscope

EDS - Energy Dispersive Spectroscopy

XRD - X-Ray Diffraction

XPS - X-ray Photoelectron Spectroscopy

TGA - Thermo Gravimetric Analysis

BET - Brunauer-Emmett-Teller

CHAPTER 1

INTRODUCTION

1.1 Importance of Nitrogen Oxide Emissions

Nitrogen oxide (NOx) emissions pose an ongoing issue in environmental pollution. Nitric oxide (NO) and nitrogen dioxide (NO_2) together are commonly represented as NOx. The environmental effects of NOx include formation of ground level ozone, acid precipitation, and fine particles, as well as reductions in visibility.

The Leighton mechanism describes ozone formation in troposphere in three simple steps given below.

$NO_2 + hv \longrightarrow NO + O^*$ ----------▶ equation 1

$O_2 + O^* + M \longrightarrow O_3 + M$ ----------▶ equation 2

$O_3 + NO \longrightarrow NO_2 + O_2$ ----------▶ equation 3

M is a generic molecule to carry away excess energy to stabilize the O_3 molecule. In equation 1, a photon of wavelength less than 430 nm splits nitrogen dioxide into nitric oxide and oxygen radical. In equation 2, the oxygen radical reacts with molecular oxygen to form ozone. In equation 3, ozone reacts with nitric oxide to reform nitrogen dioxide and molecular oxygen. NO_2 thus has to be eliminated to reduce ozone formation.

Deposition of wet and dry acidic components is called acid rain, with pH less than 5.6. NOx reacts with OH° and water vapor to form nitric acid. NOx forms small particle by reacting with ammonia, sulfate, moisture, and other compounds in the atmosphere.

The adverse health effects of NO_2 include airway inflammation and aggravation of asthma. NO_2 is thus listed by the Environmental Protection Agency (EPA) as one of the six criteria pollutants. The present primary National Ambient Air Quality Standard (NAAQS) for

NO_2, for protecting public health, is 100 ppb for a 1-hour averaging time and 53 ppb for an annual averaging time. The secondary standard to protect human welfare is 53 ppb for an annual averaging time.

1.2 Sources of Nitrogen Oxide Emissions

NOx is emitted into the atmosphere via mobile and stationary sources. The mobile sources include cars, trucks, buses, and other mobile sources using diesel as a fuel. The stationary sources are power plants, incinerators, and any combustion equipment using diesel as a fuel. .

90-95% of NOx is emitted in the form of NO from fossil fuel combustion sources, including power plants, incinerators, and mobile sources. Sources of NOx emissions for Texas and the U.S. are shown in Figure 1.1. As shown in Figure 1.1, the largest category of NOx emissions in Texas and in the U.S. is mobile sources. Emissions from mobile sources in the U.S. increase every year due to the increasing numbers of vehicles and miles travelled per vehicle.

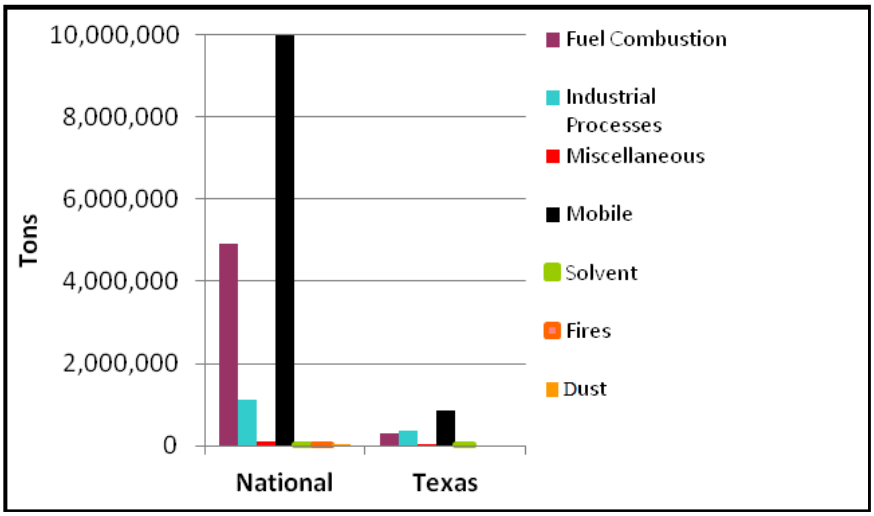

Figure 1.1: Sources of NOx emissions (EPA, 2008)

1.3 Emissions and Controls for Gasoline and Diesel Engines

Gasoline engines operate via spark ignition. Three-way catalytic converters (TCC) can effectively reduce emissions from gasoline engines, since they operate at stoichiometric conditions. Catalytic converters are made of precious metals to increase oxidation and reduction via palladium and rhodium, respectively. The three-way catalytic converter thus simultaneously oxidizes hydrocarbons and carbon monoxide and reduces nitrogen oxides to produce carbon dioxide, water, and nitrogen, as shown below.

$$2HC + 2.5O_2 \longrightarrow 2CO_2 + H_2O$$

$$2CO + O_2 \longrightarrow 2CO_2$$

$$2NO + O_2 \longrightarrow N_2 + 2O_2$$

The diesel engine was developed by Rudolf in 1897. It is widely used for its high efficiency. After 1910, diesel engines began to be used in large trucks and generating plants, and after the 1930s in automobiles. Since 1970, diesel engines have been widely used in off road and on road vehicles. As of 2007, 50% of new cars sales in Europe were diesel vehicles. Even though emissions for some pollutants are higher than gasoline engines, diesel engines are widely used due to several advantages over gasoline engines. Diesel engines can convert 45% of fuel energy to mechanical energy, and gasoline engines only convert 35% of fuel energy to mechanical energy. The life of diesel engines is twice as long as for gasoline engines. Diesel engines are also safer in many applications. Different types of diesel engines are used in passenger cars, trucks, railroad rolling stock, aircraft, marine vehicles, motorcycles, backup generators, irrigation pumps, lawn mowers, coffee de pulpers, corn grinders and much more.

Diesel engines are compression ignition and operate under fuel-lean conditions. They burn the fuel completely, and carbon monoxide and hydrocarbon emissions are thus lower than gasoline engines. NOx emissions from diesel engines, however, are higher than those from gasoline engines due to the high temperatures needed to induce compression ignition (150ºC to 450ºC). NOx formation is an exponential function of temperature. Particulate matter (PM)

emissions from diesel engines are also higher than for gasoline engines due to incombustible matter in the fuel. Diesel exhaust or diesel fumes are thus a mixture of gases, liquid aerosols, vapors and particulates. The emissions include carbon, nitrogen, water, carbon monoxide, aldehydes, nitrogen dioxide, sulfur dioxide, and polycyclic aromatic hydrocarbons.

The TCC used for emissions control from gasoline engines cannot be used for diesel engines. The PM in the exhaust clogs the surface area of TCC. In addition, the lean-burning conditions of a diesel engine lead to a high amount of oxygen in the exhaust; under these conditions, TCC cannot achieve NOx reduction (Nakatsuji, 1999).

Instead, in diesel engines a diesel oxidation catalyst (DOC) can be used to oxidize CO and HC into CO_2 and water. A DOC achieves 90 % efficiency by adding oxygen in the exhaust stream. Exhaust gas recirculation can be used to reduce NOx in both diesel and gasoline engines. It recirculates a portion of exhaust back into the combustion chamber. It thus reduces the combustion temperature and excess oxygen in the pre-combustion chamber, which reduces NOx emissions. However, EGR only achieves up to around a 50% reduction in NOx. For stationary sources, NOx may be controlled using an NH_3 injection system. However, for mobile sources, on-board ammonia systems are problematic. Hence, developing a method to reduce NOx emissions from mobile diesel sources is currently an active area of research.

1.4 Research Objectives

This study develops a selective catalytic reduction (SCR) catalyst for diesel engine NOx reduction using activated carbon. Although zeolites have been found to work well for SCR of NOx at high temperatures, a catalyst effective at lower temperature ranges is needed. A number of studies have been conducted concerning the effectiveness of metal-doped activated carbon (AC) in removing NOx from diesel engine exhaust at lower temperatures; however, no study has directly compared the effectiveness of various types of AC under similar conditions. Thus, this study proposes to do that. In particular, study objectives are:

1. To compare NOx reduction efficiency for cerium doped granular activated carbon (GAC), activated carbon fiber (ACF), and multiwall carbon nanotubes (MWCNTs) at temperatures ranging from 100º C to 400°C, and NO concentrations of 150 and 500 ppm. Reduction efficiencies for untreated AC materials will be compared as a baseline.
2. To characterize the doped catalyst and assess its durability.

Ce was chosen as a dopant in particular due to its non-toxic properties, its ability to reduce NOx and as well as oxidize HC and CO without decomposing, and its relatively low cost. No previous study, to our knowledge, has tested the effectiveness of Ce-doped ACF in particular for NOx reduction.

1.5 Dissertation Organization

This study is organized into five chapters as summarized below.

Chapter 1- Introduction: provides background on gasoline and diesel engines, environmental effects of nitrogen oxides, and research objectives.

Chapter 2- Literature Review: discusses diesel exhaust regulation history, control technologies and previous studies. This chapter also discusses catalyst media, metal oxides, characterization, measurement technologies, importance of this study and summary of literature review.

Chapter 3- Methodology: discusses details about the experimental procedure, experimental design, and characterization techniques.

Chapter 4 - Results and Discussion: contains results obtained from this study and significant findings are discussed in detail.

Chapter 5- Conclusions and Recommendations: key findings are summarized and future study recommendations are listed.

CHAPTER 2

LITERATURE REVIEW

2.1 NOx Control Technologies for Diesel Engines

EPA emission regulations for diesel engine exhaust in the U.S. have become increasingly stringent. Figure 2.1 shows exhaust emission standards for heavy-duty highway compression-ignition engines and urban buses. Several vehicle manufacturers have tried to meet emission standards for 2010 based on a combined NOx catalyst but there are still developments needed to achieve and stay in compliance with regulations.

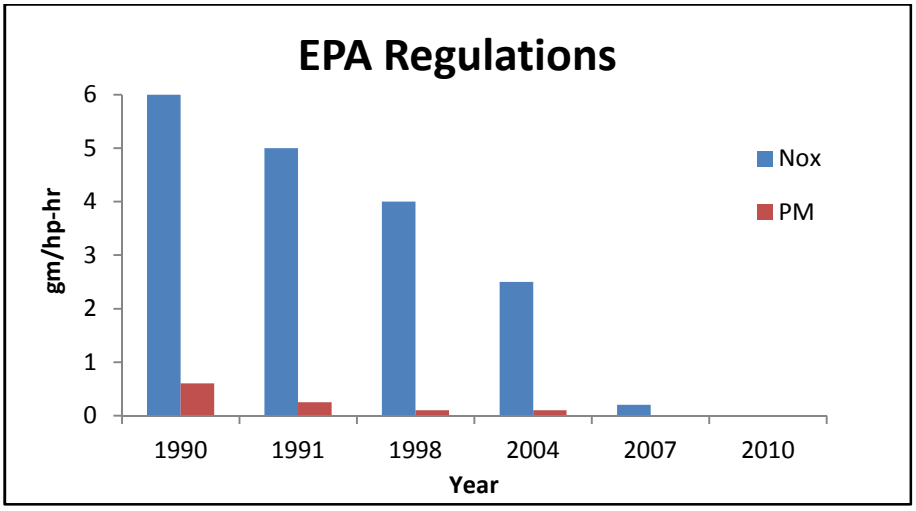

Figure 2.1: Regulation history for NOx emissions from EPA

Over the last thirty years, researchers have put substantial time and effort into developing methods to reduce NOx emissions from diesel engines. Finding a single catalyst for NOx removal has been difficult due to the wide temperature range, high flow rates, wide range of reactants in the exhaust stream, and long lifetime typical of diesel engines (Traa et al., 1999).

Elimination of nitrogen oxides in diesel engine exhaust from mobile sources is still an open relevant target in catalytic research for future researchers (Centi and Perathoner, 2007).

Several review papers for NOx abatement summarize the current status of NOx reduction technologies. Skalska et al. (2010) mention numerous factors that have to be considered in selecting a NOx abatement strategy, including type of source, amount of NOx, composition of NOx, temperature and much more. They conclude that NOx emissions from stationary combustion processes can be successfully reduced using pre and post combustion techniques; however, mobile sources have fewer options for controlling NOx emissions.

Control technologies for reducing NOx emissions from diesel engines include fuel modification, engine design modification and exhaust gas treatment. Fuel modification and engine design modification may affect the engine performance. Modifying the existing engine design may also be expensive. Exhaust gas treatment technologies are added onto the exhaust system to facilitate reduction/oxidation of pollutants to achieve required emission levels. Exhaust gas treatment can be applicable to both new vehicles and existing vehicles. Moreover, an exhaust gas treatment add–on technology often will not affect the power of diesel engine. It includes exhaust gas recirculation (EGR) and catalytic reduction. EGR system recirculates a portion of the exhaust back to the fuel/air intake; it thus reduces excess oxygen in the pre combustion mixture and reduces engine temperatures, which lowers NOx formation in the combustion chamber. However, the NOx reduction efficiency of EGR is only around 50%.

Catalytic reduction reduces NOx in three ways: non-selective reduction, selective reduction and decomposition.

2.1.1 Non-Selective Reduction

In non-selective reduction (NSR), nitrogen oxides are non-selectively reduced by hydrocarbons, carbon monoxide and other emissions in the exhaust stream, as shown in Eq. 1. There is no external source added to reduce NOx.

$$2NO_2 + 4CO \longrightarrow N_2 + 4CO_2 \qquad (1)$$

2.1.3 Selective Catalytic Reduction

Selective catalytic reduction (SCR) involves adding a reducing agent to reduce NOx in the exhaust stream, as shown in Eq. 2. The reducing agent can be ammonia, urea, or hydrocarbons such as propene and methane. SCR is always carried out in the presence of oxygen. SCR reduction efficiency is higher than other control technologies. The reduction efficiency of NOx can up to 90%, HC up to 80% and 20 to 30% for PM.

$$4NO + 4NH_3 + O_2 \longrightarrow 4N_2 + 6H_2O \quad (2)$$

2.1.3 Decomposition

Decomposition of NOx involves decomposing NOx into nitrogen and oxygen using a transition metal based catalyst, as shown in Eq. 3. It is favorable below 900° C.

$$NO \longrightarrow \tfrac{1}{2} N_2 + \tfrac{1}{2} O_2 \quad (3)$$

Roy et al. (2009) reviewed different development and progress of various catalytic media for NOx decomposition or SCR using CO, HC, H_2 or ammonia. They reported that NOx is thermodynamically unstable but has a high activation energy that must be overcome for it to decompose. A suitable catalyst can reduce the activation energy required for NOx decomposition. SCR technology with ammonia as a reductant has several disadvantages associated with transport, injection point and storage. They concluded that several challenges associated with catalyst temperature, poisoning and selectivity still need to be overcome to achieve NOx removal in diesel engines.

However, Diesel Exhaust Fuel (DEF) Addblue, a trademark held by the German Association of the Automobile Industry, eradicates some of the issues related to ammonia transportation and safety. Addblue is in the form of a liquid urea solution, which consists of 32.5% high purity urea and remaining deionized water. It is non hazardous and safe to transport in vehicles and degrades into ammonia by thermal decomposition in the exhaust after injection. It is connected to the exhaust stream through pumping. A 1:1 ratio of NOx to ammonia is required for complete reduction. The average usage of DEF is 3% per gallon. A

single urea tank positioned near SCR can be good for 10,000 miles of highway operation. Following the usage of DEF in diesel trucks, SCR technologies received more attention in research.

Following EPA's 2010 regulation of heavy-duty highway compression-ignition engines and urban buses, selective catalytic reduction became available in most of the light duty diesel engines manufactured. SCR significantly reduces NOx from diesel engines, but the effective operating temperature is above 300ºC (Li et al., 2011). For high temperatures (300°to 500℃), SCR based on Ag/Al_2O_3 and In_2O_3/Al_2O_3 for diesel engines is already giving good reduction capacity. However, SCR catalysts to work in lower temperature ranges to overcome cold start emissions are still under development. Since the temperature window of diesel engine varies, finding a high activity single catalyst for this wide temperature range is likely not possible. Thus, dual catalysts for specific window ranges can be helpful. Figure 2.2 shows the dual catalyst in a diesel engine patent in the year 2004 (Valentine et al., 2004). The research described in this dissertation will identify an appropriate diesel SCR catalyst for low temperatures ranging from 100°to 300℃.

Selective catalytic reduction of NOx is a known control technology for NOx reduction but still it is a significant target in catalytic research for lean burn engines (Genti and Perathoner, 2007; Liu and Seong, 2006). The first pilot study of an SCR process was performed on a coal fired unit in the United States (Muzio and Quartucy, 1997). Since then, substantial improvements have been achieved in SCR processes using ammonia, especially in stationary sources. According to Skalska et al. (2010), there are fewer options available for mobile sources. Studies report up to 85% NOx reduction using SCR by ammonia over TiO_2 (Barman and Philip, 2006) and zeolite (Brüggemann and Keil, 2008). According to Garcia et al. (2005), in general SCR reduction efficiency ranges from 60% to 85% .The operating characteristics of different catalysts for the SCR process have been reported: zeolite works for high temperatures (345º-500ºC) , V_2O_5/TiO_2 for medium temperatures (260º- 425ºC) and Pt-based catalyst for low

temperature (150º - 300ºC) (Heck, 1999). However, platinum is a rare earth metal and it is not an economical choice for diesel engine exhaust.

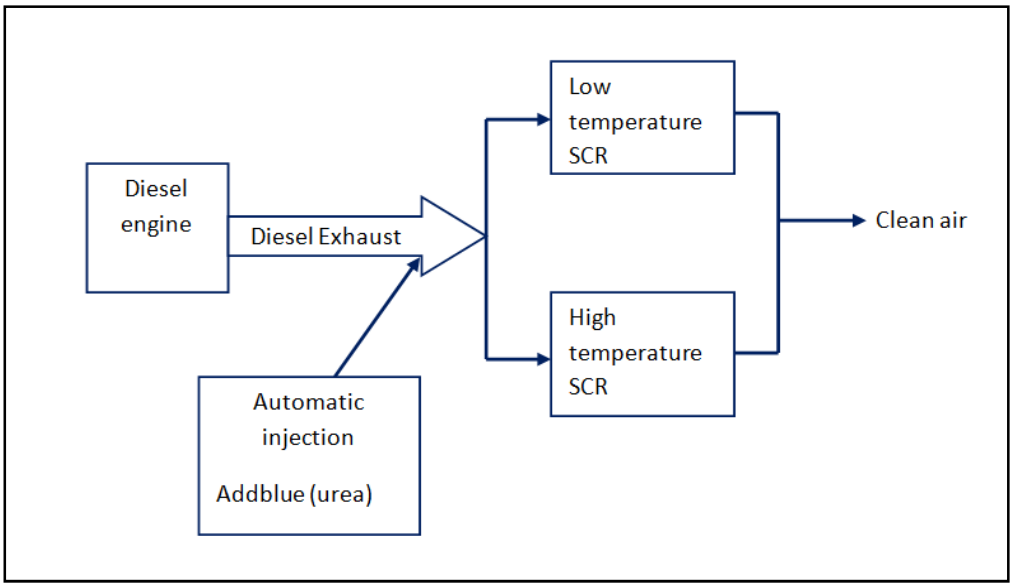

Figure 2.2: SCR dual catalyst in diesel engine

Yun and Kim (2013) studied modeling of SCR by ammonia over V_2O_5 catalyst. They varied O_2 and NH_3 concentration, space velocity, and humidity. The reduction efficiency of V_2O_5 varied from approximately 60 % to 100% for space gas velocity of 100,000/hr to 10,000/hr, respectively, at 400ºC. Space velocity is a major component in reduction efficiency which indicates the residence time of pollutant in the reactor.

2.2 Catalyst Media

Adsorbents doped with transition metals can be used to catalyze the reactions involved in NSR, SCR, or decomposition processes. Various studies have previously been conducted with several adsorbent materials such as zeolites, monolith, and activated carbon. These materials are used due to their advantage of high surface area. Various metals (cobalt, cerium, iron, magnesium, platinum, palladium, titanium, and rhodium) are doped into the high surface area media to improve NOx reduction efficiency due to their catalytic ability. Different

temperature ranges have been widely studied to determine the NOx reduction of catalyst (Huang et al., 2007; Rathore et al., 2010; Chen et al., 2011; Fan et al., 2011).

Zeolite has a natural reduction capacity due to silicon and alumina presence in the structure, and tends to work well at higher diesel exhaust temperatures, above 350ºC. There are more than 150 different kinds of zeolite available. Ion exchange zeolite catalyst shows high performance in HC-SCR but is unstable in hydrothermal conditions (Roy et al., 2009). ZSM-5 is commonly studied for the use of diesel engine exhaust catalyst. Zeolites with metal exchange have also been studied (Yahiro, 2001; Xu, 2002; Bhattacharyya, 2011). Yang (2009) studied adsorption of nitrogen oxides onto commercial powdered zeolite Na X and Na Y. The author found that due to the high number of micropores, its adsorption capacity is high even at higher humidity levels. A combination of silver and aluminum catalyst and silver modified ZSM-5 catalyst in lean burn engines were compared for reduction efficiency (Konova et al., 2006). Ag-ZSM-5 completely oxidized CO and unburned hydrocarbons but NOx reduction was comparatively efficient in bimetallic catalyst than Ag-ZSM 5.

Activated carbon coated cordierite monoliths doped with vanadium and aluminum metals for the reduction of NO by NH_3 show reduction capacity from 50% to 80% (Boyano et al., 2009). Bimetallic catalysts, potassium–copper and potassium–cobalt supported on alumina, show high removal efficiency for both NOx and soot from simulated diesel engine exhaust (Nejar and Illan-Gomez, 2007). Enhanced NOx reduction activity is found in indium (In) and gallium (Ga) doped metal oxide (Maunula et al., 1998).

Since this research examines the potential of doped activated carbons for reducing NOx emissions from diesel engines, various forms of activated carbon and previous NOx reduction studies are discussed in detail. Activated carbons have the potential to reduce NOx at lower temperatures (below 300ºC), where zeolites do not work well. Activated carbon (AC) is formed by heating a charcoal at high temperature in the absence of oxygen; then the carbon is subsequently exposed to oxygen to open up millions of pores. Depending on the raw material

burned (coal, lignite, wood, coconut shell, peanut shell, bones, petroleum coke, lignin and more), different types of activated carbon form. Activated carbon has long been recognized as one of the most versatile adsorbents due to its high porosity and the resulting high surface area (Prakash et al., 1994; Yang, 2003). The typical surface area for gas phase adsorption for carbon is 800-1200 m^2/g. AC is available in different forms. In this study granular activated carbon, activated carbon fiber and multiwall carbon nanotubes will be compared for their NOx reduction capacities.

2.2.1 Granular Activated Carbon (GAC)

Granular activated carbon is in the form of pellets with activated pores to increase surface area. Commercially available bituminous coal based GAC with mesh size 4 X 6 is used in this research. GAC has internal micro pores and external macro pores. Figure2.3 shows the mechanism of accessing the pores in GAC. It is a three stage process, involving advection and diffusion to the surface of the AC, diffusion in the internal pores of the GAC, and finally attachment to the AC surface within the pore.

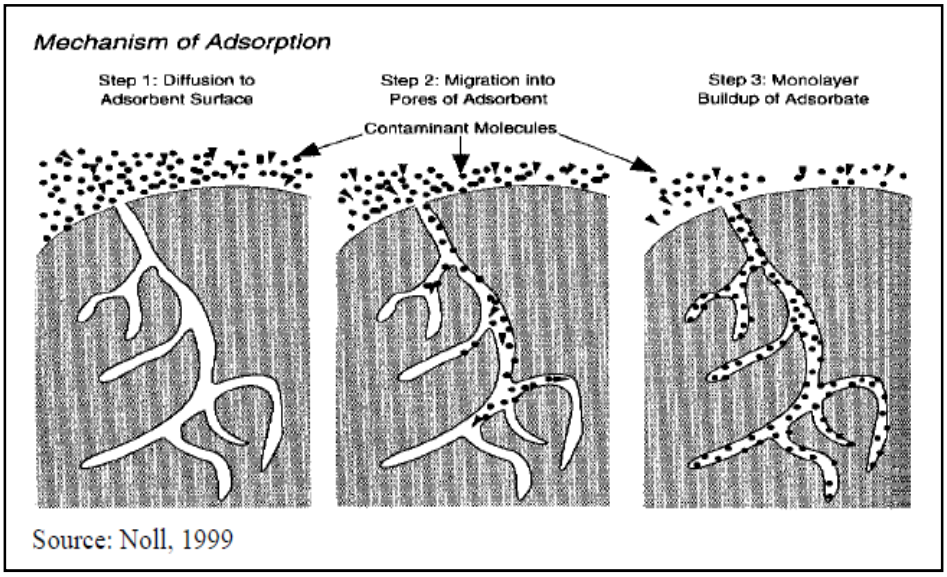

Figure 2.3: Adsorption mechanism in GAC

Previous researches have studied the effectiveness of GAC in removing NOx. A mixture of coal and coconut shell activated carbon doped with several metals was studied for its effectiveness in SO_2 and NOx removal (Gao et al., 2011). Among several metals tested, Ce was reported to have the most promising future due to its nontoxicity and high activity. Selective catalytic reduction of NOx using C_3H_6 over AC doped with several metal oxides (Pt, Pd, Fe, Co, Ni and Cu) found that Pt shows high reduction but low selectivity for N_2 (Garcia-Cortes et al., 2000). They conclude that activated carbon-supported metal catalysts have two main advantages: i) higher NO_x conversions at lower temperatures and ii) at lower temperatures, the N_2 selectivity range is same as alumina supported catalyst. Simultaneous removal of VOC and NO by cobalt, copper, iron, and nickel coated coconut shell activated carbon was studied by Lu and Wey (2007). The study found that cobalt coated GAC shows higher activity at 250ºC temperature. Simultaneous removal of SO_2 and NOx on peanut shell activated carbon (PSAC) with different calcination temperatures and metal oxide coatings showed good performance in NOx reduction and SO_2 adsorption (Sethuraman et al., 2010). The study concluded that 10 wt% of cerium-coated PSAC showed better performance than other wt% of metal coatings. The effect of calcination temperature on pollutant removal efficiency was also been studied.

2.2.2 Activated Carbon Fiber (ACF)

Activated carbon in a cloth structure is known as activated carbon fiber. It was originally invented in 1970s. It can be rolled or wrapped together as a sheet form. It has advantages of low weight, high adsorption capacity, and high regeneration capacity. The cloth surface area, at 1000-2000 m^2/g, is much higher than typical AC. It has evenly distributed micropores. In ACF, the gases can easily access the micropores exposed to the outer surface. In contrast, gases have to travel through the macro pores and transitional pores to access and fill the micro pores available in GAC. Figure 2.4 shows the difference between GAC and ACF adsorption site availability. Strong electrostatic forces developed within the cloth enable it to be highly active in adsorbing vapors. (Zorflex ACC).

A study of ACF impregnated with several reagents (ammonia, pyridine, amine, etc.) found that ammonia impregnation achieved 70% NO oxidation and 90% capturing in particulate concentration (Rathore et al., 2010). The ACF showed large adsorption due to N-containing groups. In removal of NOx and SO_2, a thinner bounding layer is favorable under rapid gas flow (Mochida et al., 2000). Thinner paper reduces the pressure drop in the system. However, the shape and size of the fiber is important in compact packing.

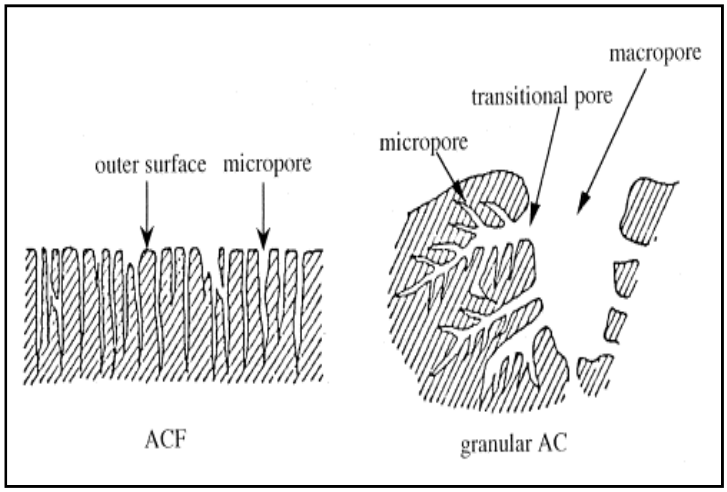

Source: Mochida et al., 2000

Figure 2.4: Adsorption site availability in GAV and ACF

The reduction efficiency of vanadium oxide loaded activated carbon fiber increases as temperature increases in the window of 120º to 240ºC (Huang et al., 2008). The V_2O_5 loading affects the NO conversion efficiency: lesser loading of vanadium oxide shows less reduction in NOx efficiency.

2.2.3 Multi-Walled Carbon Nanotubes (MWCNTs)

Carbon nanotubes have received much attention for their potential applications in pollution control since their first discovered by Iijima in 1991. They are formed by rolling a graphite sheet into a tube-shaped structure. Carbon nanotubes have high tensile strength and elastic modulus due to the covalent bonds between carbon atoms. If one sheet is rolled, then single walled carbon nanotubes (SWCNT) result. If several or more than two concentric circles

formed by rolling, then Multi-Walled Carbon Nanotubes (MWCNTs) result. Figure 2.5 shows the difference between SWCNT and MWCNTs.

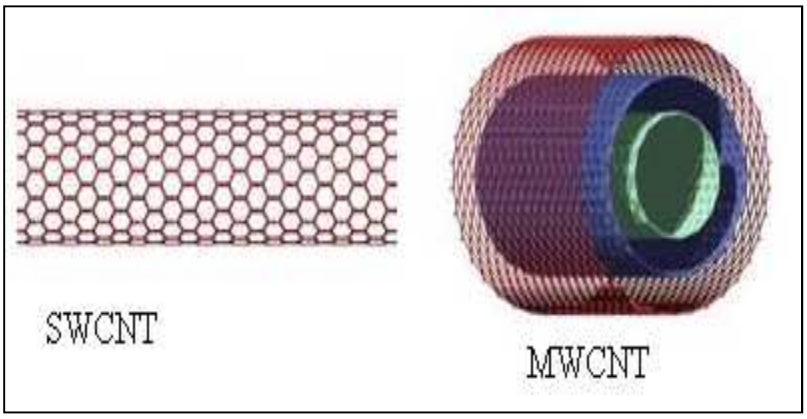

Figure 2.5: SWCNT and MWCNT Structure (Larouche et al., 2009)

The adsorption mechanism in CNTs can be explained with the help of a study by Ren et al. (2011). They explained adsorption site availability in nanotubes. According to their study, Figure 2.6 explains the possible spaces for adsorption and reduction processes: 1. Open-ended multiwall nanotubes, 2. Closed MWCNTs, 3. External wall surface where surface adhesion can occur, 4. Interstitial channel available between nanotubes and 5. External groove sites.

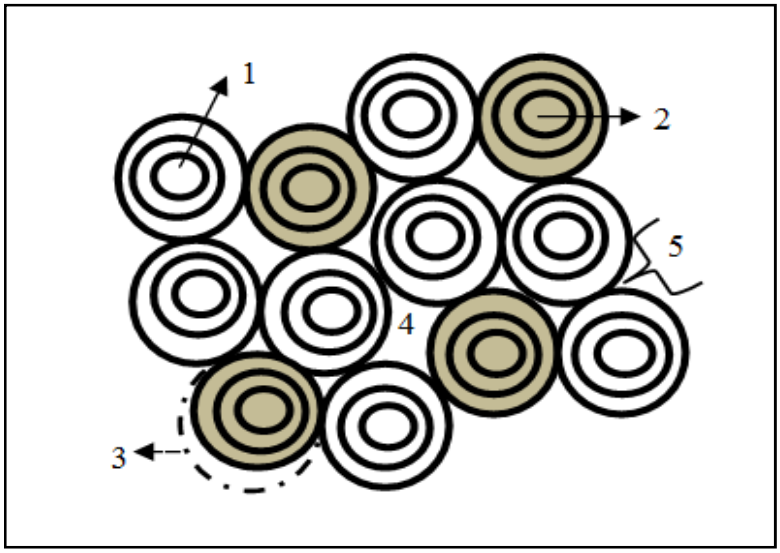

Figure 2.6: MWCNTs adsorption sites: 1, Open ended, 2. Closed cap, 3. External wall surface, 4. Interstitial channel, and 5. External groove site.

A number of studies have examined the effectiveness of MWCNT in NOx removal. Li et al. (2011) found that MWCNTs coated with titanium oxide and vanadium oxide at 10% by weight demonstrated an 89% NOx removal efficiency at 300℃ . Platinum (Pt) supported MWCNTs with propene were found to have a NOx reduction capacity comparable to Pt/Al_2O_3 **(**Santillan-Jimenez et al., 2011). The author suggests that the use of 3:1 Pt-Rh alloy catalyst will improve the efficiency of the MWCNT performance. Selective catalytic reduction of NO using NH_3 over cerium oxide-doped MWCNTs showed reduction efficiencies ranging from 70% to 90%, depending on Ce/C ratio, in the temperature window of 250℃ to 450℃ (Chen et al., 2011). Huang (2007) found that vanadium oxide (V_2O_5) supported MWCNT catalysts with NH_3 as the reductant showed good performance in the temperature range from 373 to 523 K (Huang, 2007): the loading percentage (V_2O_5) 2.35 wt% was used, and the NOx reduction efficiency achieved was 92%. De-NO_X efficiency of more than 90% was obtained over the Mn–Ce–O_X/TiO_2-CNTs catalyst at the temperature window of 75–225°C (Fan et al., 2011). A higher efficiency observed when SO_2 was introduced into the stream. Wang et al. (2012) studied the catalytic reduction of NO with NH_3 in manganese oxides supported on multi-walled carbon nanotubes. They found that high manganese loading (25 wt.%) and high calcination temperature (500℃) will reduce the dispersion and increase the crystallinity of the catalysts. They conclude that 10 wt% at 400℃ works well.

2.3 Metal Oxide Doping of Activated Carbon

Several metal oxides have been doped onto the surface of the activated carbon to improve its catalytic ability. Transition metals can be used for this application, as they possess incompletely filled outer shell electronic configurations, together with an ability to have two different oxidation states; thus, continuous oxidation and reduction processes occur in these transition metals. A number of studies have been done with cobalt, cerium, iron, magnesium, platinum, palladium, titanium, and rhodium as dopants. Cerium is reported as a promising dopant for NOx reduction in some of the researches. Among several metals tested, Ce shows

more promise than V due to its non-toxicity (Gao et al., 2011). Cerium has high capacity in storing and releasing oxygen in the surface due to the presence of cerium in two different valance states, namely Ce^{4+} and Ce^{3+} (Kaspar et al., 1999; Zimmer et al., 2002; Bjorn et al., 2002; Yanyong et al., 2002). Cerium oxide has been continuously considered as an automobile catalyst due to its stabilized dispersed state and high surface area (Travorelli, 1999)

2.3.1 Cerium Oxide

Cerium is a soft ductile metal which easily oxidizes in air. It is abundantly available, comprising approximately 0.0046% of Earth's crust weight. It has a dual valence state: Ce^{4+} (CeO_2) and Ce^{3+} (Ce_2O_3). It is usually present in compounds in both the tetravalent (Ce^{4+}) and trivalent (Ce^{3+}) states (Kilbourn, 2003; Reinhardt and Winkler, 2002). The crystallography of cerium oxide is face centered cubic structure. In cerium oxide, cerium and oxide ions are arranged in a fluorite structure, wherein oxygen atoms in the ceria are arranged in plane with one another, as shown in Figure 2.7. The oxygen moves in the outer surface of the structure. Ceria is a non-stoichiometric compound containing oxygen vacancies in its crystal structure and can be represented by the formula $CeO_{(2-x)}$. Because of the oxygen vacancies, there will be some Ce^{3+} ions in CeO_2 crystals and the number of Ce^{3+} will be twice the number of oxygen vacancies. Thus, the presence of Ce^{4+} and Ce^{3+} ions within the crystal lattice of CeO_2 makes it a very good catalyst for oxidation as well as for reduction reactions. Rapid diffusion of oxygen atoms occurs when the number of vacancies increases. It can easily take and give up oxygen in the exhaust stream. Rapid transformation from Ce^{4+} to Ce^{3+} makes cerium as a good catalyst.

The atomic number and atomic mass of cerium are 58 and 140.116, respectively. It melts at 797.8℃ and boils at 3,442°C. Cerium oxide appears as a yellow powder and takes moisture from atmosphere. It is odorless and insoluble in water. Major uses of cerium oxide include decolorizing and polishing glass, heat resistant coatings, catalyst for emission control, ceramic coatings, gemstone polishing, semiconductors and capacitors. Cerium oxide is a nontoxic and non-radioactive compound.

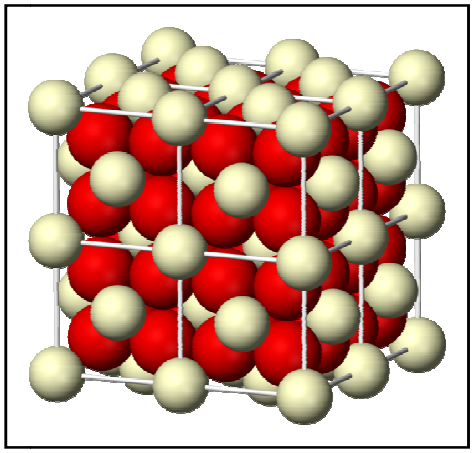

Fig 2.7: Fluorite structure of cerium

2.3.2 Reaction Mechanism

It is well known that cerium oxide has a powerful oxidizing and oxygen storage (redox conversion between Ce^{3+} and Ce^{4+}) property which could bring new surface groups like Ce–OH and Ce=O onto the surface. Under reducing conditions, these properties could reduce NO to N_2. The proposed mechanism for the cerium oxide catalyzed NO reduction in presence of NH_3 is given in Figure 2.8. The reaction cycle may takes place in three main steps. The CeO_2 (Ce^{4+}) dispersed in the surface of activated carbon contains Ce=O groups on the surface (a). In the first step (b), two Ce^{4+} (Ce=O groups) react with one NH_3 molecule to form two Ce–OH groups. The left over N–H (which is away from the CeO_2 surface) combines with another N-H to form N_2H_2 (i.e., HN=NH). In the second step (c), this HN=NH reacts with another Ce^{4+} (Ce=O group) either to form an H_2O molecule and inert N_2 molecule, or to form 2 Ce–OHs and an N_2 molecule. Thus, the Ce^{4+} (Ce=O) is reduced to Ce^{3+} (Ce–OH) by NH_3. The third step (d) is the oxidation of Ce^{3+} (Ce_2O_3) to Ce^{4+} by nitric oxide (NO) in the exhaust-gas to form H_2O plus N_2 and regenerate Ce^{4+} (e) again to make the continuous chain reaction of oxidation and reduction processes. Thus, the NO is reduced to N_2 and the overall reaction would be:

$$4NH_3 + 4NO \longrightarrow 6H_2O + 4N_2$$

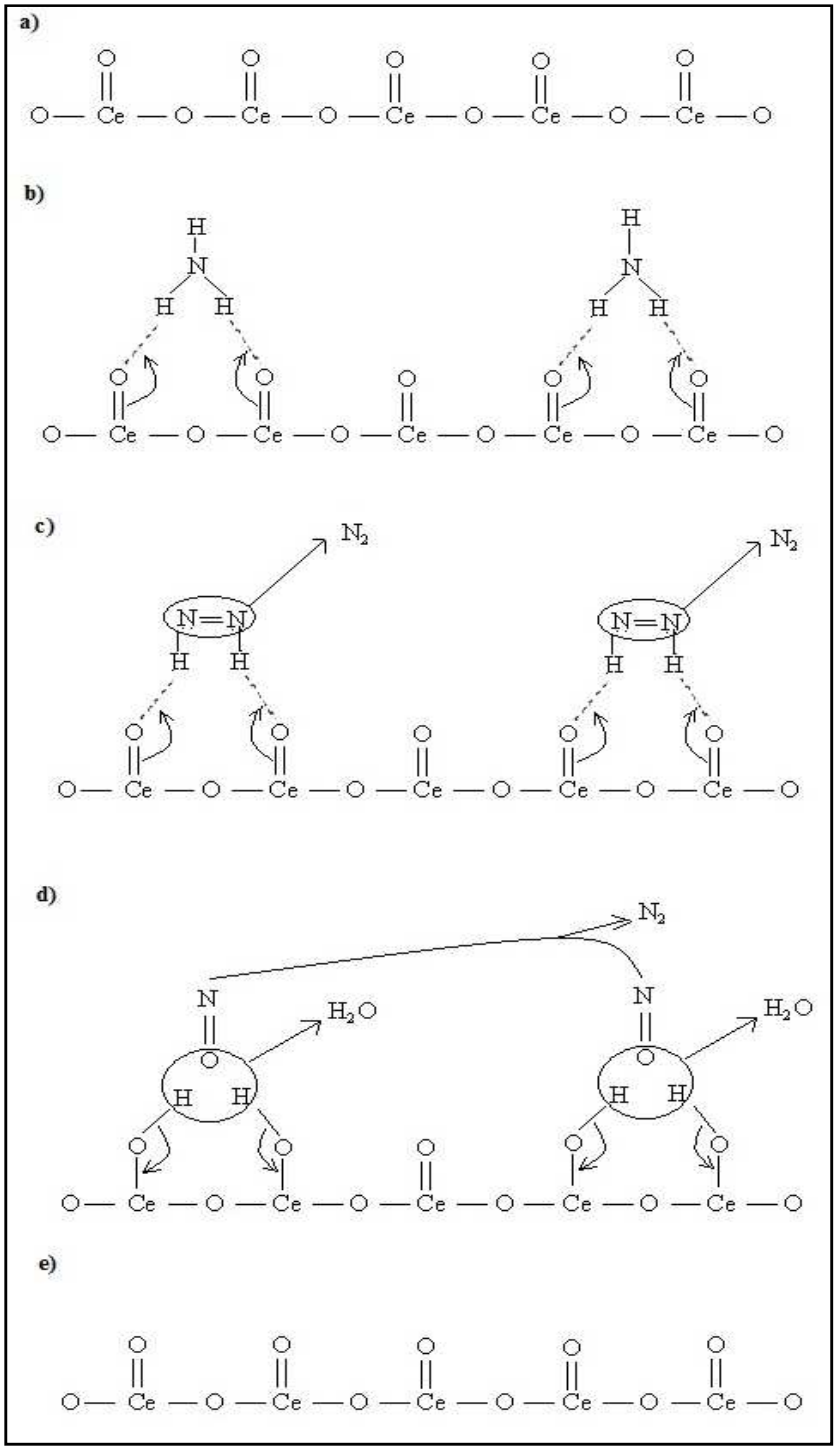

Figure 2.8: Cerium oxide NOx reduction mechanism

Activated carbon provides high surface area to spread the cerium oxide in the pores. Cerium oxide helps reduce NO into N_2 by using NH_3 to facilitate reduction and oxidation cyclic reactions. Garcia et al. (2005) explains the importance of transition metal as a catalyst in his study. It creates sorption and regeneration processes on the surface to facilitate the reaction. The decomposition of NO into N_2 in the catalyst will also form N_2O, NO_2 and unreacted NH_3 in the reaction. To overcome this effect, the exhaust gas can be recirculated to further react with the catalyst. Colombo et al. (2012) developed a dual layer ammonia slip catalyst: platinum group based metals (PGM catalyst) were placed downstream of an SCR catalyst as a thin wash coat layer to take care of the unwanted pollutant in the stream.

2.4 Catalyst Characterization

Catalyst characterization is of foremost importance in designing a new catalyst. Doping the metal oxides onto the surface of the carbon changes its structure, surface area and surface functional groups. The significance of characterization is reported in numerous articles. Several researchers have studied NOx reduction percentages related to the catalyst physiochemical properties, exhaust temperature, and percentage weight of metal doping in the surface of the materials. Physiochemical properties of several metal-doped activated carbons (Fe, Co, Ni, V, Mn, Cu and Ce) have been studied using X-ray diffraction and X-ray photoelectron spectroscopy; Cu and Fe were found to be partly reduced by carbon during preparation (Gao et al., 2011).

The oxidation state of Cerium Ce(IV) or Ce(III) can be found by XPS analysis. Gao et al. (2011) found the state of cerium oxide in core level spectra analysis through XPS and also found a total of eight peaks corresponding to cerium. Cerium (IV) has six peaks and cerium (III) has two peaks in their finding. In inert atmosphere, major amounts of $Ce(NO_3)_3$ precursor decomposed into CeO_2 (Ce(IV)). However, it also forms Ce(III) due to the transfer of electrons from the surface of activated carbon to the metal oxide (Faria et al., 2008). Tang et al. (2009) studied the characterization and catalytic activity of manganese oxide supported on activated

carbon. Manganese oxide dispersion, oxidation state, and local coordination in the prepared catalyst were characterized by X-ray diffraction (XRD), hydrogen temperature-programmed reduction (H_2-TPR), electron spin resonance (ESR), and more. The use of Raman spectroscopy to understand the functional groups in the surface of the catalyst is emphasized (Banares and Wachs, 2002; Banares and Mestl, 2009). Infrared spectroscopy is the most widely used and important characterization method to identify surface-bound molecules.

2.5 Measurement of NOx

Chemiluminescence is a reliable, leading and standard high-performance analytical measurement method for NOx. Chemiluminescence means a chemical reaction produces light. In the case of NOx, ozone reacts with a NO (nitric oxide) molecule, which is oxidized to NO_2. This reaction releases energy in the form of light, which is measured by the detector in the analyzer. The level of chemiluminescence detection is directly proportional to the NO concentration. It also calculates NOx by converting NO_2 into NO in a different channel and finds the difference between the two channels for NO_2 measurement.

Measuring NOx and ammonia in a single analyzer is challenging due to ammonia gas precipitation onto the analyzer surface, which clogs measurement. The CLD 822 cm H by Ecophysics overcame that by using heated sample line measurement. The analyzer is equipped with two parallel converters to measure N-containing compounds such as NO, NO_2 and NH_3. The operating principle of the CLD 822 CM h is shown in Figure 2.9.The metallic converter converts only NO_2 into NO and finds the total NOx. A catalyst converts NO_2 and NH_3 into NO and finds NOxamine. Ammonia is calculated by subtracting NOx from NOxamine value.

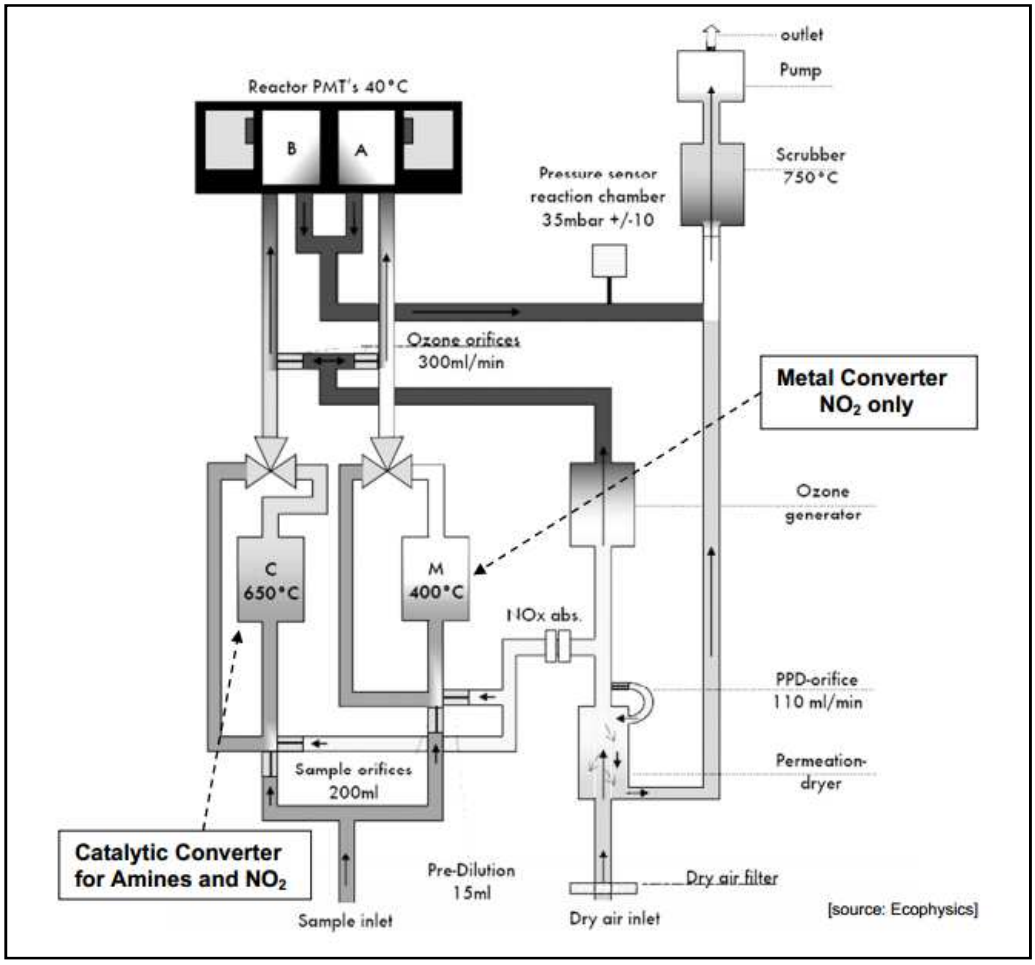

Figure 2.9: Operating Principle of CLD 822 CM h NOx/Ammonia Analyzer

2.6 Summary

Tables 2.1, 2.2, and 2.3 below summarize articles related to use of activated carbon for removing NOx.

Table 2.1: Articles Related to Granular Activated Carbon

Title: Physicochemical properties of metal-doped activated carbons and relationship with their performance in the removal of SO_2 and NO, 2011						
Authors: Xiang Gao, Shaojun Liu, Yang Zhang, Zhongyang Luo, Kefa Cen						
Catalyst	**Characterization**	**Variables**	**Concentration**	**Analysis Method**	**Other parameters**	**Conclusion**
Coal and coconut shell mixed carbon doped with Fe, Co, Ni, V, Mn, Cu and Ce	XRD, XPS, XRF, CHN, BET,	1.Temperature 2.Metal Oxide	450 ppm NO, 500 ppm NH_3, 6.5% O_2, and 8% H_2O	Chromatography	Flowrate = 0.4 L min^{-1} Amount used=1 g	V, Ce and Cu impregnation showed good activity for NO reduction using NH_3.The deposition of Fe and Ni enhanced the adsorption of NO rather than reduction.
Title: Simultaneous removal of VOC and NO by activated carbon impregnated with transition metal catalysts in combustion flue gas						
Authors: Chi-Yuan Lu, Ming-Yen Wey						
Catalyst	**Characterization**	**Variables**	**Concentration**	**Analysis Method**	**Other parameters**	**Conclusion**
Coconut shell-derived carbon	ICP-MS, XPS, FTIR, BET and SEM	Transition metals Oxygen concentration Temperature	NO600 ppm, toluene 150 ppm/N_2/O_2	Flue gas analyzer (Horiba, PG-250 and chromatograph/ flame ionization detector)	Flowrate = 500 ml/min Amount used= 992 mg	The results show that Co/AC and Cu/AC provided a high activity of around 100% for VOC deep oxidation at 250℃.

Table 2.1 – *Continued*

Title: Cerium impregnated palm shell activated carbon (Ce/PSAC) sorbent for simultaneous removal of SO_2 and NO-Process study, 2010						
Authors: S. Sumathi, S. Bhatia, K.T. Lee, A.R. Mohamed						
Catalyst	**Characterization**	**Variables**	**Concentration**	**Analysis Method**	**Other parameters**	**Conclusion**
Palm shell activated carbon (Ce/PSAC)	N/A	Temperature Humidity SO_2 and NO concentration	SO_2 (2000 ppm) (50%), NO (500 ppm) (11%), O_2 (10%), and N_2 (29%) as the balance	Flue gas analyzer (IMR5000/400)	Flowrate = 150 ml/min Amount used= 1.0 g	SO_2 and NO decreased with increasing space velocity, NO sorption increases with temperature increases from 100 to 250℃

Table 2.2: Articles Related to Activated Carbon Fiber

Title: Vanadium supported on viscose-based activated carbon fibers modified by oxygen plasma for the SCR of NO, 2008						
Authors: Huacun Huang, Daiqi Ye, Bichun Huang, Zhengle Wei						
Catalyst	**Characterization**	**Variables**	**Concentration**	**Analysis Method**	**Other parameters**	**Conclusion**
VACF	SEM, XPS, BET, XRD	1. Activity test temperature 2. Oxygen plasma and Nitric acid modification (NAM) 3. Metal loading %	1000 ppm NO, 1000 ppm NH3, 5% O_2, and the balance Ar	Flue Gas Analyzer (TH-990S)	Space velocity = 9686.8 h^{-1} Flowrate = 0.365 L min^{-1} Amount used=200 mg	NO conversion increases with increasing temperature (120–240 COPM and NAM increase the surface roughness and thus activity.
Title: Development of surface functionalized activated carbon fiber for control of NO and particulate matter, 2010						
Authors: Rajveer Singh Rathore, Dhananjay Kumar Srivastava, Avinash Kumar Agarwal, Nishith Verma						
Catalyst	**Characterization**	**Variables**	**Concentration**	**Analysis Method**	**Other parameters**	**Conclusion**
ACF impregnated with ammonia, pyridine, amine, etc.	BET, FTIR	1. Various ACF weight 2. NO concentration 3. Flowrate	variable	Chemilumin-escence NO*x* analyzer (Thermo electron Co. USA; Model: 42C	Variable	Ammonia impregnated ACF shows 70% reduction of NO and 90% removal of particulate at temperature 40%C, and oxygen concentration 20%

Table 2.3: Articles Related to Multiwall Carbon Nanotubes

Title: Manganese oxides supported on multi-walled carbon nanotubes for selective catalytic reduction of NO with NH_3: Catalytic activity and characterization, 2012						
Authors: Lishan Wang, Bichun Huang, Yanxia Su, Guangying Zhou, Keliang Wang, Hongcheng Luo, Daiqi Ye						
Catalyst	**Characterization**	**Variables**	**Concentration**	**Analysis Method**	**Other parameters**	**Conclusion**
MnOx/ MWCNTs	TEM, XRD, XPS, N_2 adsorption, H_2-TPR, and Raman spectroscopy	1. Metal loading 2. Calcination temperature 3. Outer diameter of MWCNTs 4. Experiment temperature	1000 ppm NH_3, 1000 ppm NO and 5 vol.% O_2	42i-HL, Thermo Ins.	Space velocity =40,000 h^{-1} Flowrate =0.6 L/min Amount used=180mg	High manganese loading (25 wt.%) and high calcination temperature (500℃) will reduce the dispersion and increase the crystallinity of the catalysts. 10 wt% at 400℃ works well.
Title: Selective catalytic reduction of NO over carbon nanotubes supported CeO_2, 2011						
Authors: Xiongbo Chen, Shan Gao, Haiqiang Wang, Yue Liu, Zhongbiao Wu						
Catalyst	**Characterization**	**Variables**	**Concentration**	**Analysis Method**	**Other parameters**	**Conclusion**
CeO_2/ MWCNTs	XRD, XPS, TEM, BET, and H_2-TPR	1. Ce/C ratio, 2.Reduction Temperature 3.Calcination temperature	600 ppm NO , 600 ppm NH_3, 3.5% O_2 and balance N_2	flue gas analyzer (KM9106 Quintox Kane International Limited) and Gasmet DX-4000	Space velocity = 100,000/h Amount used=0.5 g	Non-toxic SCR catalysts with good performance in the medium temperature range (250–400℃).

Table 2.3 – *Continued*

Title: Selective catalytic reduction of NO_X with ammonia over MnCe–O_X/TiO_2-carbon nanotube composites, 2011						
Authors: Xiaoyu Fan, Famin Qiu, Hangsheng Yang, Wei Tian, Tianfeng Hou, Xiaobin Zhang						
Catalyst	**Characterization**	**Variables**	**Concentration**	**Analysis Method**	**Other parameters**	**Conclusion**
Mn–Ce–O_X/TiO_2-CNTs	XRD, XPS, SEM, BET, TGA and H_2- TPR, NH_3-TPD	1. Catalyst stage 2. Reduction temperature 3. Introduction of SO_2	NO (0.025 vol.%), O_2 (6.5 vol.%), NH_3 (0.025 vol.%), and N_2 as balanced gas	Testo AG — Testo 350 and Motorola 500 Series	Space velocity = 36,000 h^{-1} Flowrate = 1200 ml/min	De-NO_X efficiency of more than 90% was obtained over the Mn–Ce–O_X/TiO_2-CNTs catalyst at the temperature window of 75–225 ℃
Title: Low temperature SCR of NO with NH_3 over carbon nanotubes supported vanadium oxides, 2007						
Authors: Bichun Huang, Rong Huang, Dongjie Jin, Daiqi Ye						
Catalyst	**Characterization**	**Variables**	**Concentration**	**Analysis Method**	**Other parameters**	**Conclusion**
V_2O_5/MWCNT	TEM, BET, FTIR, XRD and TPD methods.	1. Metal loading % 2. Reduction temperature 3. CNTs diameter	800 ppm NO, 800 ppm NH_3, 5 vol% O_2 balanced by He	FSI Model flue gas analyzer and gas chromatograph with Porapak Q column	Space velocity = 35,000 h^{-1} Flowrate = 500 ml min^{-1} Amount used=200mg	The prepared catalysts show a good catalytic activity at a temperature range of 373–523 K.

Table 2.3 – *Continued*

Title: Promotional effects of carbon nanotubes on $V2O_5/TiO_2$ for NO_X removal, 2011						
Authors: Qian Li, Hangsheng Yang, Famin Qiu, Xiaobin Zhang						
Catalyst	**Characterization**	**Variables**	**Concentration**	**Analysis Method**	**Other parameters**	**Conclusion**
V_2O_5/TiO_2–MWCNTs	XRD XPS Raman spectra TGA H_2-TPR NH_3-TPD	1. CNTs Wt % 2. Reduction temperature 3. SO_2 and H_2O	500 p m NO, 500 ppm NH_3, 6% O_2, 200 ppm SO_2, and 2.5% H_2O	Testo AG-Testo 350)	Space velocity = 22,500 and Flowrate = 500 ml/min	V_2O_5/TiO_2–CNT (10 wt.%) showed an NO_X removal efficiency of 89% at 300 ℃
Title: Carbon nanotube-supported metal catalysts for NOx reduction using hydrocarbon reductants. Part 1: Catalyst preparation, characterization and NOx reduction characteristics, 2011						
Authors: Eduardo Santillan-Jimenez, Vladimir Miljković-Kocić, Mark Crocker, Karen Wilson						
Catalyst	**Characterization**	**Variables**	**Concentration**	**Analysis Method**	**Other parameters**	**Conclusion**
Pt/MWCNTs	XPS, TGA, BET, TEM, STEM, CHN,FTIR, EDS, NH_3-TPD	1. Metal loading % and metal 2. Reduction temperature	500 ppm NO, 10% O_2, 10% H_2O and 500 ppm of propene	Eco Physics CLD 700 EL ht	Space velocity = 50,000 h^{-1} Flowrate = 1667 cm^3/min Amount used=1g	Pt supported on pristine MWCNTs was found to exhibit a comparable NO_x reduction activity with propene to Pt/Al_2O_3

Table 2.3 – *Continued*

Title: Selective catalytic reduction of NO with NH_3 over CuO_X-carbonaceous materials, 2011						
Authors: Qian Li, Hangsheng Yang, Zhaoxia Ma, Xiaobin Zhang						
catalyst	**Characterization**	**Variables**	**Concentration**	**Analysis Method**	**Other parameters**	**Conclusion**
Cu–CNTs, Cu–ACs and Cu–Gs	SEM, EDX, TPD, TPR, AAS and XPS	1. Different catalysts 2. Reduction temperature 3. SO_2 concentration	700 ppm NO, 700 ppm NH_3, 6% O_2, 100–200 ppm SO_2	Testo AG-Testo 350	Space velocity = 7500 h^{-1} Flowrate = 500 mL min^{-1} Amount used=1g	Cu–CNTs strong acid sites and good dispersion on the surface gives 67% removal at 250ºC

The NOx reduction efficiency of SCR with ammonia depends on several factors. Taking carbon as a matrix structure to load the metal, the reduction efficiency can vary depending on the type of metal, metal loading percentage, calcination temperature, concentration of NOx, NOx/NH_3 ratio, retention time in the reactor (or Gas Space Hourly Velocity (GSHV)), temperature, O_2 concentration, and humidity. Since SCR is a broad research area, this paper concentrates on the non-toxic metal cerium and tries to find the cost effective carbon matrix to dope the metal for high GSHV. Higher GSHVs would reflect real time application processes for on road diesel engines. No previous study, to our knowledge, has directly compared the effectiveness of 3 carbon matrices for SCR. In particular, no study has examined the effectiveness of Ce-doped activated carbon fiber for SCR. The doping percentages and calcination temperatures were adapted from previous work (Sumathi et al., 2010). Common O_2 concentration and NOx /NH_3 levels were maintained with variations in temperature and NOx concentrations to obtain reduction efficiency profiles.

Thus, this study compares the reduction efficiency for 3 kinds of carbon tested under the same preparation and operating conditions and finds the best practice for achieving high reduction in NOx for diesel engine exhaust. It also examines the difference in physical/chemical characteristics of the 3 kinds of carbon by material analyse.

CHAPTER 3

METHODOLOGY

3.1 Catalyst Preparation

Activated carbon fiber (ACF) and granular activated carbon (GAC) with mesh size 4X6 were purchased from Calgon Corporation. Catalytic multi-walled nanotubes (MWCNTs) produced by chemical vapor deposition (CVD) were purchased from Materials and Electrochemical Research (MER) Corporation. The nanotubes were 20-25 nm in diameter and 1-5 microns in length. According to manufacture data, impurities present in the MWCNTs are 1.8 wt% iron (Fe), 2.6 wt% alumina (Al), and traces (~0.02%) of cobalt (Co), with the rest is carbon.

Cerium (III) nitrate hexahydrate 99.5% ($Ce(NO_3)_3 \cdot 6H_2O$) was purchased from Fisher Scientific Corporation. To make the doped catalysts, a 10 wt % of cerium (Ce) was loaded onto the carbons as follows. 1g of carbon and 10 wt % of cerium (0.3099 g cerium nitrate hexahydrate) were weighed. Cerium nitrate hexahydrate was mixed with 100 ml of deionized water to obtain a cerium nitrate solution. The carbon was added to the cerium nitrate solution, which was then kept in the rotary meter for 5h with intermediate mixing. The solution was then heated to 70℃ and constantly mixed until the water completely evaporated. The wet sample was oven dried for 12h in a muffle furnace manufactured by Paragon Industries at 110℃ to remove excess water. Finally, the sample was calcinated in a tube furnace (Lindberg, type TF55035A) at 500℃ in the presence of Argon (Ar) fo r 4h. Ultra high purity argon was obtained from Matheson Trigas Corporation. The metal-doped activated carbon was then designated as CeAC. Figure 3.1 shows the experimental set up for catalyst preparation. The impregnation procedure was adapted from previous literature (Dr. Sumathi et al., 2012), in which different cerium percentages were loaded onto palm shell activated carbon; it was found that 10 wt %

loading is optimum for flue gas control treatment technology. A calcination temperature of 500° C was selected by running a thermo gravimetric analysis on cerium (III) nitrate hexahydrate in the presence of nitrogen; it was found that the cerium (III) nitrate hexahydrate calcinates at 450℃.

The catalyst bed, made in the mechanical shop at UTA, was made from stainless steel to withstand high temperatures. The steel alloy, containing 11% chromium, is resistant to stain, corrosion and rust. A 1 inch diameter steel rod was cut to a 6 inch length. It was drilled length wise for 4 inches to make a hole of 0.25 inch diameter (shown in Figure 3.2, top picture at left). To keep the catalyst in the rod, a catalyst bed was made by cutting the rod half way through in the center of the rod. It was then perforated to let the air flow to the catalyst bed, as shown in Figure 3.2 (top picture at right). The surface area of the inlet hole was matched with the total perforated hole surface area to avoid back pressure.

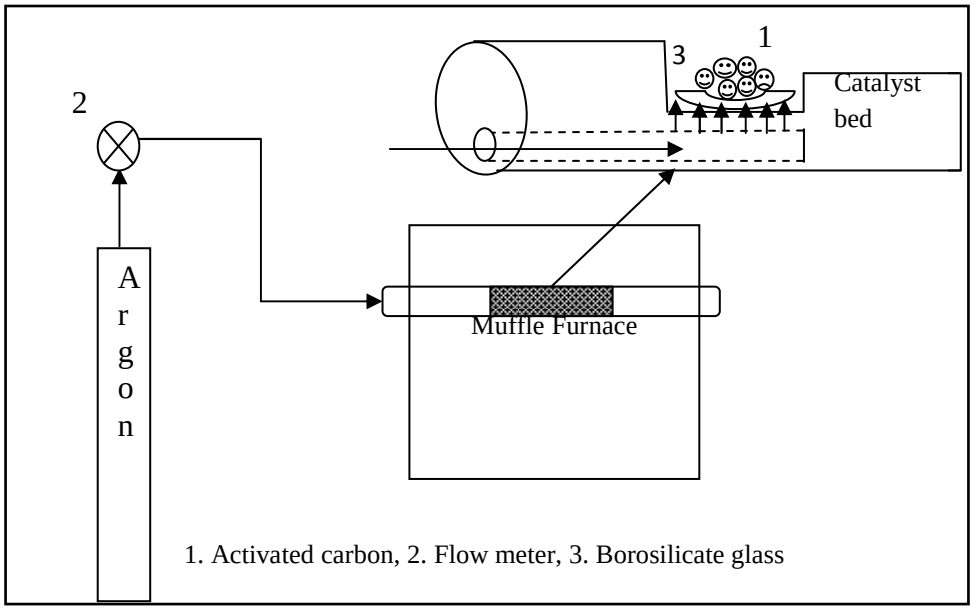

Figure 3.1: Schematic diagram of the catalyst preparation experimental set up

Figure 3.2: Catalyst preparation bed

Finally, the bed was coated with aluminum powder for finishing. To make it air-tight, it was rolled with a chromium rod (shown in bottom picture in Figure 3.2) while installing it in the tube furnace. Deactivated borosilicate glass wool (shown in bottom picture in Figure 3.2) was bought from Fisher Scientific Corporation. It was placed on top of the perforated holes to regulate and distribute the flow evenly through the carbon and to avoid losing the carbon particles during the experimental runs. Samples were placed in the wool and were thus kept in the perforated tray structure. Trial runs were made to choose the amount of borosilicate used to avoid back pressure. Approximately 0.05 g of wool was placed during each experimental run.

3.2 Catalyst Characterization

Characterization is important in understanding and analyzing the catalyst. Raw untreated samples of each of the 3 types of carbon were characterized, along with Ce-doped samples. Material analysis techniques included as Scanning Electron Microscope (SEM) imaging; Energy Dispersive Spectroscopy (EDS); carbon, hydrogen, and nitrogen (CHN) analysis; X-ray Diffraction (XRD) analysis; Raman spectroscopy; X-ray Photoelectron spectroscopy (XPS); Thermo gravimetric analysis (TGA); and Brunauer-Emmett-Teller (BET) surface area analysis. Each of these methods is discussed in turn.

3.2.1 SEM/EDS

Prepared catalysts were analyzed for metal adherence on the surface, distribution of cerium, pore openings or blockage, and impurities. A scanning electron microscope is capable of capturing high resolution back scatter electron and secondary electron images. The images are produced by passing a high-energy beam of electrons, which interacts with the atoms of the sample, in a raster scan pattern. The high energy beam of electron carries a significant amount of kinetic energy that dissipates when it interacts with sample. The beam position and detected signal together produce an image for analysis. The electron microscope images show the sample's surface topography, properties, and composition.

Energy dispersive X-ray Spectroscopy, commonly known as EDS, is used to identify the chemical composition of the sample. A beam of electrons is introduced to the sample inside SEM. It collides with electrons within the sample and causes some of them to be knocked out of the sample. The vacant places in the orbitals are then filled with high energy electrons provided in the beam; the sample thus emits x-rays as a signal. It determines the elemental composition of the sample or it can map out the lateral distribution of the element in the sample. The detector chamber is kept under vacuum at liquid nitrogen temperature.

A HitachiS-3000 N integrated with EDS in UTA’s Material Science Department (shown in Figure 3.3) was used throughout the project for image capturing. A small amount (less than 100 mg) of sample is loaded into the specimen chamber. Secondary electron images with high vacuum, 25 kV magnification and working distance 15 to 25 mm were used to capture high resolution images in sub-micron and nanometer range.

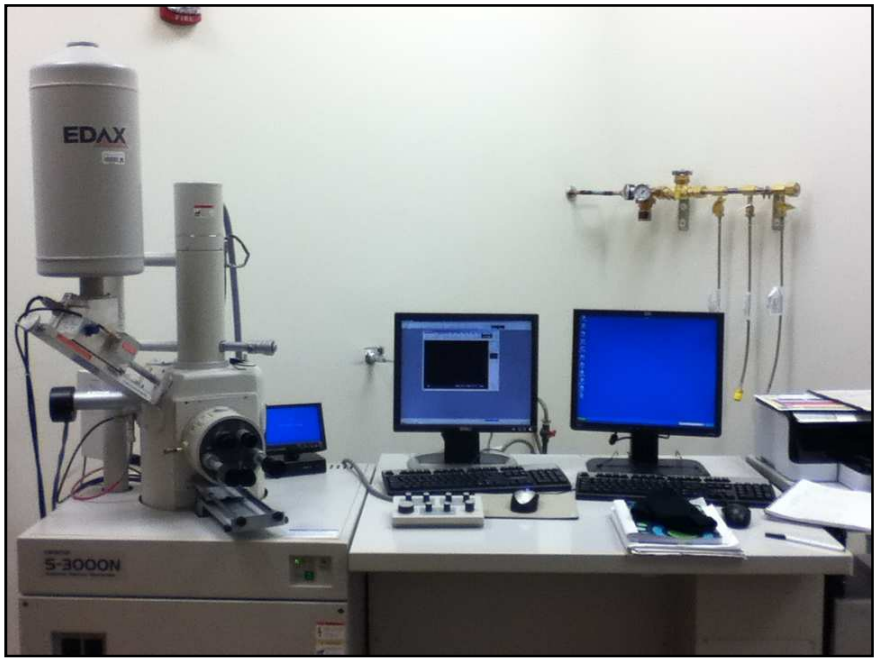

Figure 3.3: HitachiS-3000 N integrated with EDS

SEM-EDS together give a better understanding about phase identification, micro chemical analysis, failure analysis and defect characterization. Specific areas of interest in the sample were selected in the SEM image capturing screen and EDS was activated for the analysis. SUTW- Sapphire detector type was used in this instrument. EDS with same 25 KV magnification, zero tilt, detention time of 20 to 40% was used to identify the chemical compounds in the surface. The distribution of cerium was also identified by capturing images in the map.

3.2.2 CHN

CHN analysis is the most common quantitative and qualitative elemental analysis in analytical chemistry. It is a combustion analysis which provides abundant amount of oxygen during the analysis and gives complete combustion. The products of combustion such as carbon dioxide (CO_2), water (H_2O) and nitric oxide (NO) were measured carefully to determine C, H and N composition, respectively.

The CHN analysis was done by using Perkin Elmer 2400 Series II CHNO/S analyzer located in UTA Chemistry Department, as shown in Figure 3.4. Results were obtained for C%, H%, N% of each compound tested.

Figure 3.4: Perkin Elmer 2400 Series II CHNO/S analyzer

In this research the CHN analysis is considered as a quick check for carbon loss in the sample during impregnation. Detailed measurements for oxygen and other elements were obtained from EDS analysis.

3.2.3 XRD

X-ray Diffraction (XRD) analyses help to find the physio-chemical characteristics and crystallographic structure of the material, including chemical characterization, amount of crystallinity in the material, residual stress, and texture analysis. X ray beams interact with sample loaded in the goniometer during the analysis. Part of the beam is absorbed, refracted, scattered and diffracted by the plane of atoms in the sample. The diffracted beam is detected to determine the crystallography of the sample. Each mineral diffracts differently depending upon

the atoms in the crystal lattice. The data acquisition software DIFFRACplus was used to collect data. XRD was performed on the sample to measure the distribution of the cerium. A Bruker D8 Discover Diffractometer with Cu K alpha source and scintillation detector located in UTA Chemistry Department was used for XRD analysis, as shown in Figure 3.5. Experiments were run with 0.01 step sizes, dwell time of 1 sec and 2□ from 20°to 80°.

Figure 3.5: Bruker D8 Discover Diffractometer

3.2.4 Raman Spectroscopy

Raman spectroscopy analysis was used to find the cerium oxide present in the prepared catalyst. It works by having a monochromatic light source at a specific wavelength which hits the sample through focused optics. The scattered light from the sample is then passed through a filter to eliminate the unwanted light and then passes through detector for determining the sample finger print. The detected signals were collected in lab spec application software.

Samples were run by the Yvonne Jobin Lab using a Horiba Ram Aramis Spectrometer with 633 nm and 473 nm laser located in UTA's Chemistry Department, as shown in Figure 3.6.

The data were obtained in the computer using Lab view software, intensity Vs wave number. Samples were run from 200 /cm to 600 /cm wavenumber.

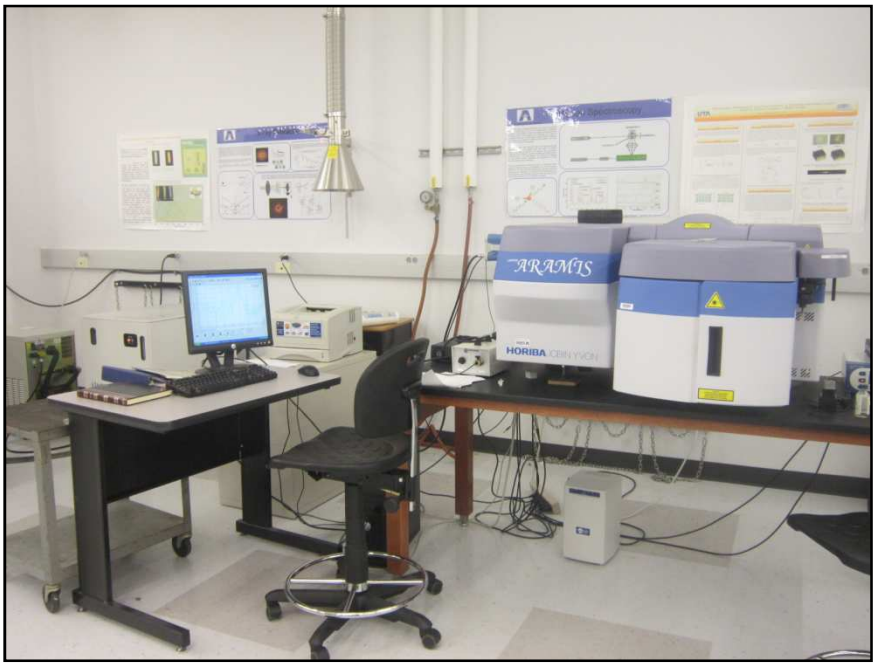

Figure 3.6: Horiba Ram Aramis Spectrometer

3.2.5 XPS

XPS analysis was used in this research to find out the ionic form of cerium (Ce3+ or/ and Ce4+) in the sample. It is a quantitative chemical analysis. A monochromatic beam of photons pass through the sample under vacuum conditions; the sample then emits excited electrons. The excited electrons are captured by electron spectrometer and compared with the energy of x ray for determination. The peaks were obtained in the computer using ----software, intensity Vs binding energy. The intensity and strength of the peaks are proportional to the chemical elements and valance state of the chemical. Vision processing version 2 software is used for data acquisition.

XPS was done by using a Kratos Axis Ultra DLD Spectrometer with Al K alpha source located in UTA's Chemistry Department, as shown in Figure 3.7. Survey scans were run with a step size of 1, dwell time of 0.01, and pass energy of 160 eV. High resolution scans were run

with 0.01 step sizes, 0.01 dwell times, and pass energy of 10 eV. A neutralizer was used when necessary to offset sample charging.

Figure 3.7: Kratos Axis Ultra DLD Spectrometer

3.2.6 TGA/DSC

Thermogravimetric analysis and Differential Scanning Calorimetry are types of durability tests. TGA determines the changes in weight according to a temperature program in a controlled atmosphere. DSC measures changes in enthalpy due to change in physical and chemical properties of the sample as a function of temperature. It gives the amount of heat needed to increase the temperature of the sample. These tests determine the maximum temperature a catalyst can withstand without losing its weight.

An SDT Q600 V20.9 Build 20 instrument located in UTA's Chemistry Department, as shown in Figure 3.8, was used for the analysis. The temperature was raised up to 1000°C at a ramp of 5°C/min in the presence of nitrogen at a flow rate of 100 ml/min. Results were displayed in TA universal analysis 2000 software.

Figure 3.8: SDT Q600 V20.9 Build 20 instrument

3.2.7 BET

BET analysis works by using adsorption techniques. The amount of gas is adsorbed is directly proportional to the surface area available in the sample. Nitrogen is usually used for this analysis due to its high purity and strong interaction with solids. The BET isotherm plots the amounts of gas adsorbed versus relative pressure. In this research, BET analysis was performed for MWCNTs to identify surface area modification before and after cerium doping. It also identified total pore volume, microporosity volume and average pore diameter of samples before and after the cerium doping process.

The BET analysis was conducted using a N_2 adsorption/desorption volumetric gas adsorption instrument (Micromeritics, ASAP 2000 Series, Germany) located in Universiti Tunku Abdul Rahman, Malaysia. The samples were sent to Malaysia for this analysis. Prior to analysis, each sample (about 0.1 g) was placed in an analysis tube and degassed at 300℃ for at least 5h to remove any adsorbed species from the surface. After degassing, the sample was transferred to the analysis station, where it was cooled in liquid N_2 environment at temperature

77K. The adsorption-desorption processes were done automatically by software linked to the analyzer.

3.2.8 Density

The inverse of the gas residence time in the catalyst chamber is named as gas hourly space velocity. It is the volumetric gas flow rate divided by the catalyst volume. The catalyst volume can be determined by knowing the bulk density of the catalyst. The bulk density of the activated carbons and catalysts were measured approximately in the lab. Each sample was filled up to 1ml in the small vial after tared and weighed in digital weighing machine with 4 significant digits. Three replicates were made and averaged for the density values.

3.3 Catalyst Activity Testing

3.3.1 Experimental Design

Typical diesel engine exhaust temperature ranges from 150°to 450℃ (Nejar and Illan-Gomez, 2007). Considering the exhaust temperature variation, seven different temperature levels (100°, 150°, 200°, 250°, 300°, 350°, and 400 ℃) were selected for the experiment. Ce-GAC and Ce-AFC were tested only up to 300°and 350° C, respectively, due to their limitations in temperature found in the TGA analysis.

Typical concentration of NOx in diesel exhaust ranges from 50-700 ppm (Majewski, 2007). Two different concentrations were tested in this research: a low concentration of 150 ppm and high concentration of 500 ppm.

The experimental design can be summarized as follows: two different concentrations (150 ppm NO, 150 ppm NH_3, 5.6% oxygen and 500 ppm NO, 500 ppm NH_3, 5.6% oxygen) were tested at the seven temperatures (100°, 150°, 200°, 250°, 300°, 350°, and 400℃), for the 3 types of catalyst (Ce-GAC, Ce-AFC, and Ce-MWCNTs), both treated and untreated .

The stoichiometric ratio of ammonia to nitrogen ratio is 1. Higher NH_3/NOx ratio results in increased ammonia emission known as ammonia slip. In another hand, lower NH_3/NOx ratio

may result in lower NOx reduction efficiency. The SCR process is always carried out in the presence of air.

3.3.2 Experimental Set-Up

The schematic diagram of the experimental setup for catalyst evaluation is shown in Figure 3.9. Figure 3.10 shows the experimental set-up in lab.

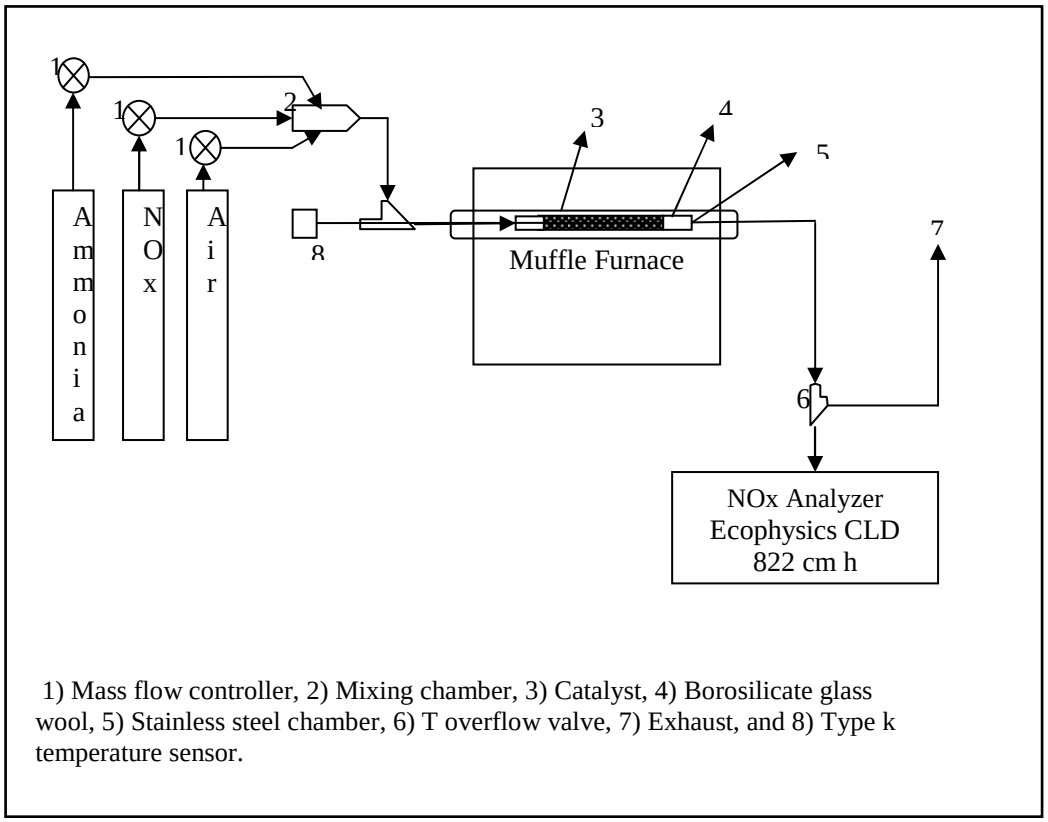

1) Mass flow controller, 2) Mixing chamber, 3) Catalyst, 4) Borosilicate glass wool, 5) Stainless steel chamber, 6) T overflow valve, 7) Exhaust, and 8) Type k temperature sensor.

Figure 3.9: Schematic diagram of catalyst activity test experimental set-up

A NOx cylinder containing 300 ppm of NO, balance nitrogen, and zero air with 99.9% ultra high purity were bought from Matheson Trigas Corporation. Cylinders of 1000 ppm of NO, balance nitrogen, and ammonia 2000 ppm were purchased from Metroplex Welding Company. All the gas cylinders were connected to mass flow controllers (#1 in Fig. 3.3) purchased from Cole Parmer. The mass flow controllers were calibrated using bubble calibrators before the experiments. The total gas flowrate was kept at 200 ml/min. All the flow lines were made using

Teflon tubing with OD ¼ inch and connections using swagelok fittings. Gases were mixed in the mixing chamber (#2 in Fig. 3.3) before entering the line in the tube furnace.

Figure 3.10: Experimental set-up in lab

NOx reduction reactions were performed in a tube furnace to achieve the appropriate temperature (Lindberg, Type TF55035A). The 5/8 inch OD stainless tube (#5) was used for loading the catalyst (#3). The stainless steel chamber was placed in the center of the tube furnace. A type k thermocouple (#8) was placed in the center of the stainless steel chamber contacting the surface of the catalyst to measure the chamber temperature.

1/8 inch OD stainless steel tube fittings were used to feed the gas from the tube furnace to the analyzer sample port. The analyzer sample line flow rate was 50 ml/min. An over flow tube more than 6 ft long was attached before the sample port to let the excess air pass through (#6 and 7). Sample lines were wrapped with heating tube (100°C) and covered with glass wool and aluminum foil as a top layer to eliminate condensation and thus provide good ammonia readings in the analyzer.

NO and ammonia concentrations were measured using a CLD 822 cm h Ecophysics Analyzer. This analyzer measured NO using chemiluminescence technology. NO concentration was measured in NOx NO NO_2 mode in the analyzer and NH_3 was measured in NO_x NOxamine NH_3 mode.

3.3.3 Experimental Procedure

For each experiment, 200 mg of catalyst was loaded between the plugs of deactivated borosilicate glass wool. The furnace was held at each experimental temperature until steady state NO concentration was achieved (change in reduction efficiency of + or -2% in 20 minutes). Inlet concentrations were measured once before each experiment and outlet concentrations were measured continuously using the CLD 822 cm h Ecophysics Analyzer in 10 second increments. NO measurement was made first; once NO had reached steady state, NH_3 measurements were done by changing the mode in the analyzer. The data was obtained through Excel using data acquisition software compatible with the analyzer.

Two replicates were conducted for all three types of catalyst at 200℃. The data were analyzed using ANOVA for repeatability. In addition, a 12 hour activity run for Ce-GAC was made to check the steady state reduction efficiency and stability of the catalyst.

CHAPTER 4

RESULTS AND DISCUSSION

4.1 Material Analysis

4.1.1 CHN Analysis

Results obtained from the characterization analyses are presented in this section. Table 4.1 and Figure 4.1 show the CHN analyses for raw samples and cerium doped samples. Each sample was tested twice and results averaged to obtain the percentage of C, H and N shown in Table 4.1. The results for all runs are given in Appendix B. All the treated samples lost carbon in the catalyst preparation process.

Table 4.1: CHN analysis results

Types of sample	**Elemental analysis (%)**		
	C	**H**	**N**
GAC	83.0	0.31	1.47
Ce-GAC	80.1	0.855	1.33
ACF	71.45	2.14	0
Ce-ACF	56.55	1.47	0
MWCNTs	94.38	1.07	0
Ce- MWCNTs	85.87	0.67	0

The carbon loss percentages for CeGAC, CeACF, and CeMWCNTs were 3.49%, 20.8%, and 8.92%, respectively. Granular activated carbon lost less carbon than other types of activated carbon. ACF as a netted structure falls apart at the edges while mixing it; thus, the loss of carbon is high for the activated fiber cloth compared to other forms of carbon. In MWCNTs the loss of carbon may indicate opening of ends of the treated carbon and thus increased surface area. Surface area was determined via BET analysis, as will be discussed later. The hydrogen content in the treated sample was increased in CeGAC but decreased in both CeACF and CeMWCNTs. There was no nitrogen present in the ACF and MWCNTs before

and after treatment. The nitrogen content of GAC did not show much difference after doping. The macro pores and inside pores in CeGAC provide surfaces for water molecules adherence during impregnation, which may explain the increase in the hydrogen content of the sample.

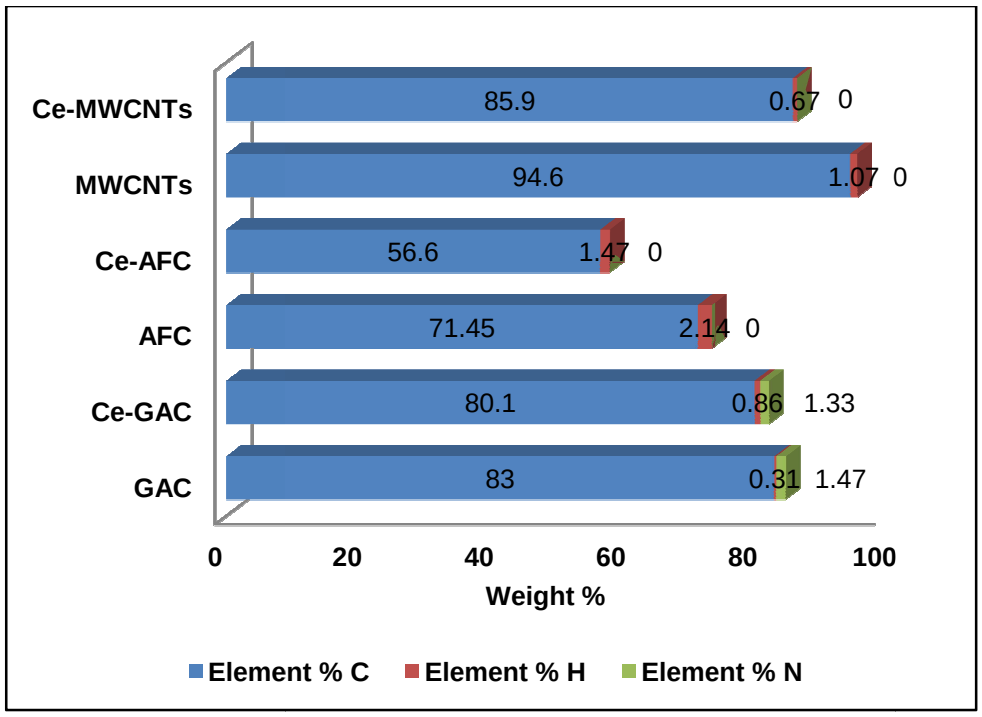

Figure 4.1: CHN analysis results

4.1.2 BET Analysis

The surface area of the catalyst plays a significant role in providing active sites for the NOx and NH_3 to adsorb and react. Table 4.2 summarizes the specific surface area and pore volumes, and Appendix B provides the detailed results. Figure 4.2 shows the surface area and pore volume difference for all types of carbon before and after impregnation. The specific surface area of the CeMWCNTs increased by 50 m^2/g compared to the MWCNTs. Nitrate present in the cerium nitrate hexahydrate precursor forms nitric acid when mixed with water, which might have opened more ends in multiwall carbon nanotubes. However, surface area may not be the determimning factor in low temperature SCR reduction efficieny (Li et al., 2007).

Table 4.2: BET analysis results

Types of Carbon	Specific surface area (m^2/g)	Pore volume (cm^3/g)
MWCNTs	170	0.365
CeMWCNTs	220	0.410

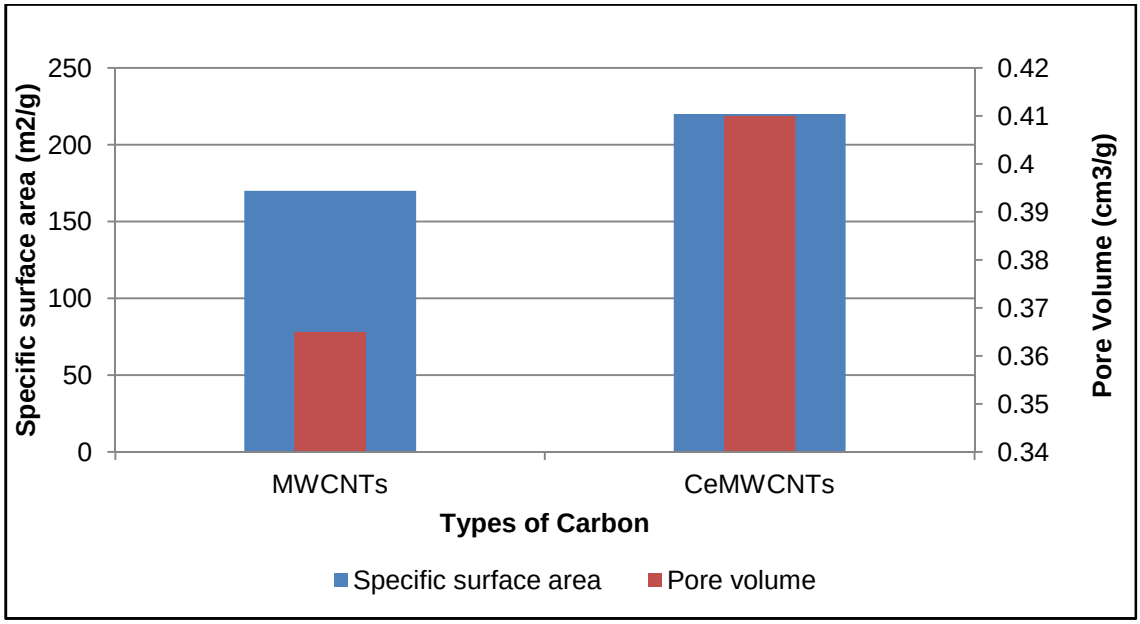

Figure 4.2: BET analysis results

4.1.3 SEM Analysis

Figures 4.3,4.4 and 4.5 show the SEM images of GAC, ACF and MWCNTs. The left sides of the images show raw samples and the right sides represent samples after cerium doping process. All the images were captured using secondary electron high resolution image capturing with the same working distance magnification and zoom level before and after the doping process.

For GAC, the surface of Figure 4.3 b) looks brighter and has more white spots than 4.3 a), which indicates the cerium adherence on the surface of the carbon. In 4.3 c), before doping process the surface is flat with no porous structure shown, but in 4.3 d), after doping the surface

is more porous due to loss of carbon, which was also indicated in CHN analysis report. In 4.3 e) and 4.3 f), it is significant that even after doping, the pores were clear from blockage.

The ACF surface in figure 4.4 right side looks brighter and has more brighter white spots than left side which indicates the cerium adherence on the surface of the activated carbon fiber. In Figure 4.4 c), before the doping process the surface is flat with no deposition shown, but in 4.4 d) after doping, cerium is deposited evenly on the surface wall of the fiber. Figures 4.4 e) and 4.4 f) significantly showed the cerium adherence even at the ends of the fiber and excess loading of metal in the surface. The thin film on the the surface of ACF represents the monolayer deposition of the chemically bonded species with carbon layer (Hunag et al., 2008).

The MWCNTs surface morphology shown in 4.5 b) looks brighter and has more white spots than 4.5 a), which indicates the cerium adherence in the MWNTs. The nanaotubes are more clearly shown in Figures 4.5 d) and f) compared to 4.5 c) and e), which indicates open ends and also cerium doping inside the nanotubes. More open ends promotoes increased surface area which may increases removal efficiency due to more active sites. The BET surface area test provided evidence of open ends in the sample, since the surface area increased by by 50 m^2/g after the doping process.

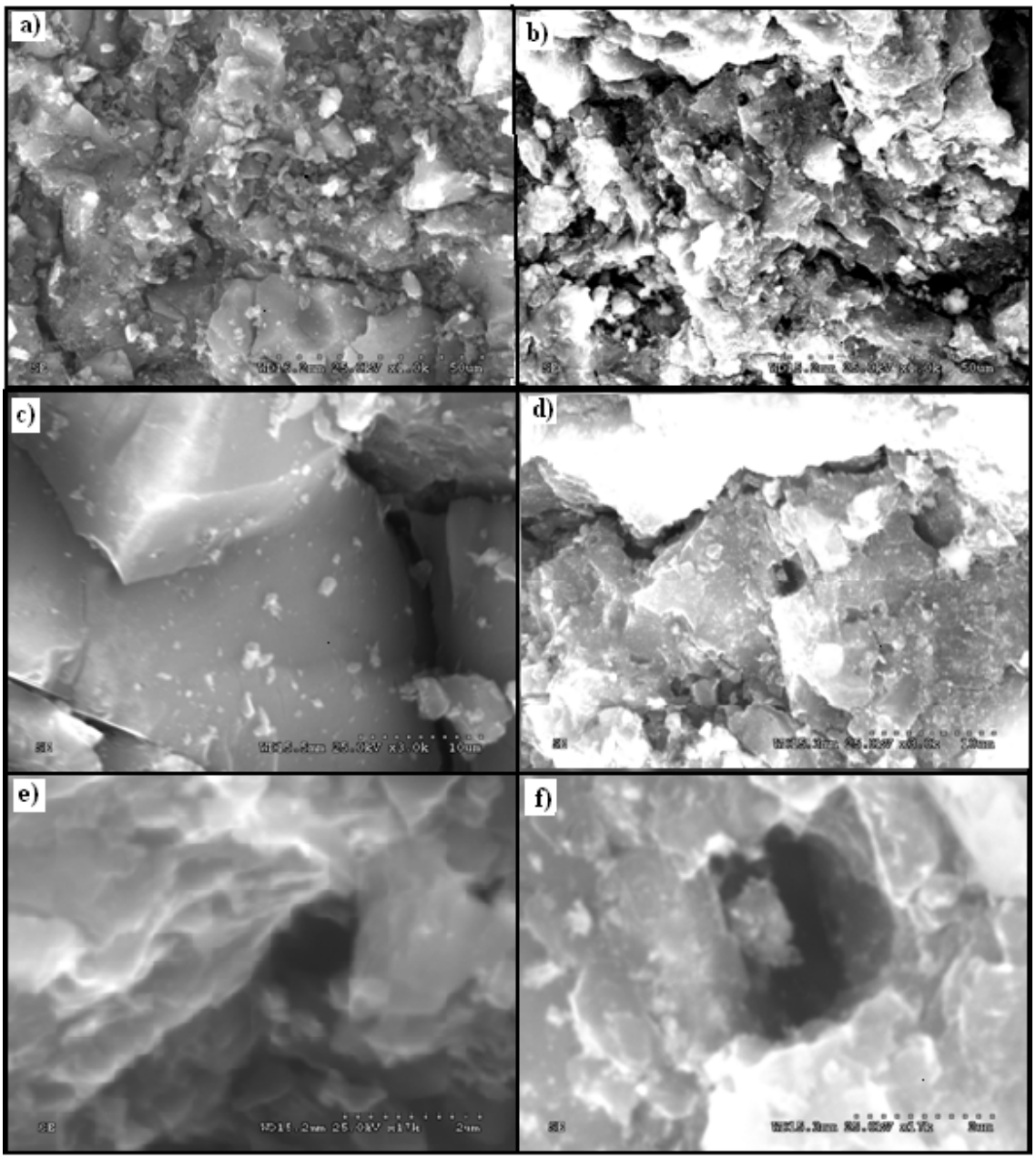

Figure 4.3: SEM imaging of GAC and CeGAC a) GAC 50 µm, b) CeGAC 50 µm, c) GAC 10 µm, d) CeGAC 10 µm, e) GAC 2 µm, and f) CeGAC 2 µm.

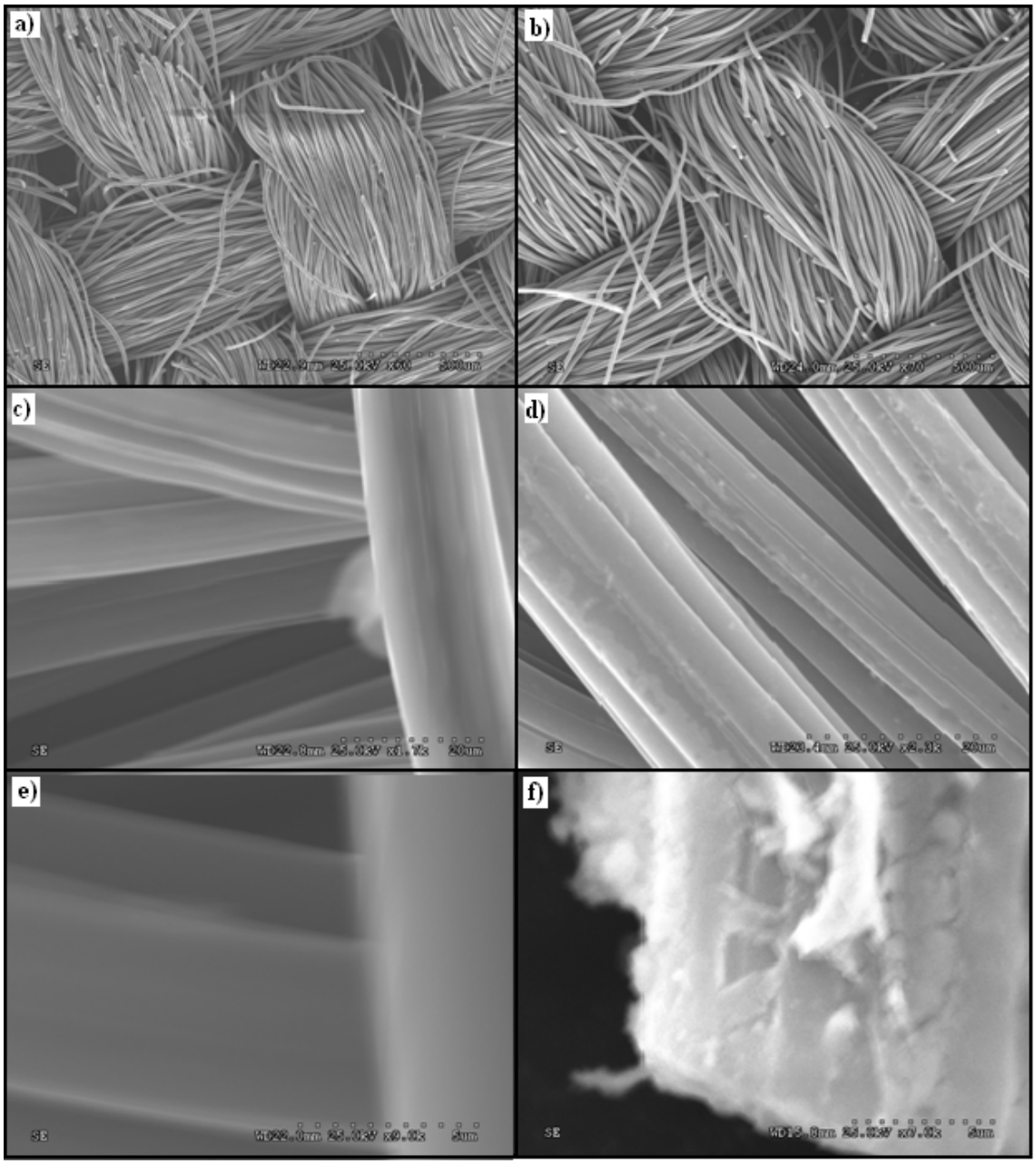

Figure 4.4 : SEM image of ACF and CeACF. a) ACF 500 µm, b) CeACF 500 µm, c) ACF 20 µm, d) CeACF 20 µm, e) ACF 5 µm, and f) CeACF 5 µm.

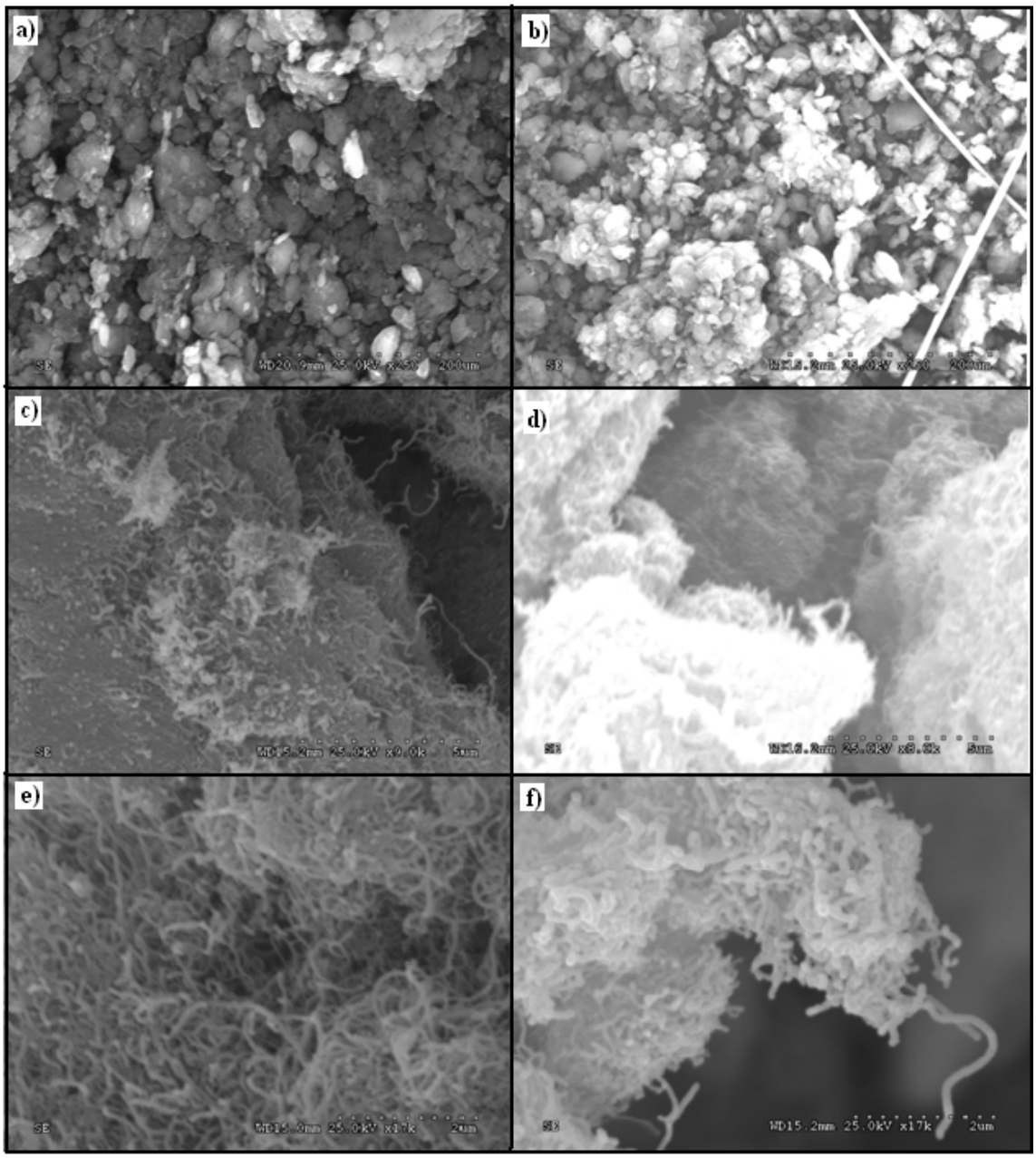

Figure 4.5: a) MWCNTs 200 µm, b) CeMWCNTs 200 µm, c) MWCNTs 5 µm, d) CeMWCNTs 5 µm, e) MWCNTs 2 µm, and f) CeMWCNTs 2 µm.

4.1.4 EDS Analysis

The cerium distribution mapping for CeGAC, CeACF and CeMWCNTs is shown in Figure 4.7 on the right, along with SEM images of the carbons on the left. The figures 4.7 b,d, and f show even distribution of cerium for CeGAC, CeACF, and CeMWCNTs, respectively. CeGAC (4.7 a and b) shows inside applicability of the process by showing cerium distribution even inside the pores. From Table 4.3 and figure 4.6, the percentage of cerium distribution was identified as 84.16%, 12.19% and 2.73 % for CeGAC, CeACF and CeMWCNTs, respectively. The cerium distribution percentage in the surface is in the order of CeGAC > CeACF > CeMWCNTs. The pore size and pore volume would be the deciding factor in distribution. Since GAC has more macro pores, the distribution of cerium is higher than the other types of carbon.

Table 4.3: EDS analysis results

Element	***Weight %***					
	GAC	***CeGAC***	***ACF***	***CeACF***	***MWCNTs***	***CeMWCNTs***
C	96.03	13.57	81.86	69.62	93.93	89.1
O	0	1.4	4.66	10.25	4.45	6.8
Si	1.59	0.87	0	0	0	0
Ce	0	84.16	0	12.19	0	2.73
Al	1.38	0.87	2.95	3.22	0.28	0.22
Zn	0	0	10.33	4.33	0	0
S	1	0	0	3.22	0	0
Fe	0	0	0	0	1.2	0.58
Cu	0	0	0	0	0.15	0
F	0	0	0	0	0	0.57

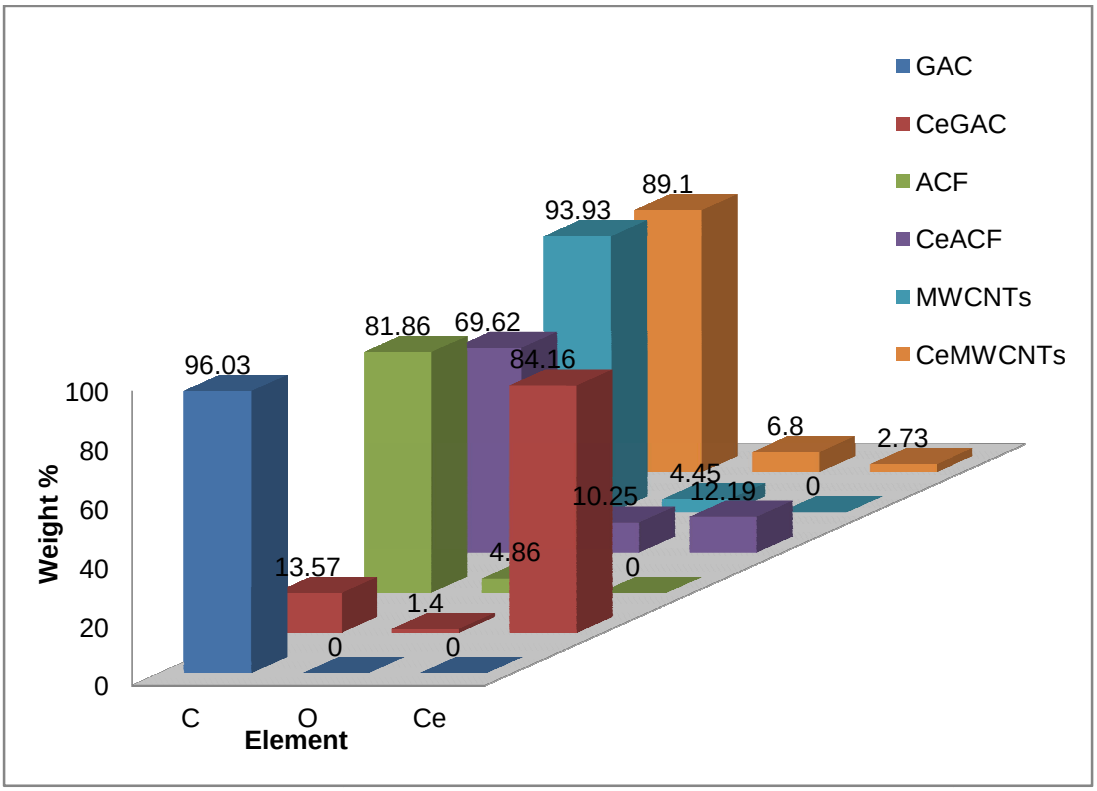

Figure 4.6 : EDS analysis results

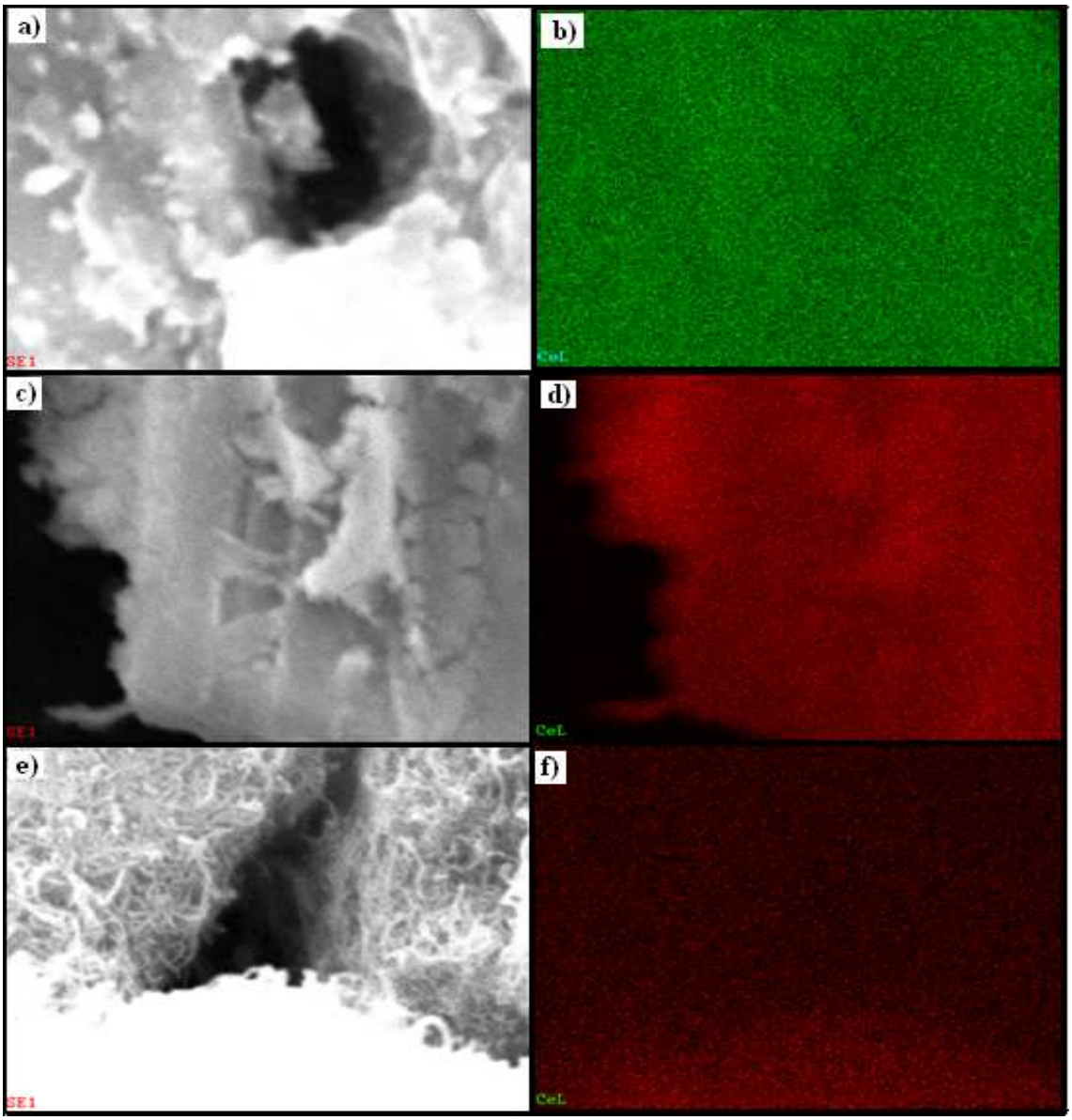

Figure 4.7: EDS mapping of cerium distribution a) Ce-GAC, b) Ce-GAC EDS map, c) Ce-ACF, d) Ce-ACF EDS map, e) Ce-MWCNTs, and f) Ce-MWCNTs EDS map.

4.1.4 TGA

Thermogravimetric analysis is an efficient and cost effective way of analyzing the range of thermal events associated with combustion (Warne, 1991). Cerium (III) nitrate hexahydrate 99.5% ($Ce(NO_3)_3 \cdot 6H_2O$) was used as a precursor for cerium doping in this study. The calcination temperature of 500°C used during the impregnation procedure was chosen by looking at the TGA analysis report for cerium (III) nitrate hexahydrate using nitrogen, as shown in Figure 4.8. It is shown that cerium (III) nitrate hexahydrate completely decomposes into cerium (III) oxide (Ce_2O_3) and cerium(IV)oxide (CeO_2) in the inert atmosphere. Cerium nitrate hexahydrate, with a molecular weight of 434.2, decomposes into cerium nitrate by releasing crystal water (freely available in the surface) and coordinating water (bonded with metal). Cerium nitrate again decomposes by releasing nitric oxides and forms cerium oxides. The remaining percentage of weight loss stays about 40%, which is an indication of cerium oxides left in the chamber during TGA analysis.

The reaction is shown below.

$Ce(NO_3)_3.6H_2O$	$\xrightarrow{-6H_2O}$	$Ce(NO_3)_3$	$\xrightarrow{-NOx}$	CeO_2	or / and	CeO_3
MW 434.32		324.32		172.16		188.16
(100%)		(74.36%)		(39.6%)		(43.3%)

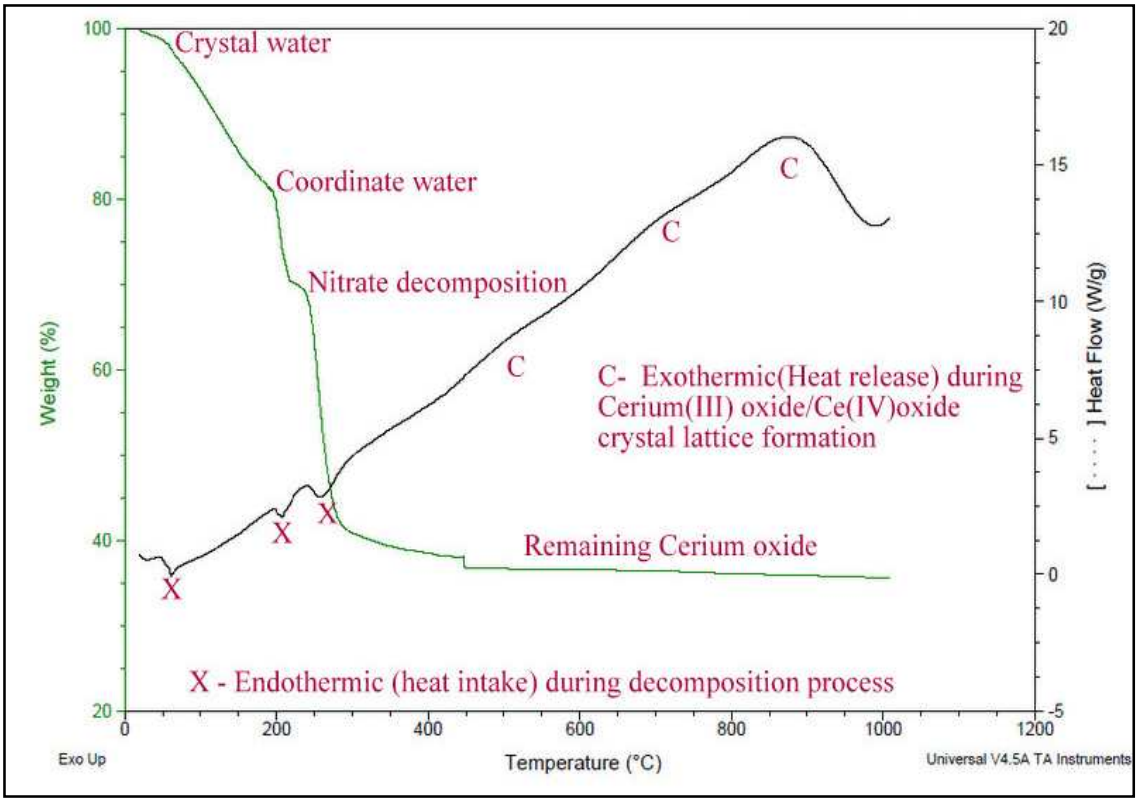

Figure 4.8: Cerium nitrate hexahydrate TGA result

TGA profiles using air for all types of raw carbon and catalyst are shown in Figure 4.9. The order of raw sample thermal stability is GAC > MWCNTs > ACF. After doping with cerium oxide, the thermal stability is decreased and the order of stability is CeMWCNTs > CeACF > CeGAC. CeGAC remains stable until 310º C, CeACF until 321º C and the CeMWCNTs until 412ºC. Santillan-Jimenez et al. (2011) stated that MWCNT catalysts for SCR are stable up to 400 º C. There is a slight weight gain in raw MWCNTs due to the chemisorption of oxygen onto the surface (Benfell et al., 1996). The slight drop in weight % in both ACF and Ce-ACF is due to water loss.The ACF are very more active in absorbing vapor content than other types of activated carbon. ACF is a very effective adsobent for high vapor concentrations; this is one of its major applications.

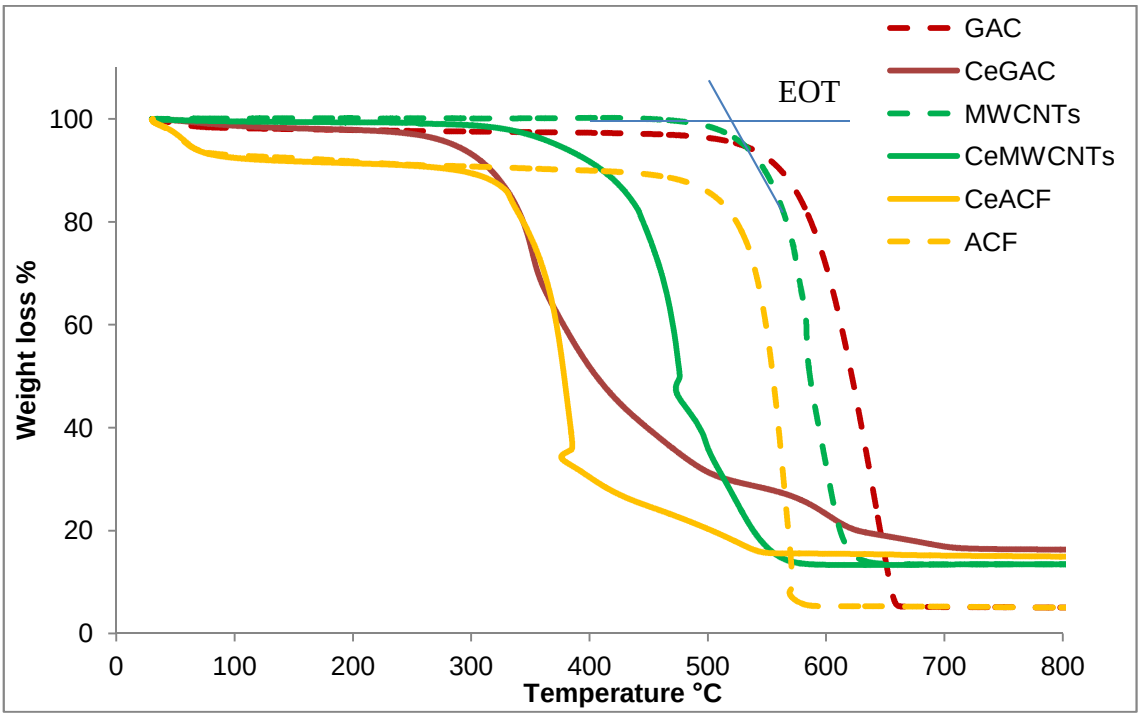

Figure 4.9 : TGA curves for AC before and after cerium doping

Nejar et al. (2007) explained the reactivity of carbon by taking TGA profiles. They calculated the Extrapolated Onset Temperature (EOT), the temperature at which 50% of carbon loss occurs (T50%), and oxygen and hydrogen content to explain the reactivity. Based on this, the values were calculated in this study as shown in Table 4.4 and figure 4.10 to understand the thermal stability of the catalyst.

Calculated EOT and T50% values from TGA results are compared with hydrogen and oxygen content from the EDS report to briefly explain the changes in temperature profile.

Table 4.4: EOT and T50% vs. Hydrogen and Oxygen

Types	EOT	T50%	H	O
GAC	570	622	0.31	0
Ce-GAC	**310**	406	0.86	1.4
ACF	525	555	2.14	4.66
Ce-ACF	**321**	379	1.47	10.25
MWCNTs	550	586	1.07	4.45
Ce-MWCNTs	**412**	476	0.67	6.8

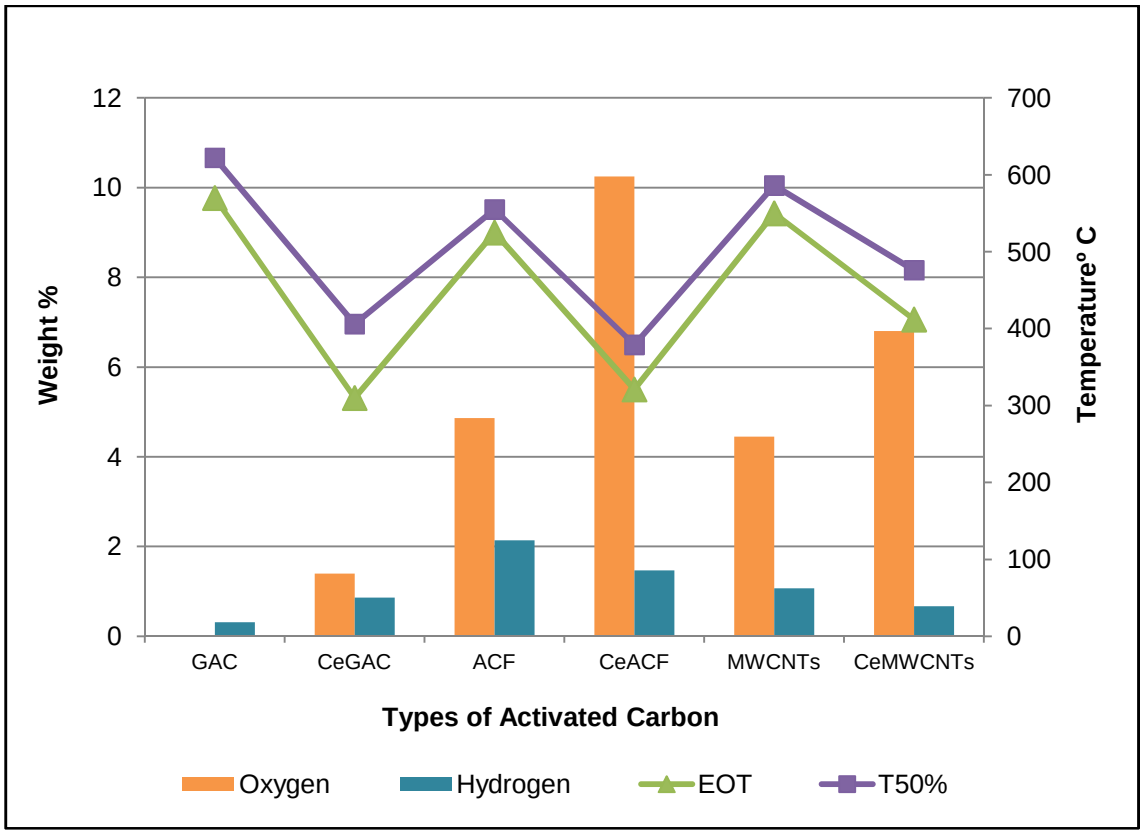

Figure 4.10 : TGA in air vs hydrogen and oxygen content for different types of carbon

As shown in Figure 4.10, the thermal stability decreases when oxygen and hydrogen content increases for all types of carbon. The oxygen and hydrogen content in the carbon is related to surface complexes, which increase the carbon reactivity ((Setiabudi et al., 2004 and Muller et al., 2005)) during combustion and thus decreases the thermal stability.

4.1.6 Raman Spectroscopy

Raman spectroscopy results are shown in Figures 4.11, 4.12 and 4.13 for GAC vs. CeGAC, ACF vs. CeACF and MWCNTs vs. CeMWCNTs, respectively. The cerium oxides (CeOx) peak is shown at 451.9, 455.5 and 453.7 wavelengths for all three catalysts, which corresponds to CeO_2 (Suzana et al., 2002 and Hamlaoui et al., 2009). The shift of the band may correspond to the valance state (Ce^{3+} or Ce^{4+}) of cerium in the cerium oxide (Siokou et al., 2006) and cerium oxide crystal size (Wang et al., 2001). The variation in peak width explains

the grain size variation (Kosacki et al., 2002). The presence of cerium oxide is determined using Raman spectroscopy but the oxidation state of the cerium ion was determined using XPS analysis in this study.

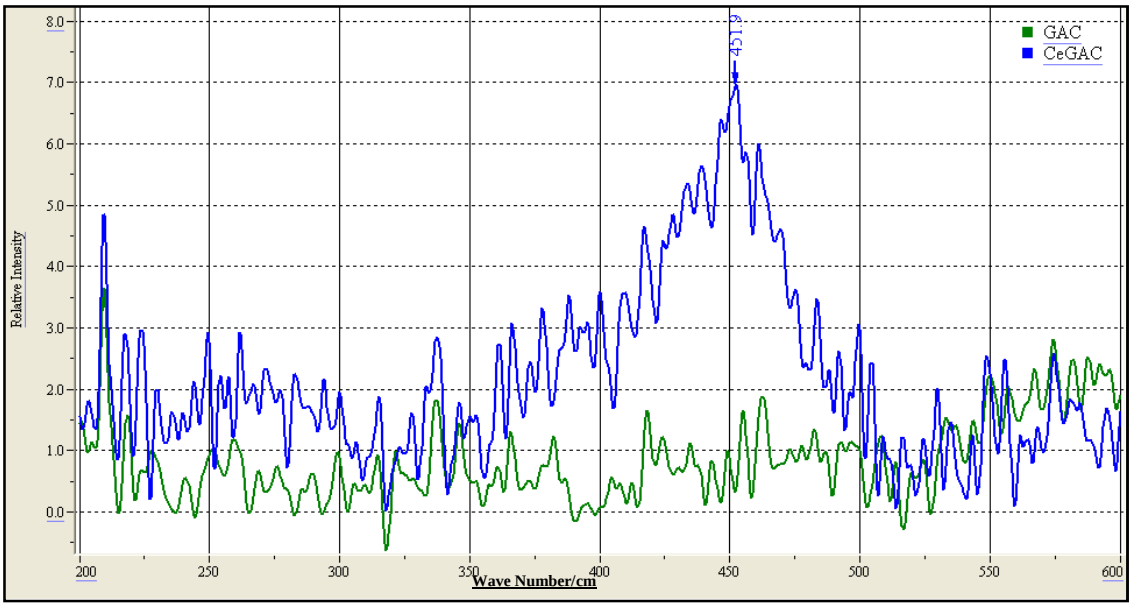

Figure 4.11: Raman spectroscopy results for GAC vs. CeGAC

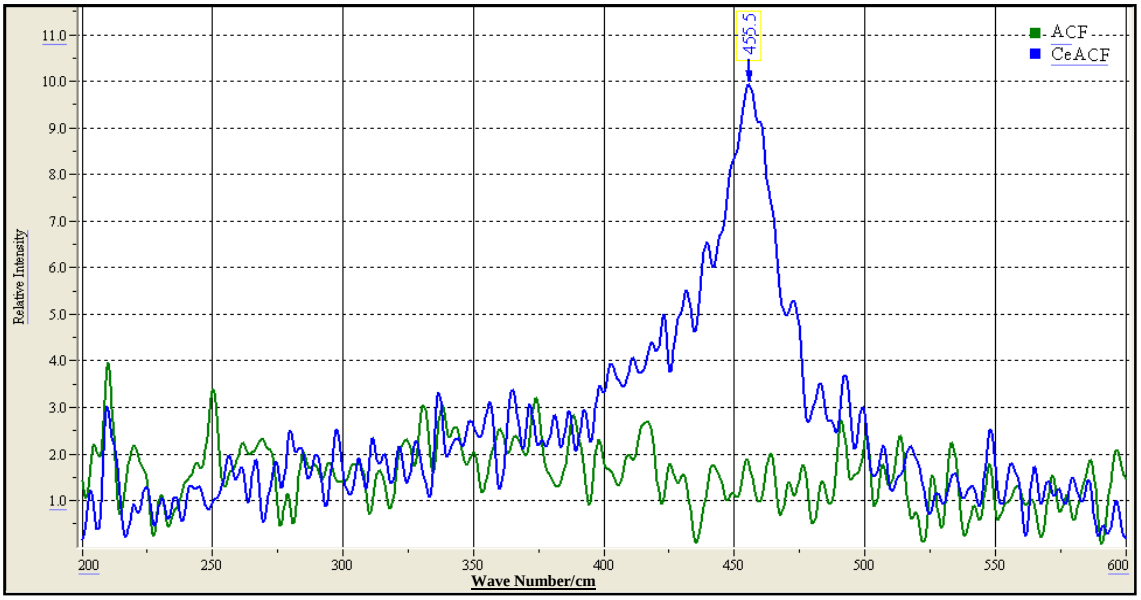

Figure 4.12: Raman spectroscopy results for ACF vs. CeACF

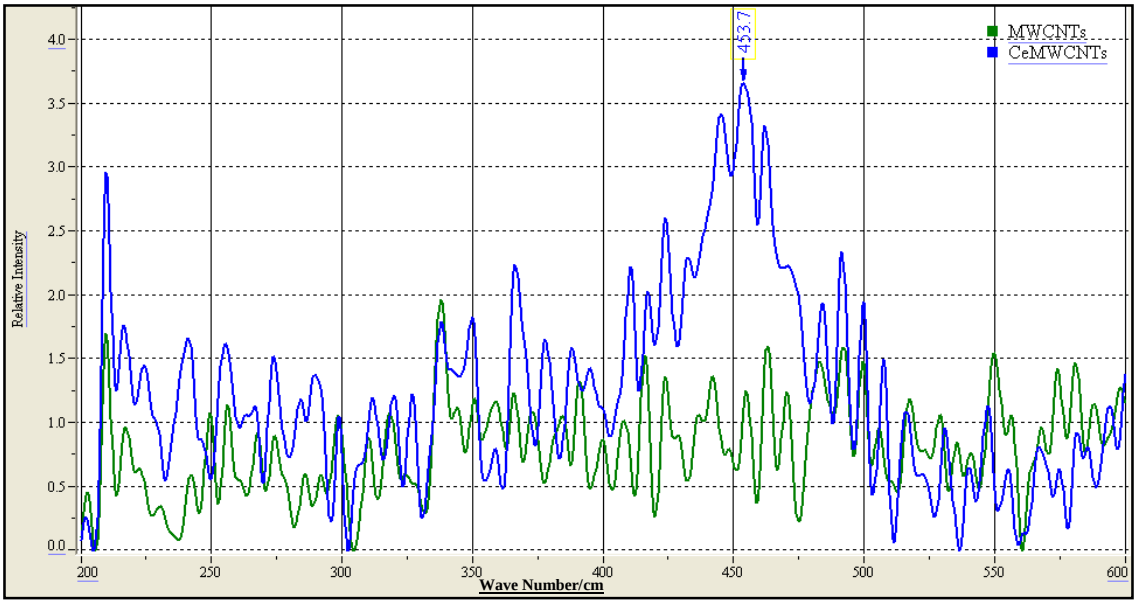

Figure 4.13: Raman spectroscopy results for MWCNTs vs. CeMWCNTs

4.1.6 XPS Analysis

The XPS results gave a precise oxidation state of cerium in the sample. However, concentrations found by XPS do not directly provide the element concentration measurement (Zhang et al., 2004). It measures the concentration at the top surface at selected spot. Figures 4.14, 4.15 and 4.16 show XPS results for GAC vs. CeGAC, ACF vs. CeACF, and MWCNTs vs. CeMWCNTs, respectively. The binding range from 875 to 915 eV is shown in these graphs and the full scale range graphs are given in Appendix B. There are 10 peaks in general for CeOx, six peaks (916.9, 907.4, 901, 888.9, 882.5, and 898.5 eV) for Ce^{4+} ion and 4 peaks (903.3, 898.7, 884.8, and 880.2 eV) for Ce^{3+} ion (Matharu et al., 2011). Table 4.5 shows the Ce^{3+} and Ce^{4+} peaks for the types of catalyst tested in this study. Ce^{4+} ion dominates in the samples; having both valance states improves the reduction efficiency by enabling Ce to change its ionic state from Ce^{3+} to Ce^{4+}. The increased presence of Ce^{4+} indicates that cerium nitrate hexahydrate precursor decomposes into CeO_2. Major amounts of cerium nitrate precursor decomposed into CeO_2 in the inert atmosphere (Gao et al., 2011).

Table 4.5 XPS results for Ce^{3+} and Ce^{4+} ion

Peaks corresponds to	Catalyst		
Ce^{4+}	**CeGAC**	**CeACF**	**CeMWCNTs**
882.5	X	X	X
888.9	Small peak	X	Small broad peak
898.5	X	X	X
901	X	X	X
907.4	X	X	X
916.9	X	X	X
Ce^{3+}			
880.2			
884.8	Small peak		
898.7	X	X	X
903.3		X	X

Note: “X” means presence of cerium in the catalyst

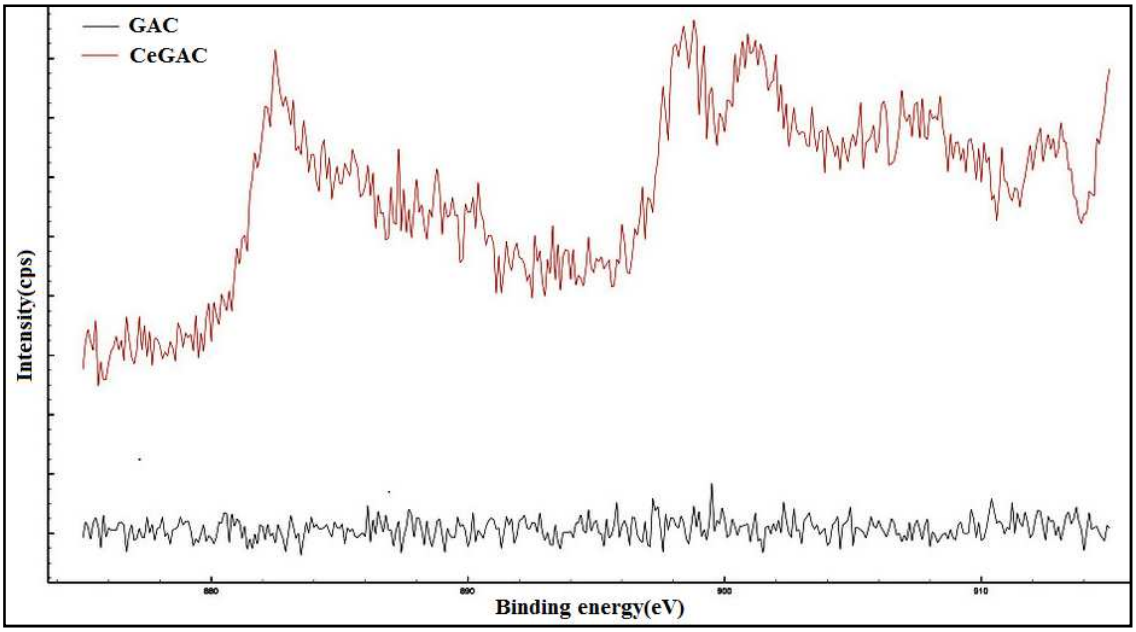

Figure 4.14: XPS results for GAC and CeGAC

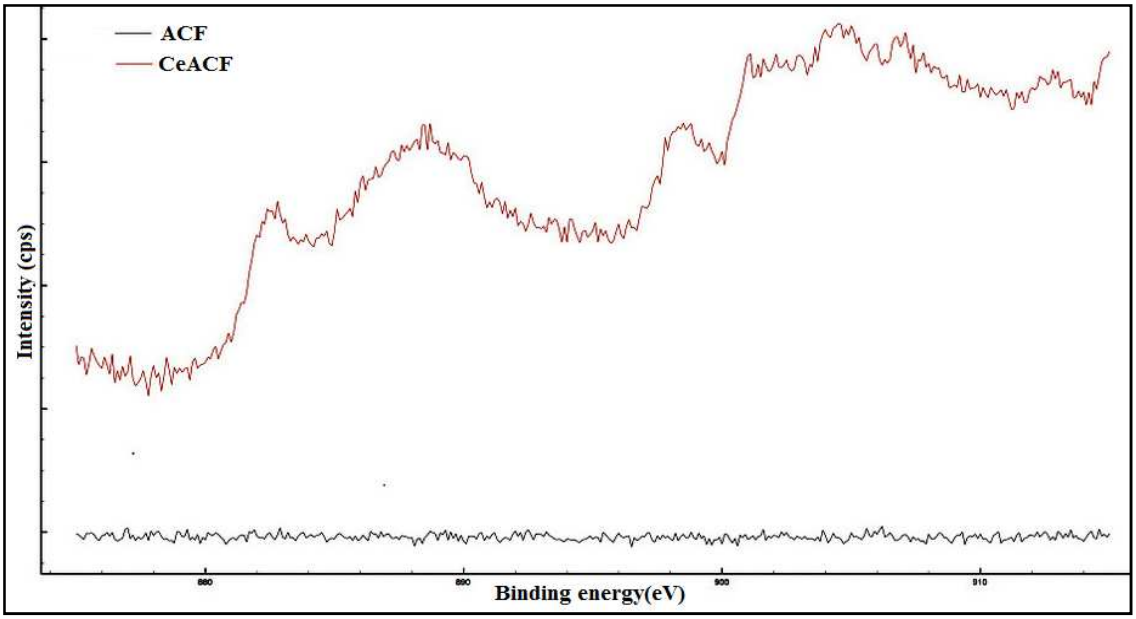

Figure 4.15: XPS results for ACF and CeACF

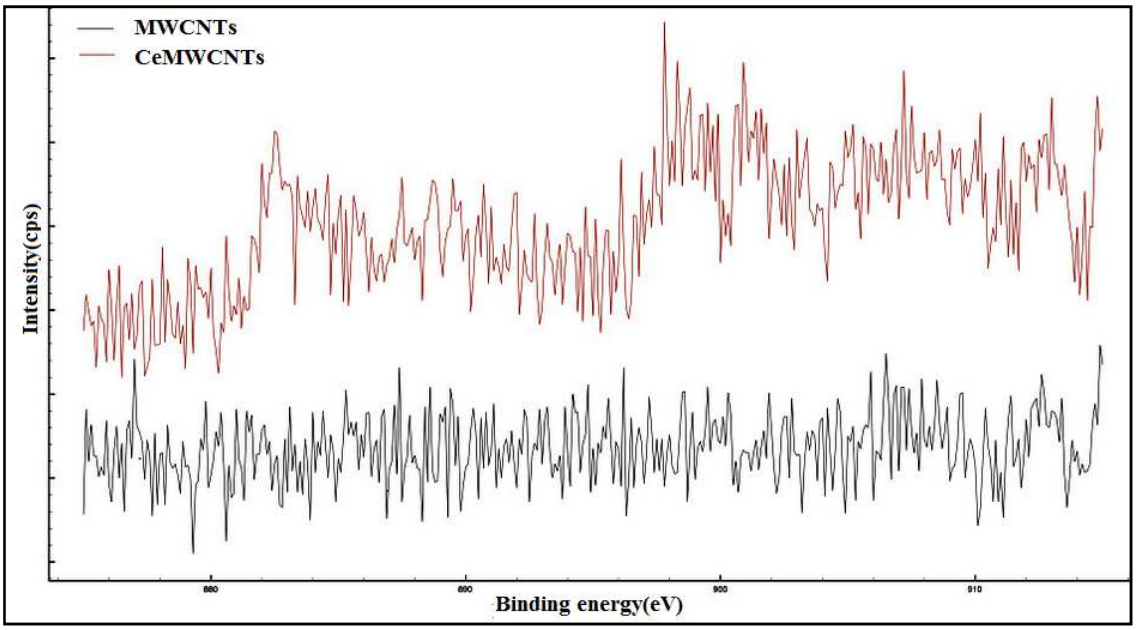

Figure 4.16: XPS results for MWCNTs and CeMWCNTs

4.1.8 XRD Analysis

The figure 4.17, 4.18, 4.19, and 4.20 show XRD results for GAC vs. CeGAC, ACF vs. CeACF, MWCNTs Vs. CeMWCNTs and catalyst comparison respectively. Peaks corresponding to CeO_2 in XRD at 2θ are 28.6°, 33.1°, 47.6° and 56.4° (Chong et al., 20 07; Gao et al., 2011). All these peaks belong to the crystal phase of cerium oxide. The cerium oxide diffraction peaks for CeACF are more intense than for the other types of catalyst. This indicates that CeMWCNTs and CeGAC have good dispersion of Ce across their surfaces, compared to CeACF. The strong diffraction peaks in the results are marked with cubic symbols, representing the face center cubic crystal structure of cerium. When the metal oxide loading exceeds the monolayer dispersion capacity, the excess metal oxides will show in the crystalline phase (Gao et al., 2011). The prominent CeACF peaks are thus caused by excess loading. This is also shown in SEM image report for CeACF, with excess loading at the edges of fiber.

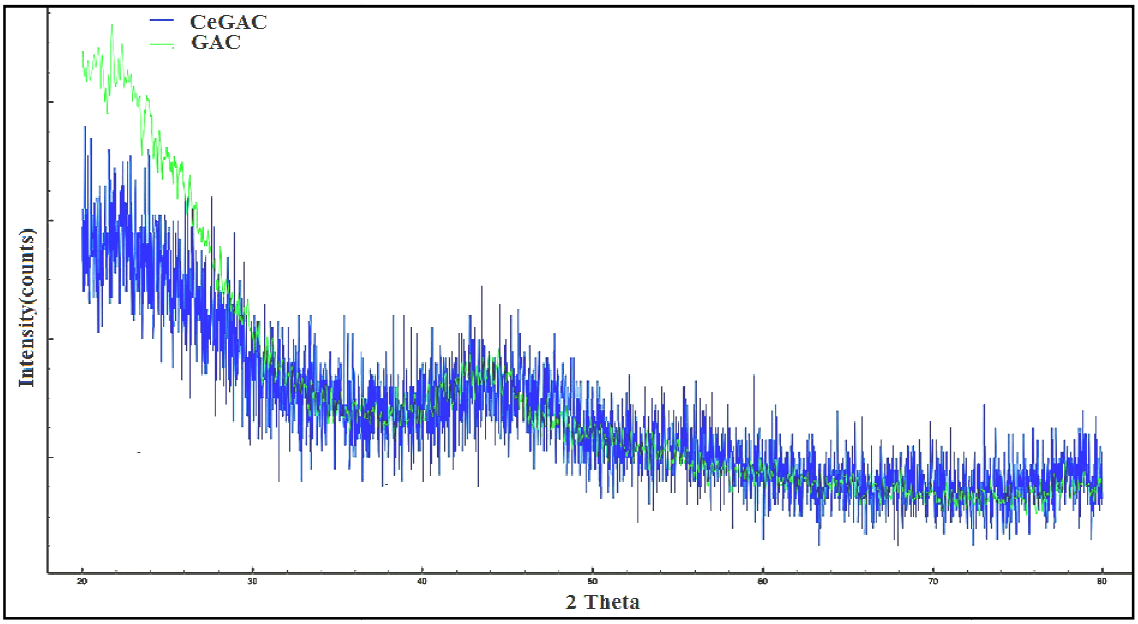

Figure 4.17: XRD results for GAC and CeGAC

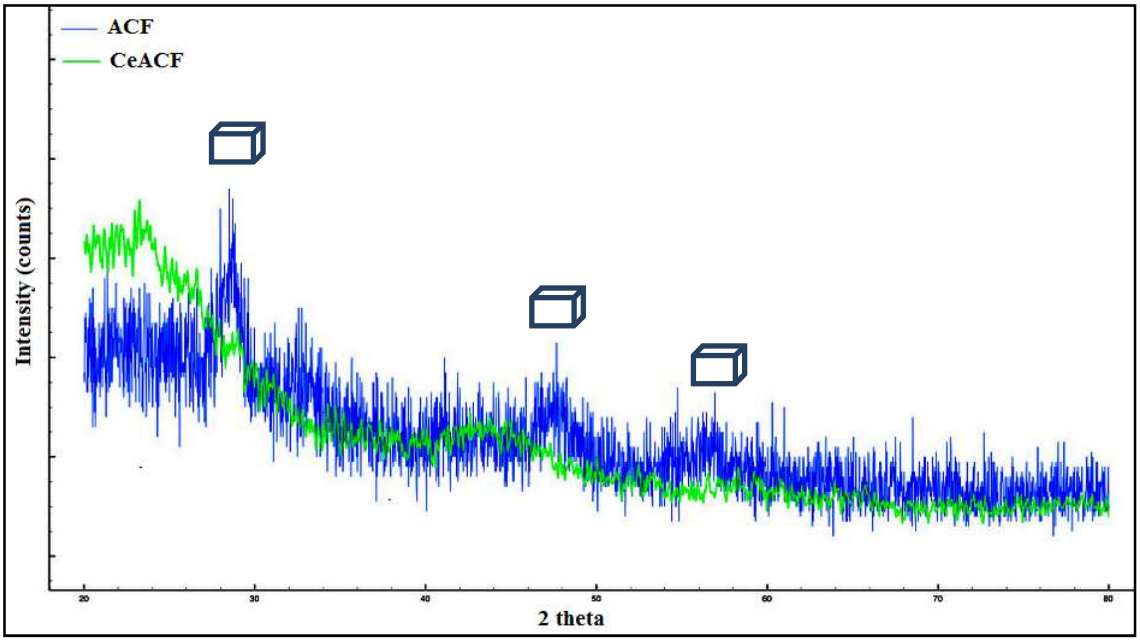

Figure 4.18: XRD results for ACF and CeACF

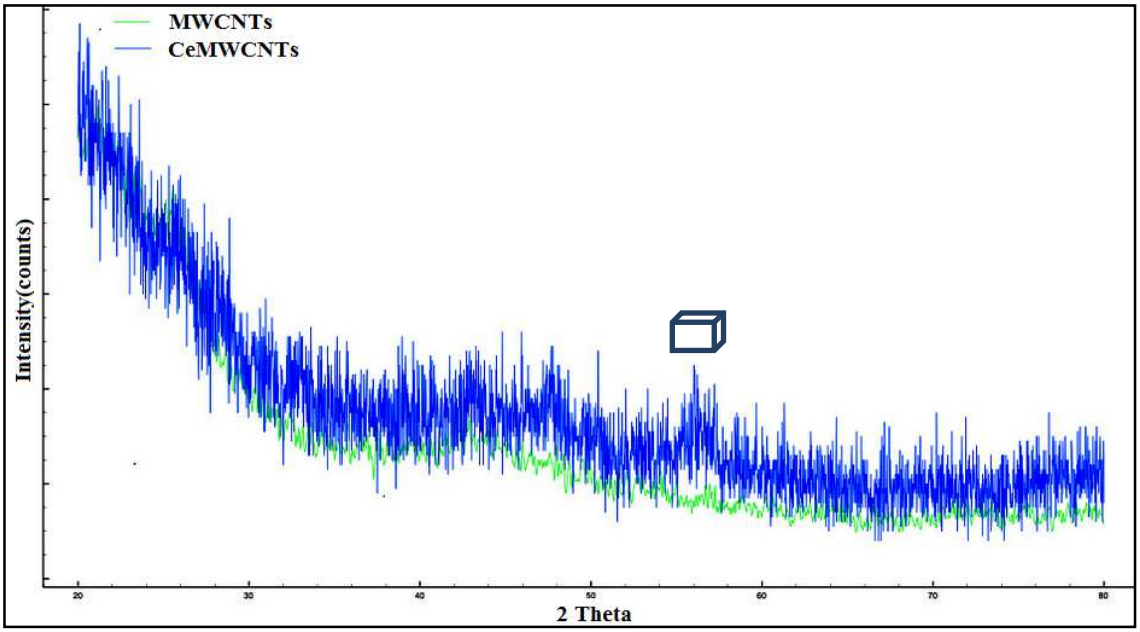

Figure 4.19: XRD results for MWCNTs and CeMWCNTs

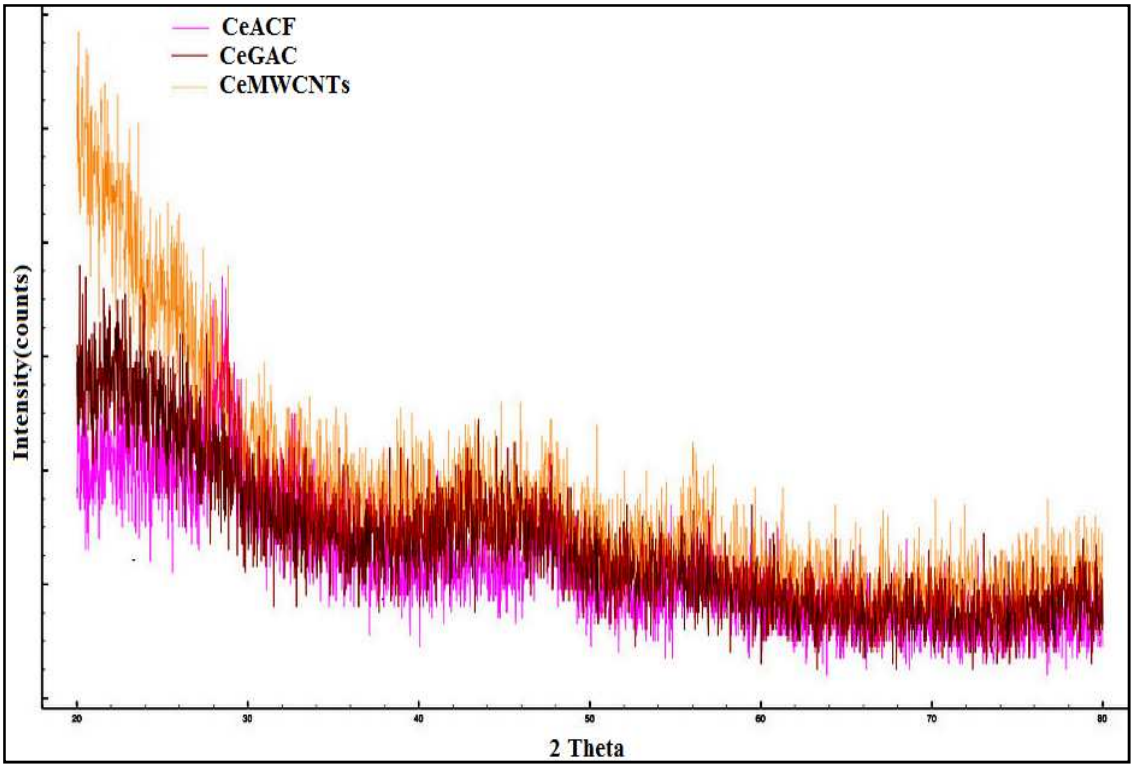

Figure 4.20: Comparison of XRD results for various catalysts

The broad peaks at 22°and 43°in all the results c orrespond to amorphous carbon (Liu et al., 2008; Maldonado-Hodar et al., 200). The crystallinity of amorphous carbon was reduced after impregnation for CeACF and CeGAC; this agrees with carbon reduction indicated in the CHN and EDS analyses and more porous structure shown in the SEM image for CeGAC.

4.1.9: Density Analysis

The density results for all samples are shown in Table 4.6. Three replicates were taken and averaged for density values. The density of CeGAC, CeACF and CeMWCNTs increased after impregnation due to the adherence of cerium oxide on to the surface of carbon. The space velocity calculation is given in Appendix A.

4.2 Catalyst Activity Test

In this study, two different NOx concentrations at various temperatures were tested: low NOx of 150 ppm and high NOx of 500 ppm, with a NH_3/NOx ratio of 1:1 (according to the reaction stoichiometry) and oxygen concentration of 5.6%. The total flow rate in the reactor was kept as 200 ml/min. 0.2 gram of catalyst was used in each experimental run. Oxygen concentration of 5% was originally targeted as a value within the typical O_2 concentration range (3 to 17%) in SCR catalyst, but 5.6% was used to make the total flow rate to 200 ml/min. The flow rate calculation is given in Appendix A.

4.2.1: The Effects of Gas Hourly Space Velocity

The space velocities for all the catalysts are shown in Table 4.7. For the same amount of sample and same impregnation procedure, the gas hourly space velocity (GHSV) is in the order of CeACF<CeMWCNTs<CeGAC. Lowering the space velocity increases the residence time, which leads to improved NOx reduction efficiency. However, if the reactor volume increases, the cost of the SCR increases and the reactor may be hard to place in the vehicle downstream due to its increased size (Yun and Kim, 2013). According to this result, CeGAC would be the most cost effective option for the SCR process. It is also showed higher cerium percentage doping in EDS analysis and even distribution in EDS mapping.

Table 4.6: Space Velocity

Catalyst	Density g/ml	Reactor volume (ml)	Gas Hourly Space Velocity (hr^{-1})
GAC	0.4931	0.4056	29,584
CeGAC	0.5101	0.3921	**30,604**
ACF	0.1074	1.8616	6446
CeACF	0.1292	1.5480	**7752**
MWCNTs	0.0333	6.0000	2000
CeMWCNTs	0.1547	1.2928	**9282**

4.2.2: The Effect of Type of Catalyst

The NOx reduction percentages for low NOx (NO 150 ppm, NH_3 150 ppm, and 5.6% oxygen) are shown in Table 4.8 and Figure 4.21. Steady state reduction graphs are presented in Appendix C (contact author for raw data). NOx percentage reduction is calculated from Equation 1 below and the emissions of NO and ammonia slips together are calculated using Equation 2. In CLD 822 cm h analyzer, two different modes were used to find the NO_2+NH_3 value. NOxamine values were obtained from the NOx, NOxamine, NH_3 mode and NO values were obtained from the NOx, NO, NO_2 mode. The NOxamine measurement accuracy exceeds 99% but NO_2 measurement accuracy is below 95%. Therefore, the direct measurement of NO_2 is not reported in this study.

$$\text{NOx reduction \%} = \frac{NOx_{out} - NOx_{in}}{NOx_{in}} \times 100 \quad \text{---------- Equation 1}$$

where
NOx_{out} = Outlet concentration (ppm)
NOx_{in} = Inlet concentration (ppm)

NO_2+NH_3 = NOxamine - NO ---------- Equation 2

Baseline measurements were made using raw activated carbon. The reduction efficiency for ACF and GAC generally stayed around 8 to 11% removal, which would be due to adsorption rather than reduction. The baseline for MWCNTs was not measured in this study due to the difficulties in loading the sample in the column.

4.2.2.1 Low NOx

According to the results, CeGAC yields the highest reduction efficiency of 77.5% at temperature 300ºC. At all the temperature levels, CeGAC achieves higher reduction efficiency than CeACF and CeMWCNTs and more stable (less deviation) reduction than other types of catalyst. CeGAC has more than 30% reduction even at 100ºC. Yoshikawa et al. (1998) studied Mn_2O_3 loaded on ACF and GAC for temperatures ranging from 51ºC to 151ºC and found that ACF had a higher reduction efficiency, ranging from 28% to 93%, compared to GAC, with a

reduction efficiency ranging from 20% to 46%. However, this research showed higher reduction for cerium doped GAC than ACF; this might be due to the transition metal (cerium) used in this research. CeGAC was tested up to 300℃ due to the l oss of carbon found from TGA analysis beyond that temperature level.

Table 4.7: Low NOx results

Temperature ºC	Reduction %				
	CeMWCNTs	CeACF	CeGAC	GAC	ACF
100	4.6	26.7	32.7	0.0	0
150	10.6	36.9	42.4	8.0	10.87
200	21	47.3	52	6.8	9.73
250	40.7	64.4	64.2	7.0	10.53
300	70.3	52.1	77.5	8.4	11.53
350	57	52.3			16.7
400	23.4				

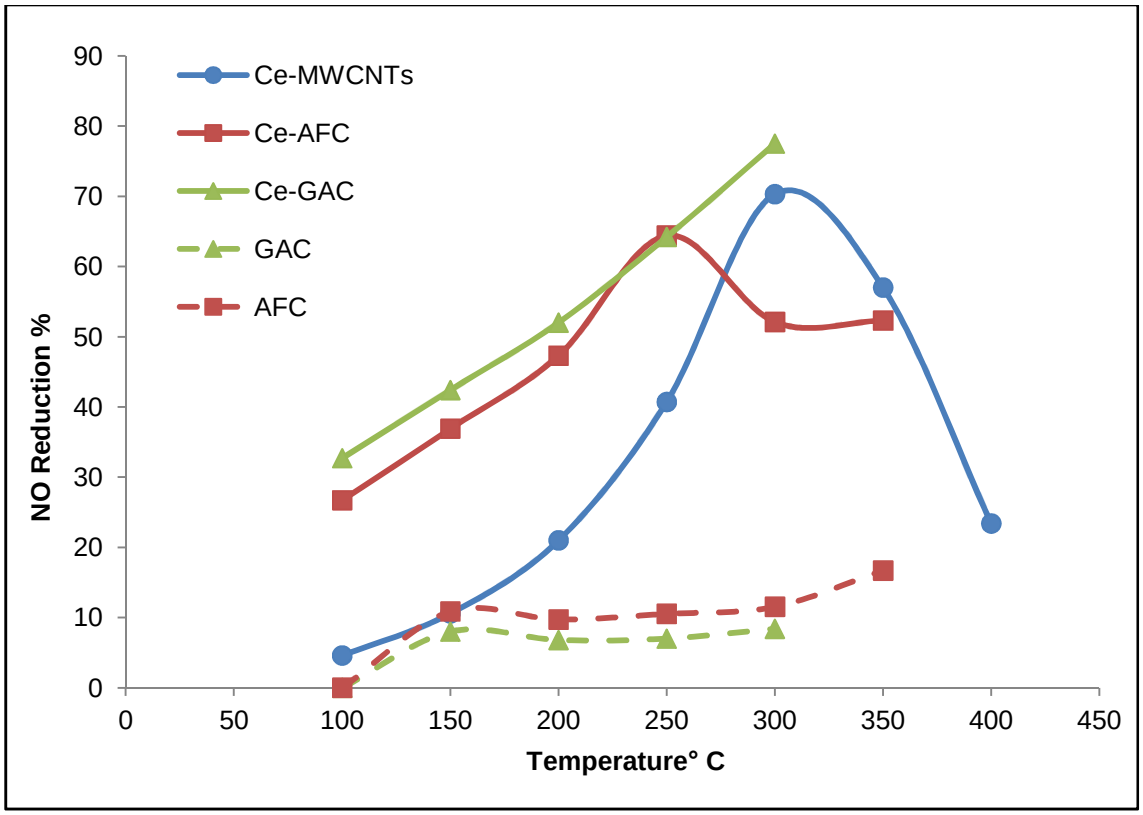

Figure 4.21: Low NOx results

CeACF and CeMWCNTs form bell shaped curves in reduction efficiency, with higher reductions at 250ºC (64.4%) and 300ºC (70.3%), respectively. CeMWCNTs reduction efficiency is highest over the range from 200º to 400°C. CeMWCNTs reduction efficiency is below 20% up to 200ºC. Both CeACF and CeMWCNTs work well above 200ºC.The bell shape reduction efficiency curve and the medium temperature operating range from 200º to 400°C are in agreement with Chen et al. (2011), as shown in Figure 4.22, which shows the NO reduction percentage for cerium oxide (about 20 to 25%) and MWCNTs (below 5%). A bell-shaped curve in efficiency vs. temperature is common in processes that involve adsorption followed by chemical reaction. Chemical reaction rates increase as a function of temperature, but adsorption rates decrease, meaning that a mid-range temperature often shows an overall peak in efficiency.

Lu et al. (2010) reported about 70% reduction efficiency for 10 % wt CeO_2/ACF at 5000/hr space velocity loaded with 0.5g of catalyst activity test at 150ºC and more stable reduction from 250ºC to 450ºC. However, this study deals with a higher GHSV and very low concentration, which impacts the reduction efficiency. Furthermore the temperature limit on CeACF was determined by the TGA analysis to be 350ºC. Operating the catalyst at higher temperatures would burn the carbon structure in the sample, leaving only cerium oxide powder.

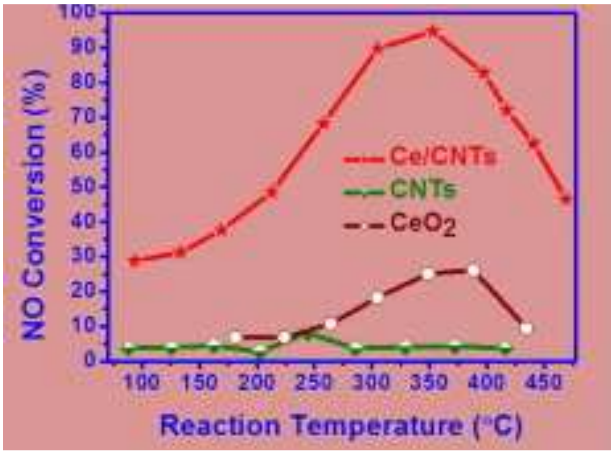

Source: Chen et al., 2011

Figure 4.22: Comparison of CeMWCNTs reduction efficiency

4.2.2.2 High NO_X

The NOx reduction percentages for high NOx (NO 500 ppm, NH_3 500ppm, and 5.6% oxygen) are shown in Table 4.9 and Figure 4.22.

Table 4.8: High NOx results

Temperature ºC	Reduction %				
	CeMWCNTs	CeACF	CeGAC	GAC	ACF
100	5.1	27.1	27.3	5.5	8.4
150	11	40.8	39.3	2.34	3.4
200	25	54	50	1.1	1.88
250	53	76.4	63	1.5	3.3
300	85	79.6	77.6	2.9	3.9
350	82	69.5			6
400	43				

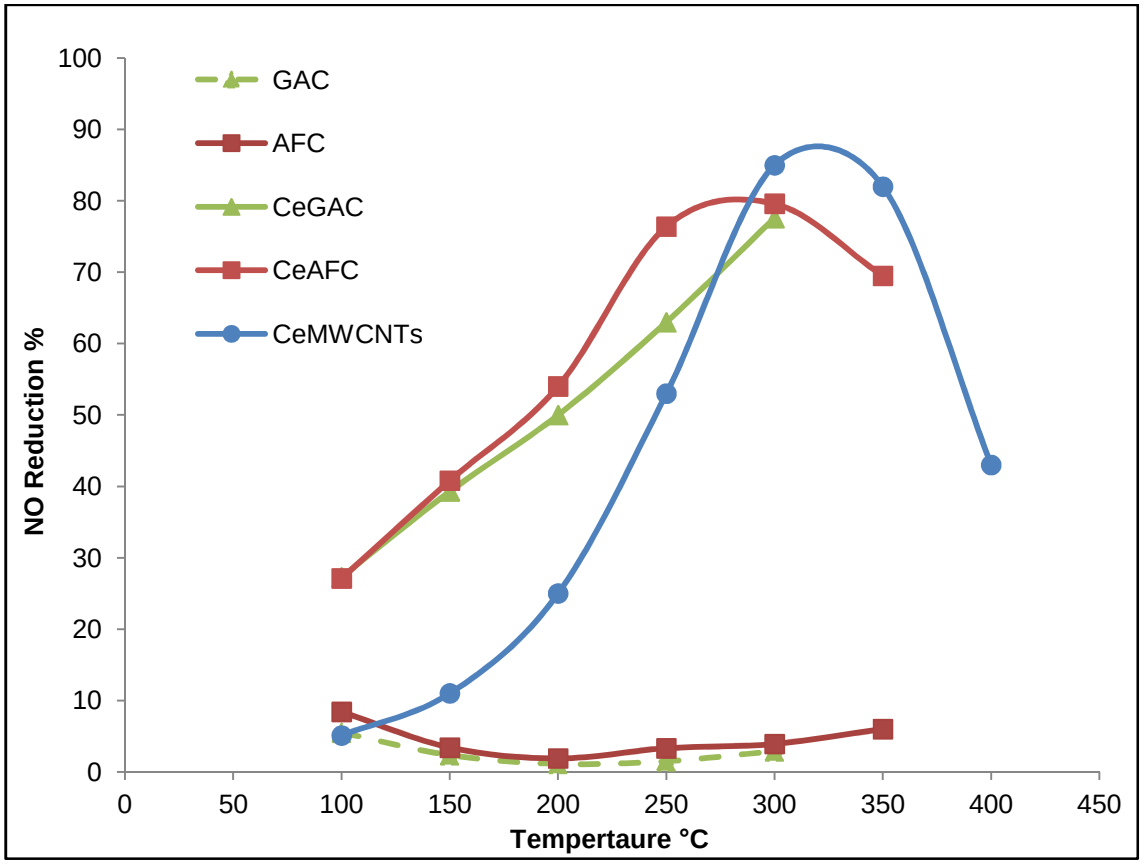

Figure 4.23: High NOx results

The highest reduction efficiency of 85% is achieved by CeMWCNTs at 300ºC. The highest reduction efficiency for a specific temperature may depend on the type of metal loaded in the sample. CuCNTs higher reduction efficiency at 250ºC (Li et al., 2011), PtMWCNTs show higher reduction at 220ºC (Santillan-Jimenez et al., 2011), V_2O_5/TiO_2–MWCNTs show higher reduction efficiency at 300ºC (Li et al., 2011), and V_2O_5/MWCNTs show higher reduction efficiency at 188ºC (Huang et al., 2007). The reduction efficiency of the sample may depend on the valence state of the metal loaded.

Again, CeACF and CeMWCNTs results show bell-shaped reduction efficiency curves. CeACF reduction efficiency is higher than CeGAC at all temperature levels. The CeACF reduction efficiency stays more stable after 250ºC, which is in agreement with Lu et al. (2010) and Li et al. (2008). CeGAC reduction efficiency increases as temperature increases but the maximum operating temperature found by TGA report is 310º C. Addition of thermally stable metals along with cerium may increase the thermal stability of the catalyst, which would provide higher operating temperatures.

4.2.3: The Effects of NOx Concentration

The low NOX and high NOx curves for all doped catalysts are compared in Figure 4.23. As the concentration increases, reduction efficiency also increases for CeACF and CeMWCNTs. CeGAC shows about same percentage reduction for both concentration levels. Increasing the concentration and keeping the GSHV the same provides more NOx and NH_3 molecules per gas phase volume, which leads to high interaction with the catalyst and higher reduction. On the other hand, when the pores are not easily accessible, increasing the concentration in the gas phase does not increase the reduction efficiency. Although CeGAC has more inner pores then CeACF and CeMWCNTs, this pore space is not accessible. ACF pore accessibility is easier than GAC (Mochida et al., 2000). Increasing the concentration and the lowering GSHV would likely increase the CeGAC reduction efficiency. CeMWCNTs yield higher reduction in higher concentration but starts working only above 200ºC.

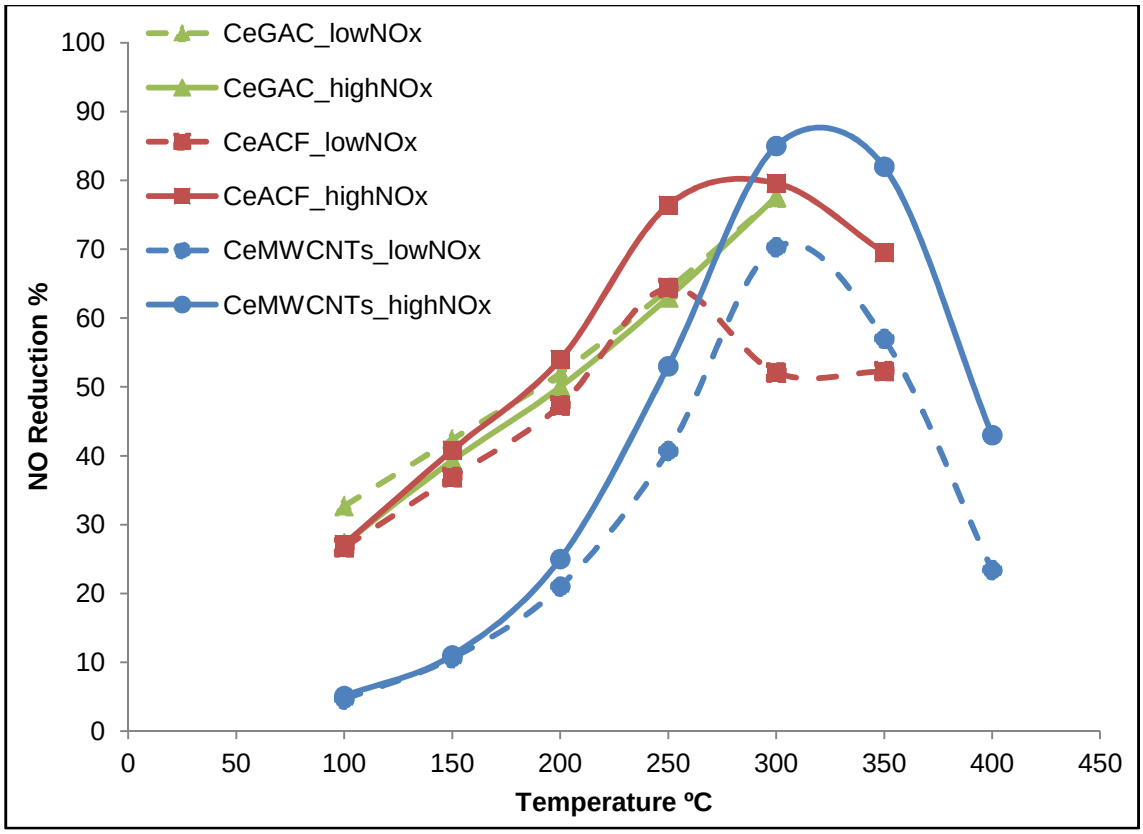

Figure 4.24: Comparison of Low NOx and High NOx Results

4.2.4: The Effects of NO Oxidation and Ammonia Slip

NO oxidation and ammonia slip are major concerns in SCR processes. NO oxidation occurs when excess oxygen is present in the exhaust, according to:

$$NO + \tfrac{1}{2} O_2 \longrightarrow NO_2$$

Unreacted NH_3 that exits the exhaust is called ammonia slip. NO_2 and ammonia together were measured in this study and reported in Table 4.10 and Figure 4.24. The NO_2 + NH_3 exiting the reactor is inversely proportional to the NO reduction efficiency. If the reduction efficiency increases, then the NO_2 plus ammonia concentration decreases. Comparing all catalysts for the high NOx, the NO_2 plus ammonia is in the order of CeACF<CeGAC<CeMWCNTs. For the low

NOx concentration, CeACF and CeGAC show similar amounts of NO_2+ammonia slip.

CeMWCNTs again with high emission for NO_2 oxidation plus ammonia slip.

Table 4.9: NO Oxidation and Ammonia Slip

Temperature, ℃	NO_2 + NH_3 concentration (ppm)					
	Low NOx			High NOx		
	CeGAC	CeACF	CeMWCNTs	CeGAC	CeACF	CeMWCNTs
100	110.1	105.2	150	365	352	470
150	85.58	92.18	148.6	298	288	444
200	61	61.26	135.6	227	206	382
250	34.3	18.76	95.62	147	79	245
300	13	33.48	25.65	0	14	66
350		24.5	1.2		51	1
400			3.5			4

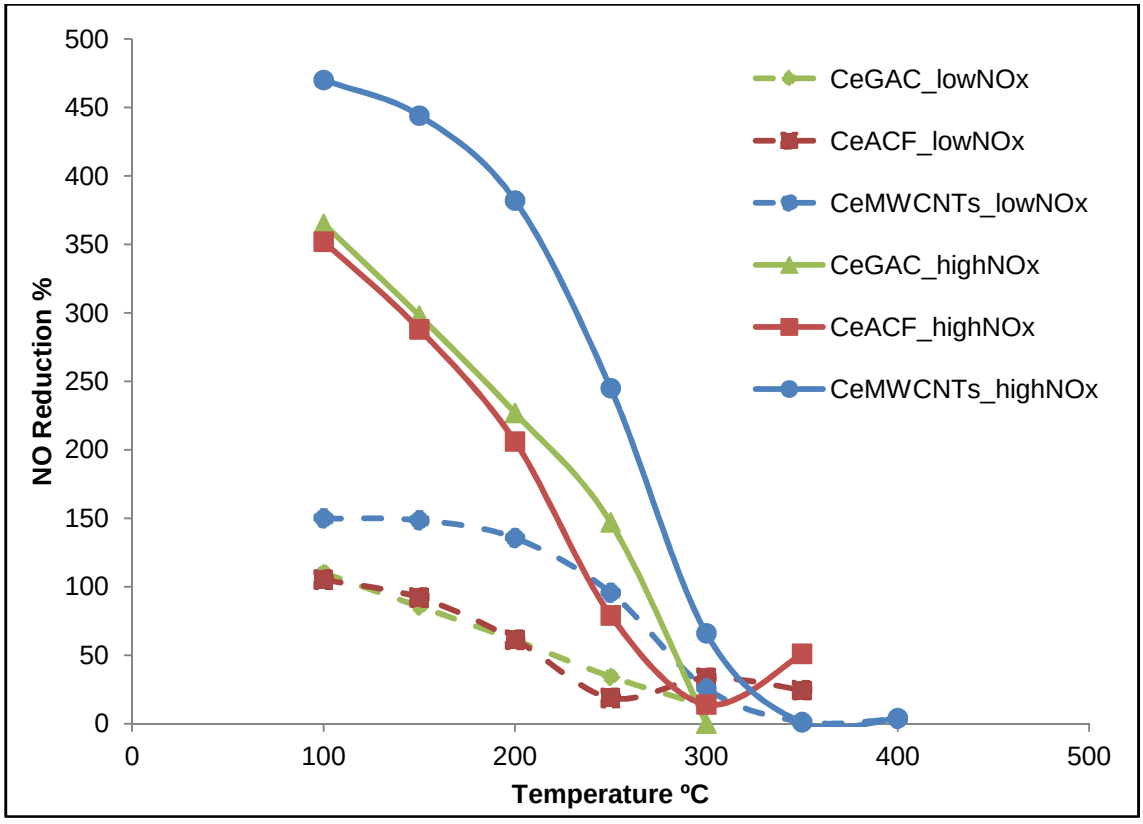

Figure 4.25: NO Oxidation and Ammonia Slip

4.2.5: Stability of the Catalyst

The catalyst stability is a significant test to see the performance of a catalyst over a long period of time. This study performed a 12-hr catalyst stability check for CeGAC at temperature 300ºC for high NOx, as shown in Figure 4.25.

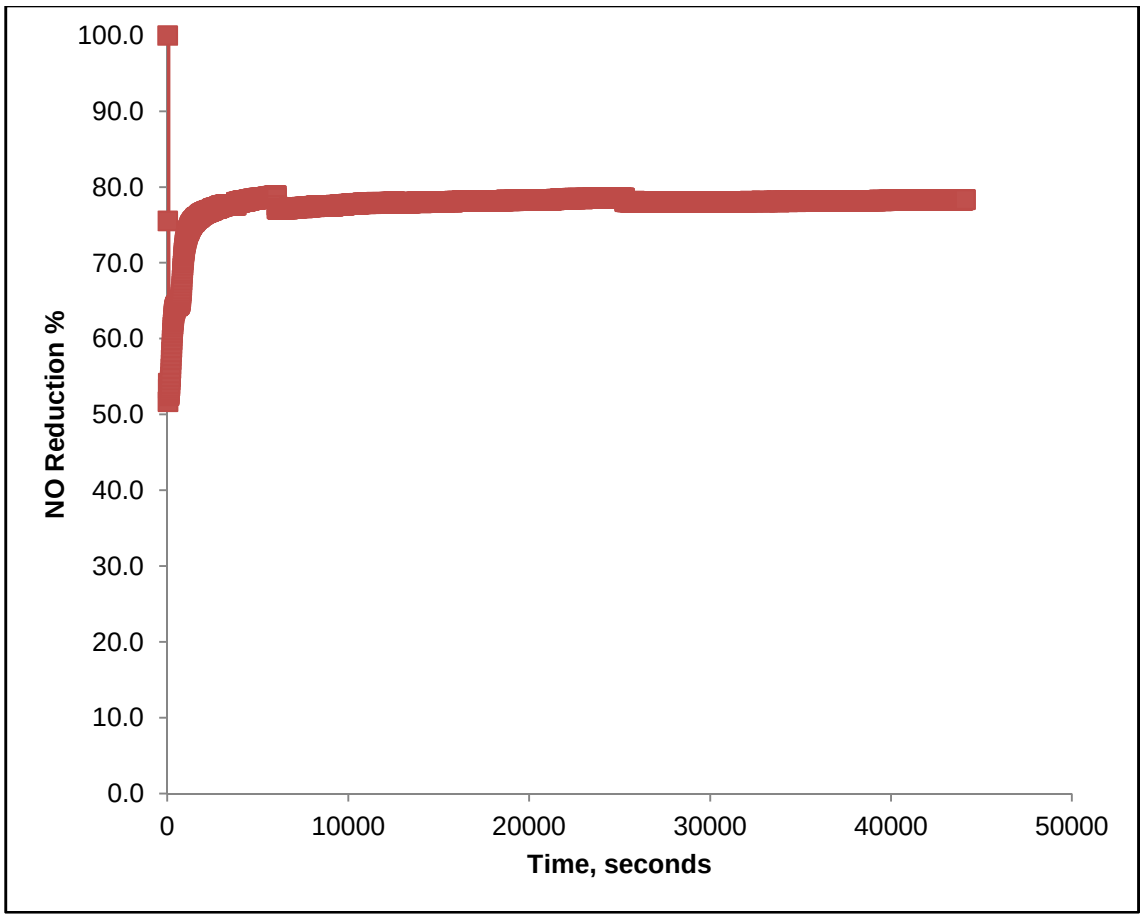

Figure 4.26: CeGAC Stability Test

As shown in the Figure 4.25, the stability of the catalyst is good. The reduction efficiency was maintained at about 80% throughout the 12-hr test. The initial hike of 100% removal efficiency was noted in all the steady-state curves for CeGAC and CeACF, but not for CeMWCNTs. Steady-state curves are provided in Appendix C. Moreover, the height of the hike is higher in CeGAC than CeACF, which is due to the availability of macropores and micropores.

After adsorption takes place in the initial stage of process and the flow becomes even in the pores, then the reduction efficiency stays same.

4.2.6: The Effect of NOx/NH_3 Ratio

A quick check was made for NOx to ammonia ratio for CeGAC at 100º C at high NOx condition. The NO reduction efficiency and the NO_2+NH_3 concentration after steady state are plotted in Figure 4.26. The reduction efficiency stays about the same but the NO_2 plus ammonia concentration goes down for 1:0.9 ratio of NOx/NH_3. At 1:1 ratio, the reduction efficiency is about 30 % and NO_2 plus ammonia slip concentration in the exhaust is 395 ppm. Lowering the ratio to 1:0.9 maintains the same reduction efficiency but lowers emission of NO_2 plus ammonia by 73 ppm. On board injection method would be helpful to reduce ammonia slip and NO oxidation in the exhaust stream. Moreover, it is more common practice method of ammonia injection in SCR catalyst.

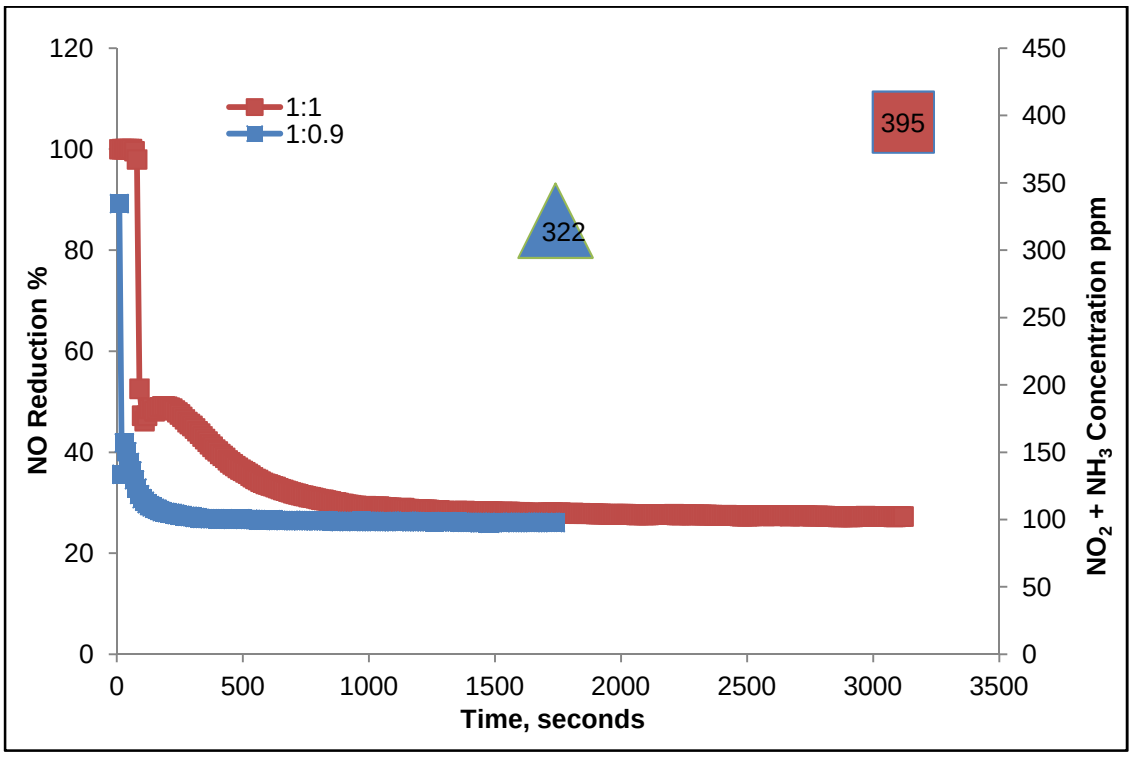

Figure 4.27: The Effects of NOx/NH_3 Ratio

4.2.7: Repeatability of Results

Replicates results were collected for CeMWCNTs at low NOx conditions at three temperature levels as shown in Table 4.10 below. The one-way ANOVA results in Table 4.11 show that the F value is well above the critical F value, with P value zero; thus the null hypothesis is rejected. It concludes that there is a significant difference between reduction efficiency due to temperature variation. The data satisfies the normality assumption.

Table 4.10: Replicate Results for CeMWCNTs

Temperature ^{o}C	**CeMWCNTs**		
	Run 1	**Run 2**	**Run 3**
100	4.6	5.9	4.3
150	10.6	13.3	11.2
200	21	21.9	20.7

Table 4.11: One-Way ANOVA Results

SUMMARY

Groups	*Count*	*Sum*	*Average*	*Variance*
100	3	14.8	4.933333	0.723333
150	3	35.1	11.7	2.01
200	3	63.6	21.2	0.39

ANOVA

Source of Variation	*SS*	*df*	*MS*	*F*	*P-value*	*F crit*
Between Groups	400.6422	2	200.3211	192.4109	3.62E-06	5.143253
Within Groups	6.246667	6	1.041111			
Total	406.8889	8				

Replicates for CeACF and CeGAC were collected at 200ºC in high NOx condition without changing the catalyst bed, as shown in Table 4.12. A standard deviation of less than 1% in reduction efficiency is noted for the catalyst tested.

Table 4.12: Replicates Results for CeACF and CeGAC

Replicates	NO Reduction %	
	CeACF	CeGAC
Run 1	54.00	50.00
Run 2	54.00	51.20
Run 3	54.80	51.80
Mean	54.27	51.00
Standard deviation	0.46	0.92

4.2.8 Characterization of Used Catalyst

The used catalysts were tested via Raman spectroscopy for metal adherence after the reduction experiments. The peaks were plotted (wave number vs. relative intensity) and compared with raw AC and after cerium doping. The results for CeGAC, CeACF and CeMWCNTs are shown in Figures 4.27, 4.28, and 4.29.

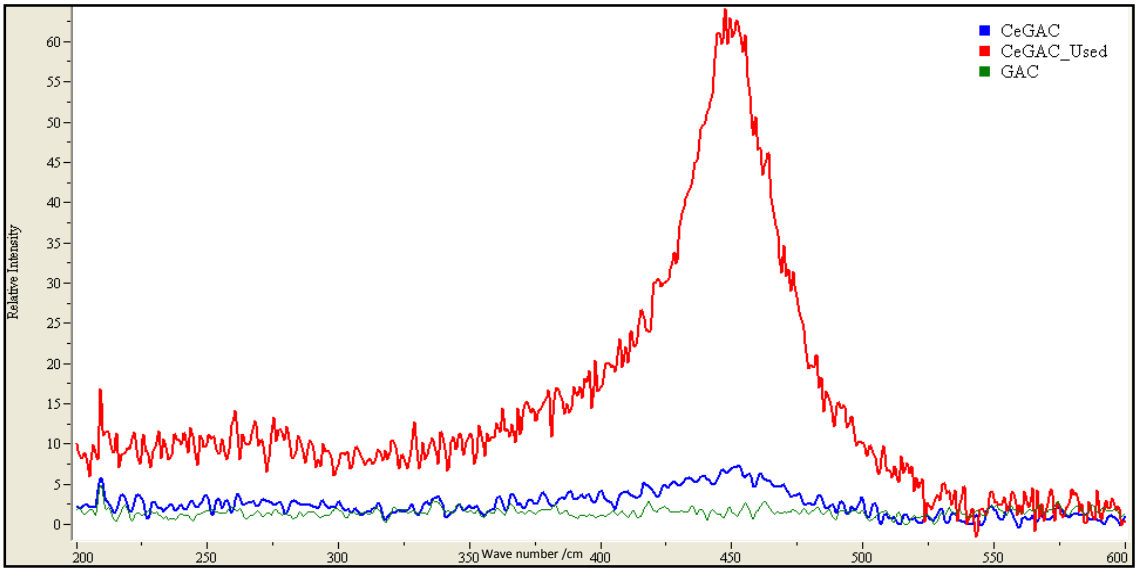

Figure 4.28: Raman Spectroscopy Results for Used CeGAC

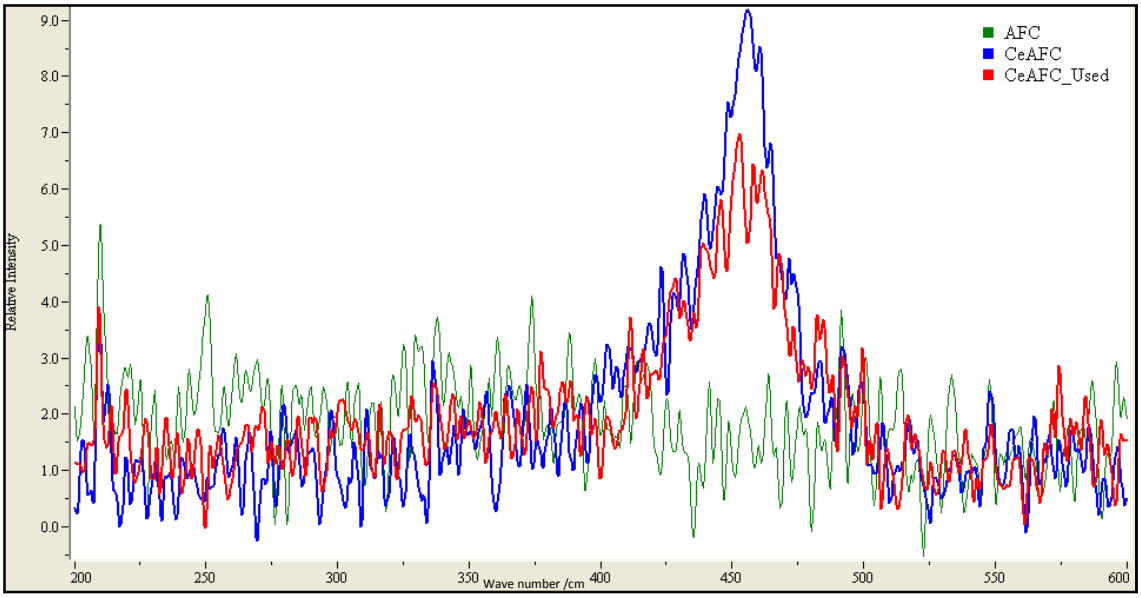

Figure 4.29: Raman Spectroscopy Results for Used CeACF

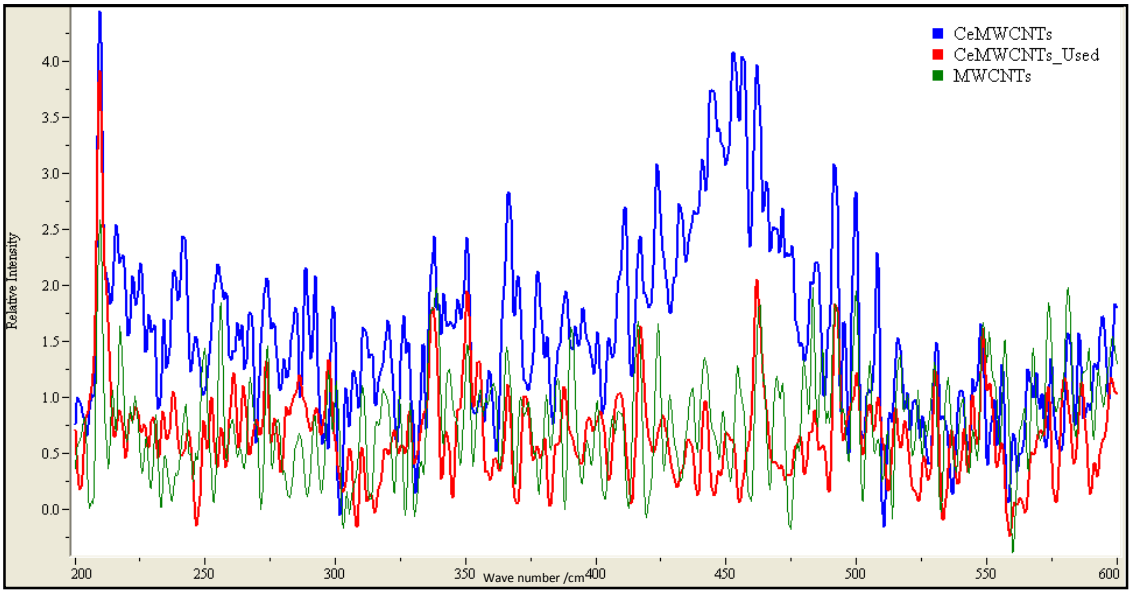

Figure 4.30: Raman Spectroscopy Results for Used CeMWCNTs

CeGAC and CeACF catalyst showed cerium oxide peaks around 450/cm. The used catalyst peaks were predominant in GAC due to carbon loss during the activity test. CeACF cerium deposition is predominant (exceeding monolayer deposition as seen from characterization results). Losing the cerium deposition on the surface would be the reason for

lower peak of used CeACF compared to CeACF. CeMWCNTs showed loss of cerium in the activity test, which explains the reduction efficiency fall after 350ºC. Pre-treating the MWCNTs before impregnation could improve the adherence of metal in nanotube surface walls.

CHAPTER 5

CONCLUSIONS AND RECOMMENDATIONS

5.1 Conclusions

The material analyses were conducted for raw granular activated carbon (GAC), activated carbon fiber (ACF), and multi-walled carbon nanotubes (MWCNT), as well as Ce-doped samples of the 3 carbon forms:

- Cerium distribution was found to be even throughout the surface of all types of catalyst, as shown by EDS mapping.
- The percentage of cerium doped was found to be highest for CeGAC. SEM images for CeGAC provide evidence that cerium doping did not affect the pore openings in the surface of the activated carbon.
- XRD showed that deposition of metal in ACF exceeded monolayer coverage at 10% weight. During impregnation procedure, the carbon weight loss for ACF was higher than for the other two types of carbon, indicating that it may require a different procedure for impregnation.
- The surface area of CeMWCNTs increased after impregnation, which likely signifies the open ends of nanotubes during the impregnation process.
- Raman showed cerium oxide present in all types of catalyst and XPS showed that most cerium nitrate hexahydrate decomposes into CeO_2 (Ce^{4+}).
- Maximum operating temperature found in TGA analysis shows high temperature of 400ºC for CeMWCNTs, the most thermally stable of the 3 carbon forms tested. CeGAC and CeACF work well at temperatures below 300º C and 350º, respectively.
- Considering the same amount of catalyst for each experimental study, different types of carbon yield different density measurements, and thus GHSV varies for the same flow rate

through reactor. CeGAC has higher GSHV than other types of catalyst, which increases its cost advantage over the 2 other types of catalyst.

CeGAC was found to be a promising catalyst for reducing NOx at low temperatures (100-300ºC); it could be used as part of a dual catalyst system, as discussed in Section 2.1, with zeolites handling NOx reduction at higher temperatures. Specific findings were as follows.

- For low concentration NOx (150 ppm), CeGAC exhibited higher reduction efficiency compared to the other two types of Ce-doped carbon over all temperatures tested. CeGAC reduction efficiency was 20% higher than CeMWCNTs for temperatures below 300ºC, and 20% higher than CeACF at 300ºC. The peak CeGAC reduction efficiency was 80% at 300ºC.
- For high concentration NOx (500 ppm), CeMWCNTs exhibited 7% higher reduction efficiency than CeGAC at 300°C, and CeACF exhibited 13% higher reduction efficiency compared to CeGAC at 250°C. For temperatures from 100-200°C, CeGAC reduction efficiency was comparable to CeACF and substantially higher than that of CeMWCNTs.
- NO oxidation and ammonia slip emission in the exhaust was higher for CeMWCNTs than for the other types of catalyst.
- The 12-hour stability test for CeGAC showed a steady reduction percentage throughout the test.

Granular activated carbon is the most economical of the three carbons tested, and unlike multiwall carbon nanotubes, poses no potential concerns regarding human health and safety. Given its superior performance for the low NOx concentration tested, and its generally comparable performance at the high NOx concentration tested, CeGAC is recommended as the most promising Ce-doped carbon form for SCR.

5.2 Recommendations for Future Research

Thermal stability limits the performance of CeGAC removal efficiency above 300°C. Future research to improve the thermal stability of CeGAC would increase its applicability to a wider range of temperatures.

High reduction efficiency with added advantages of safety and low-cost warrant additional testing of CeGAC-based SCR for mobile sources. Additional investigation could include varying the type of metal for doping, metal loading percentage, calcination temperature, GHSV, O_2 concentration, type of GAC, and humidity.

Field testing the catalyst system to match real world conditions such as variation in exhaust gas flow rates, vibration during driving and available reductants in the exhaust stream itself would be needed before applying the catalyst system in vehicles.

APPENDIX A

CALCULATIONS

TOTAL FLOW RATE CALCULATION

A.1 Cylinder concentrations

- NOx 301 ppm
- NOx 1015ppm
- Ammonia 2199 ppm
- Zero air (20% oxygen)

Need to match 1:1 concentration of NOx and ammonia, Low NOx concentration is 150 ppm and high NOx concentration is 500 ppm and desired flow rate is 200 sccm

A.1.1 High concentration calculation

$$\frac{X}{200\text{sccm}} * 1015\text{ ppm} = 500\text{ ppm}$$

X = 98.5 sccm

Mass flow controller flowrate for ammonia = Y

$$\frac{Y}{200\text{sccm}} * 2199\text{ ppm} = 500\text{ ppm}$$

Y = 45.5 sccm

Mass flow controller flow rate for air = Z

X+Y+Z = 98.5+45.5+Z = 200 sccm

Z= 200-(98.5+45.5)

Z = 56 sccm (therefore, need not to be balanced with nitrogen.)

$$\frac{56 * 20\ \%}{200\text{sccm}} = 5.6\%\text{ oxygen}$$

A.1.2 low concentration calculation

Mass flow controller flow rate for NOx = X

$$\frac{X}{200\text{sccm}} * 301\text{ ppm} = 150\text{ ppm}$$

X = 99.7 sccm = 100 sccm

Mass flow controller flowrate for ammonia = Y

$$\frac{Y}{200\text{sccm}} * 2199\text{ ppm} = 150\text{ ppm}$$

Y = 13.6 sccm

Mass flow controller flow rate for air = Z

$$\frac{Z}{200\text{sccm}} * 20\ \% = 5.6\%$$ (To match the oxygen concentration in HighNOx)

Z = 56 sccm

X+Y+Z = 100+13.6+56 = 169.6

Remaining Nitrogen = 200-169.6 = 30.4 sccm

A.2 Gas Hourly Space Velocity

Sample calculation:

CeGAC bulk density = 0.5101 g/ml

Sorbent weight = 0.2 g

CeGAC volume in the reactor = 0.2 g / 0.5101 g/ml

= 0.3921 ml

Volumetric flow rate = 200 ml/min = 12,000 ml/h

$$\text{Gas hourly space velocity (GHSV)} = \frac{\text{Total volumetric flow rate}}{\text{Volume of the sample}}$$

$$= \frac{12{,}000\text{ml/hr}}{0.3921\text{ ml}} = 30{,}604\ h^{-1}$$

APPENDIX B

MATERIAL ANALYSIS

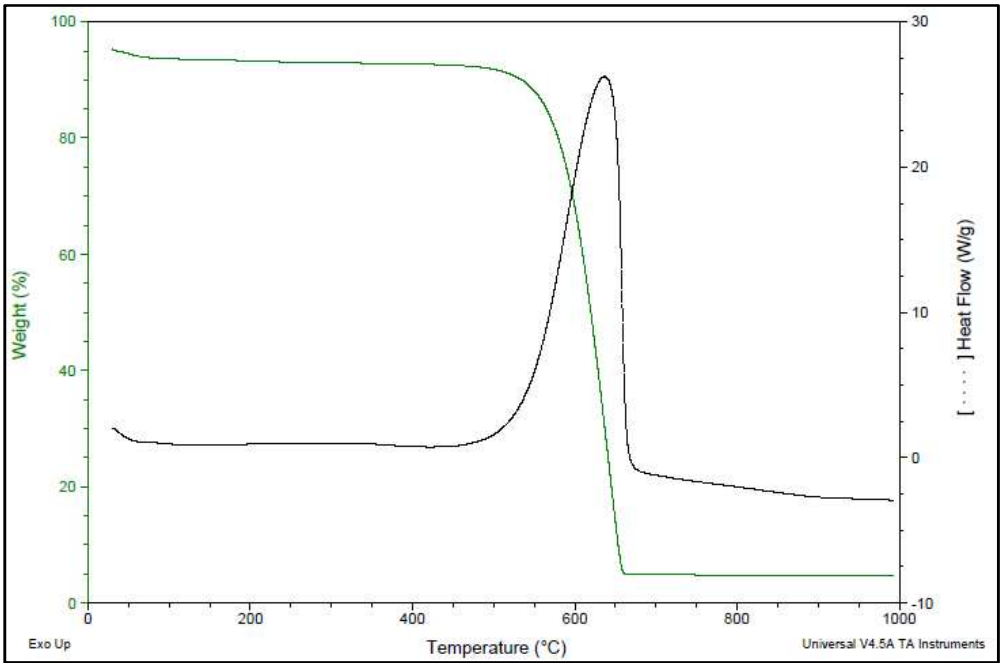

Figure B.1: DSC-TGA report for GAC

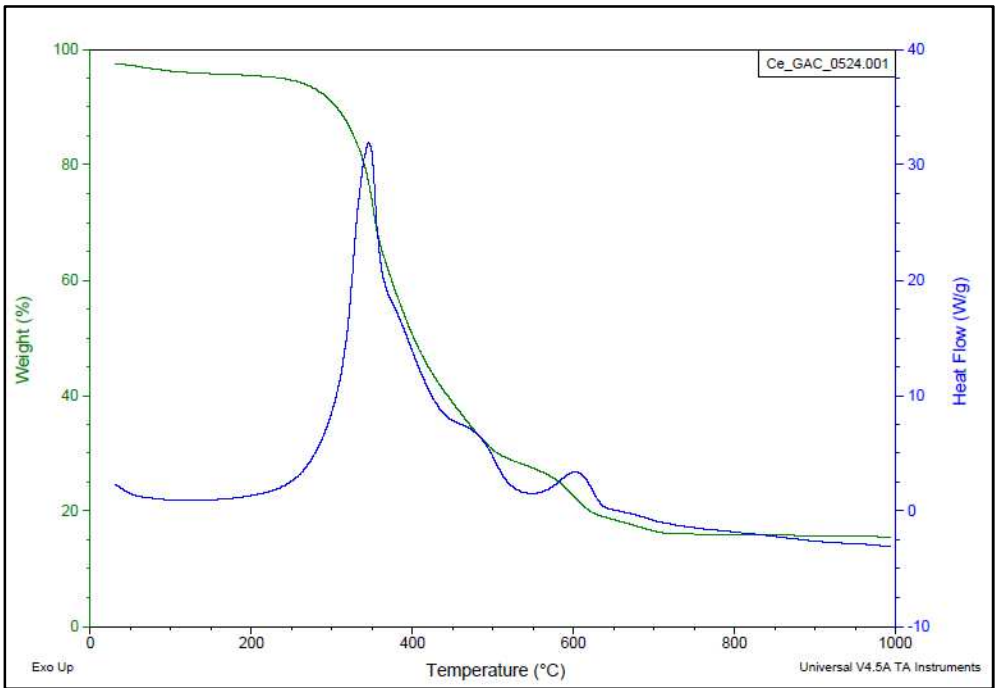

Figure B.2: DSC-TGA report for CeGAC

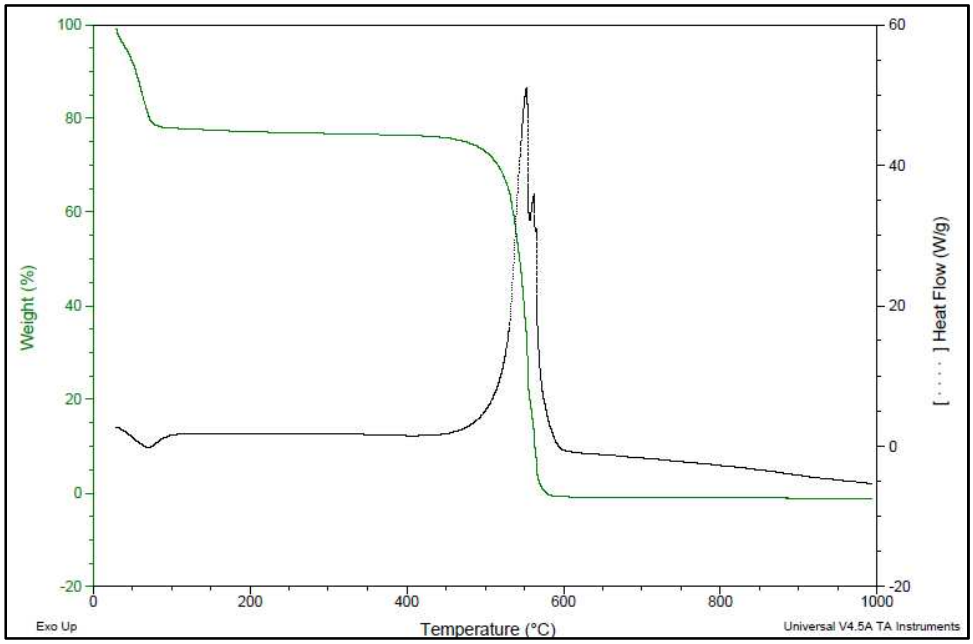

Figure B.3: DSC-TGA report for ACF

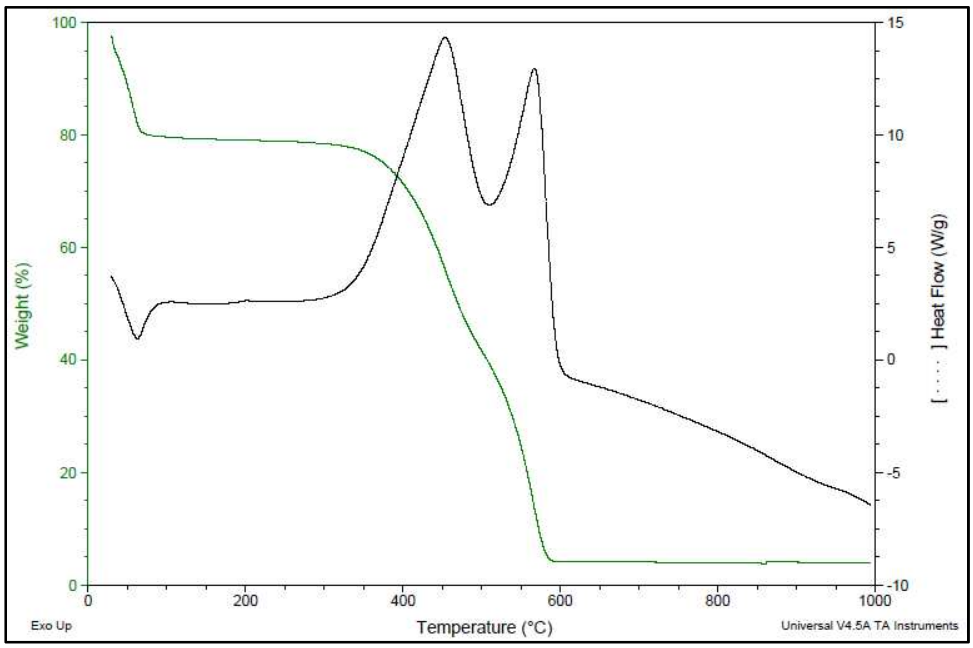

Figure B.4: DSC-TGA report for CeACF

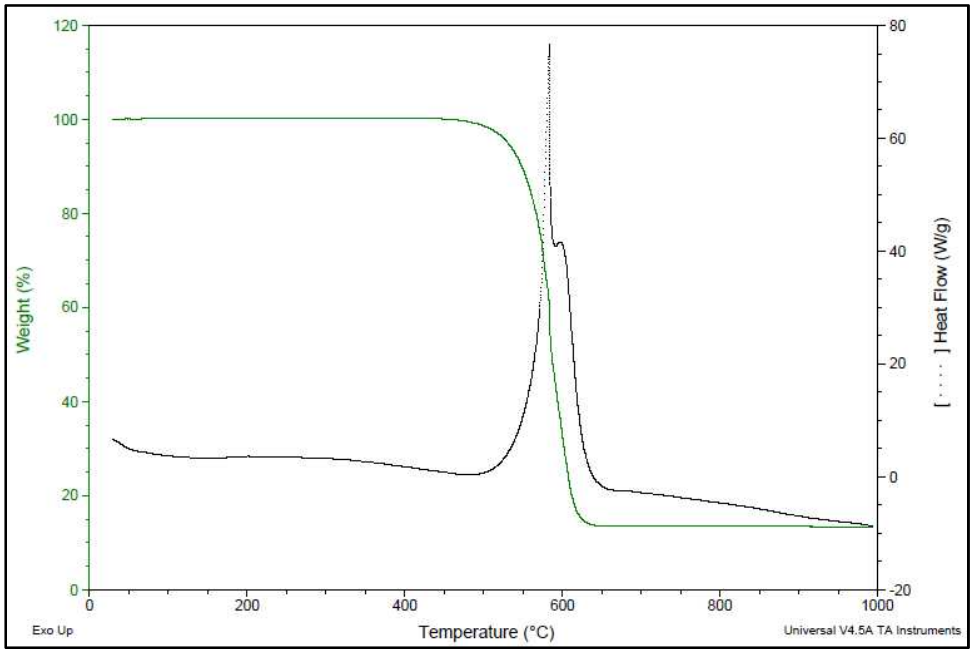

Figure B.5: DSC-TGA report for MWCNTs

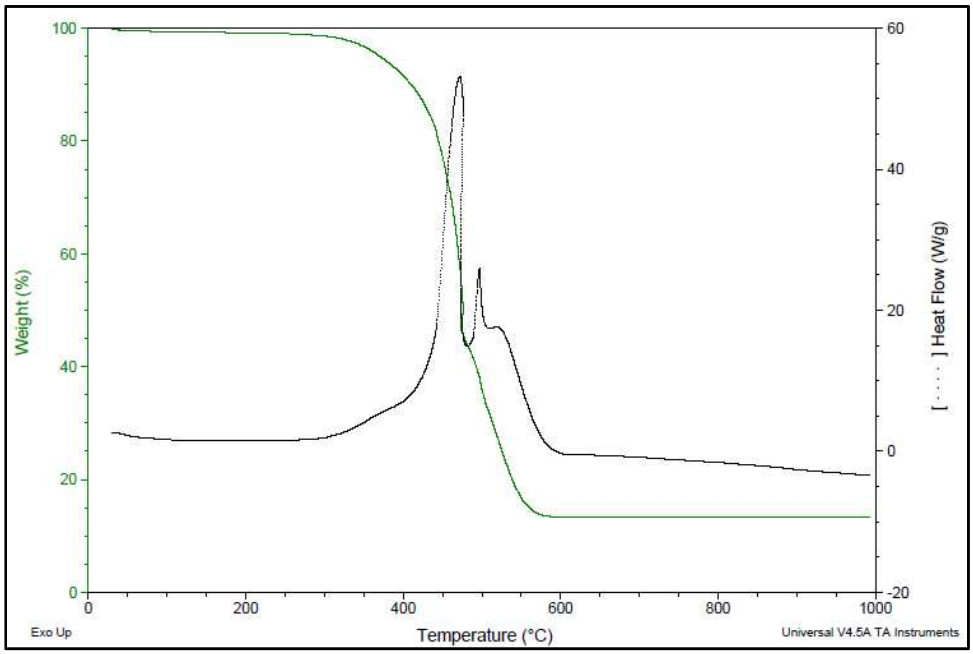

Figure B.6: DSC-TGA report for CeMWCNTs

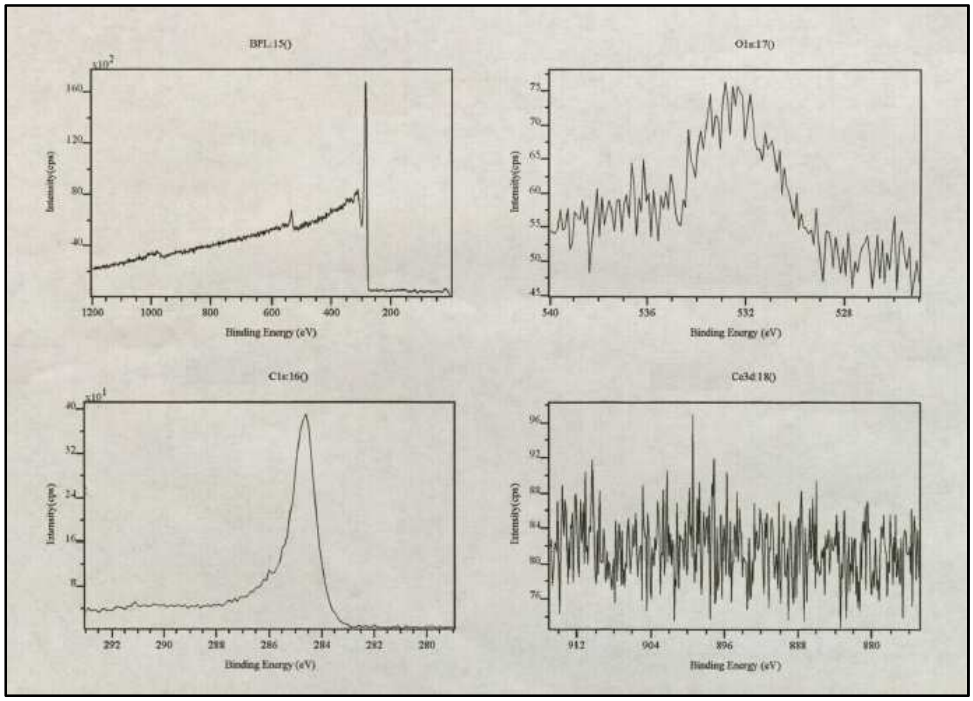

Figure B.7: XPS Results for GAC

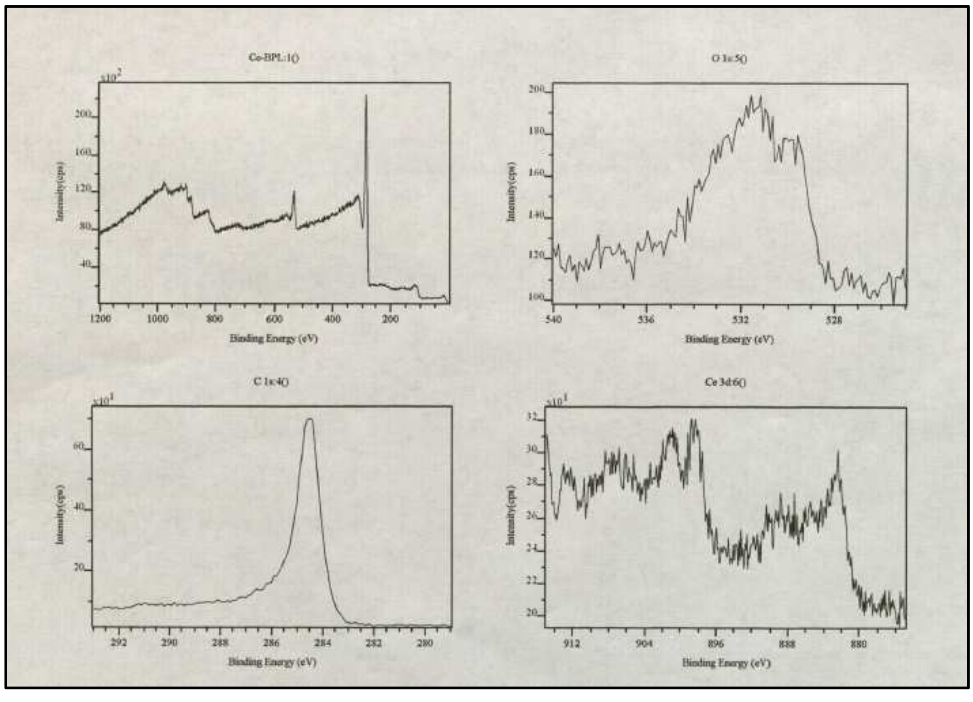

Figure B.8: XPS Results for CeGAC

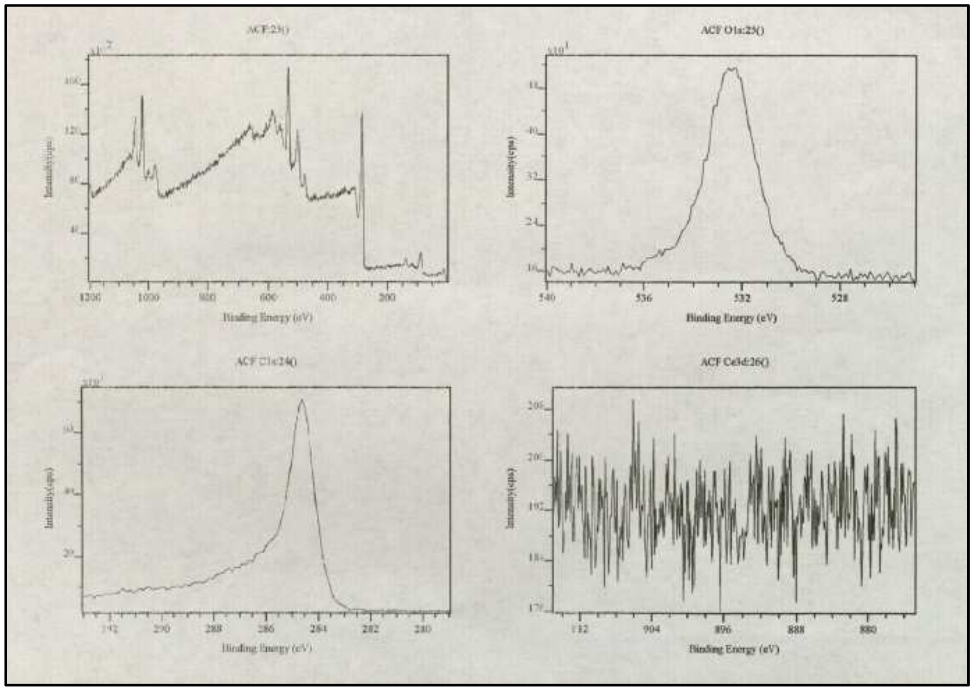

Figure B.9: XPS Results for ACF

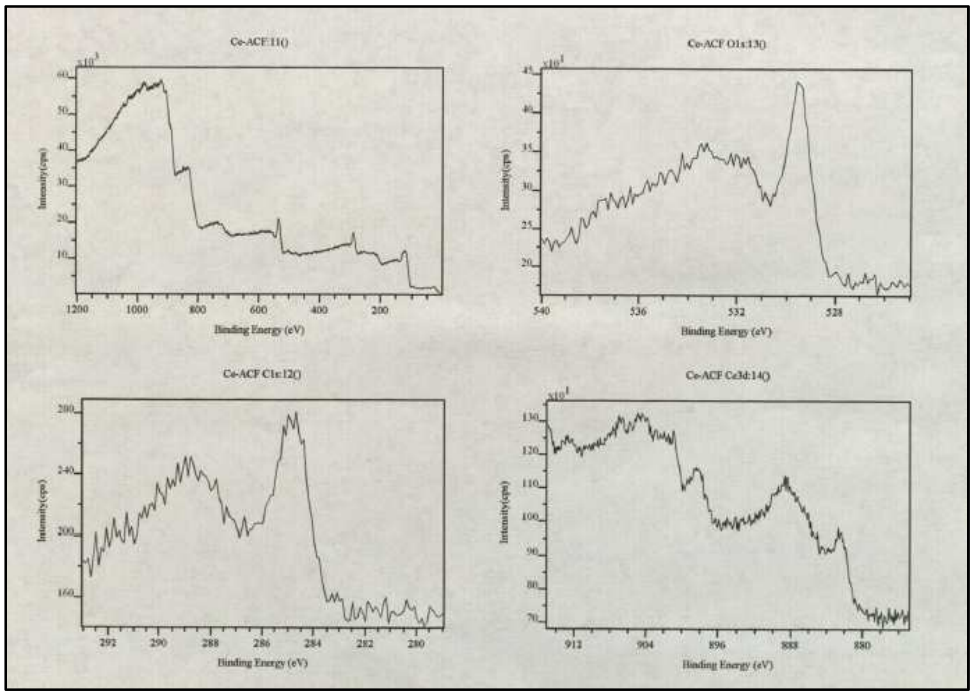

Figure B.10: XPS Results for CeACF

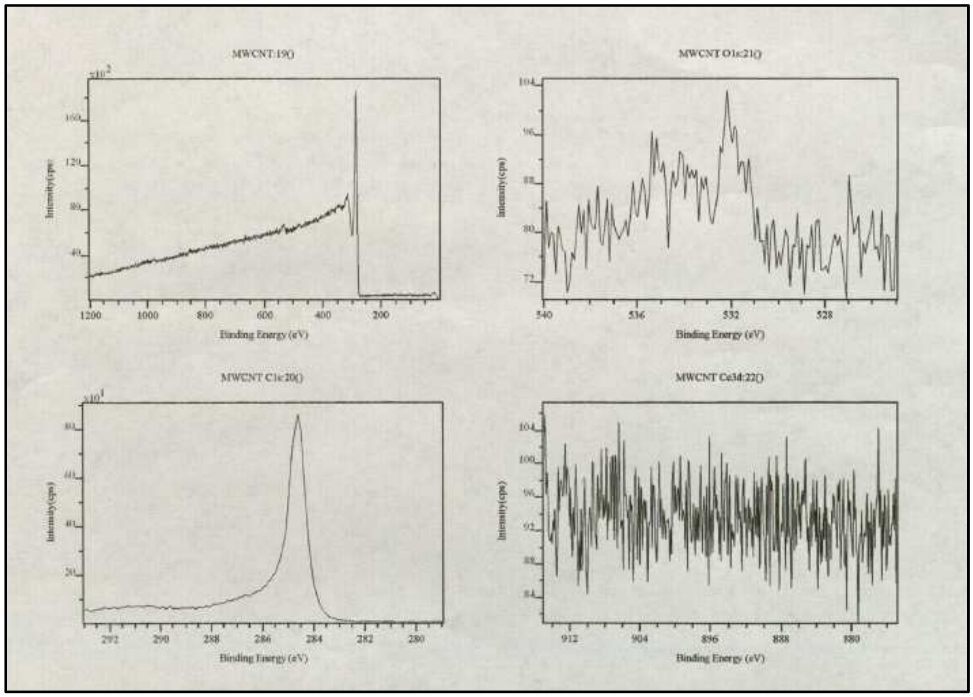

Figure B.11: XPS Results for MWCNTs

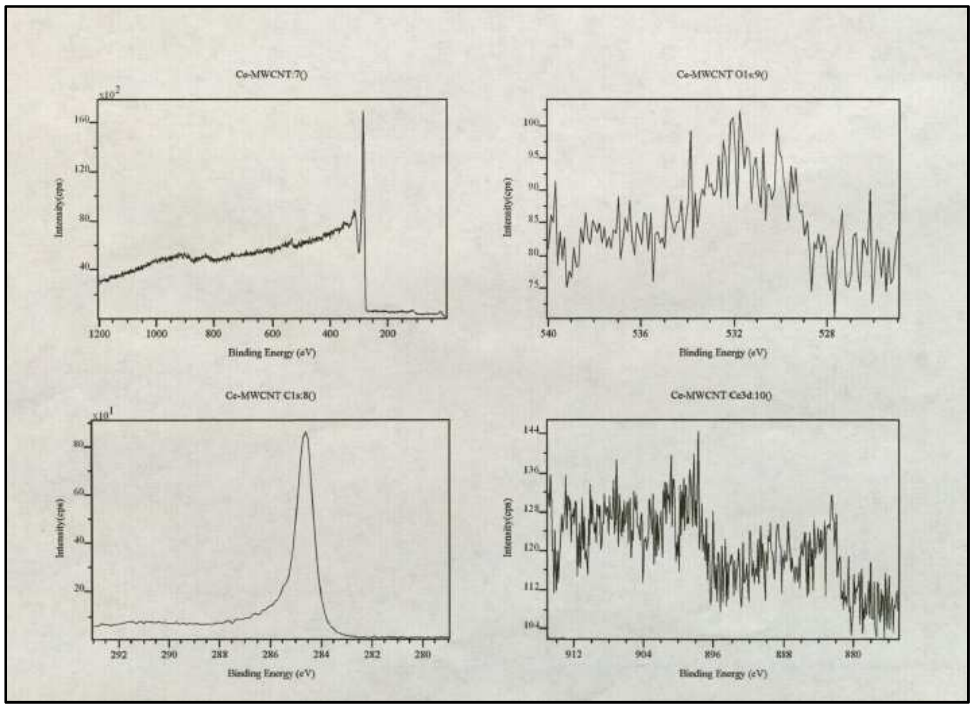

Figure B.12: XPS Results for CeMWCNTs

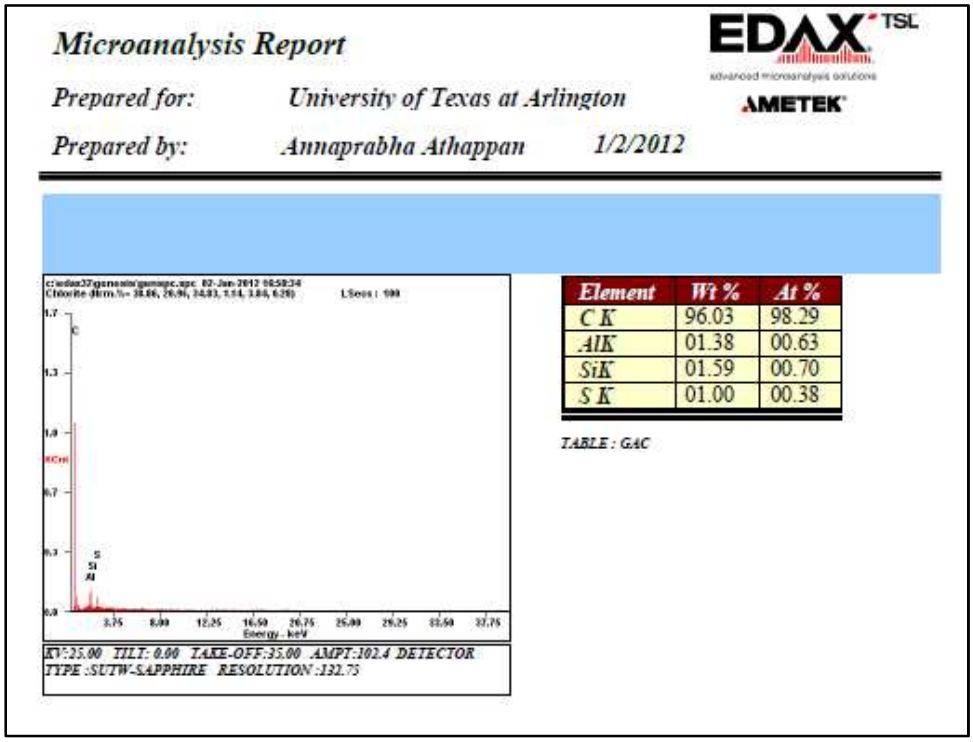

Figure B.13: EDS Results for GAC

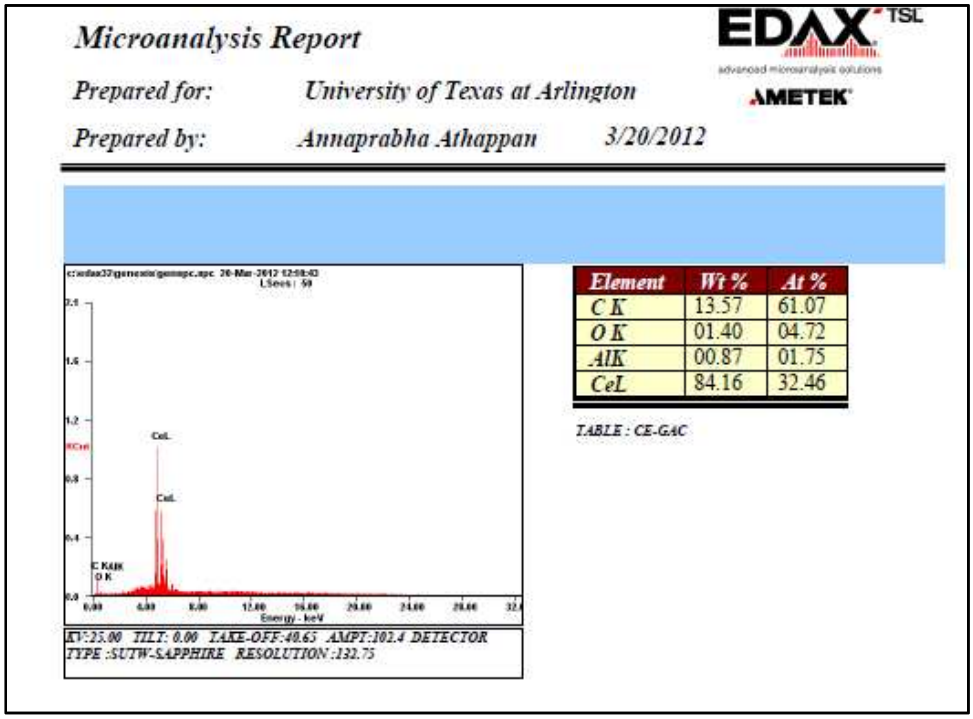

Figure B.14: EDS Results for CeGAC

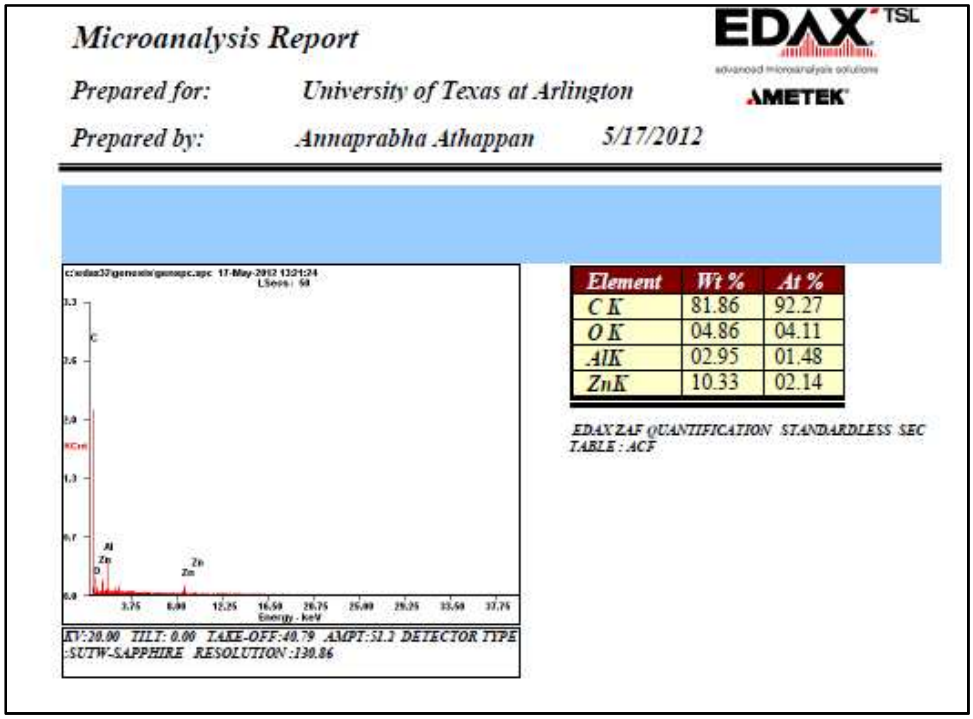

Figure B.15: EDS Results for ACF

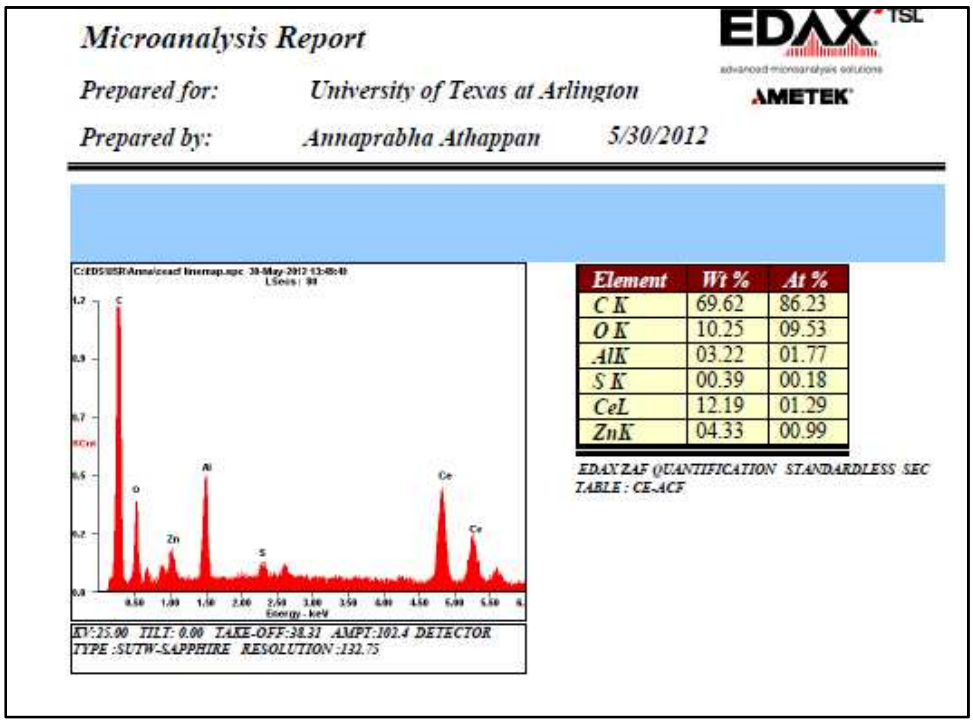

Figure B.16: EDS Results for CeACF

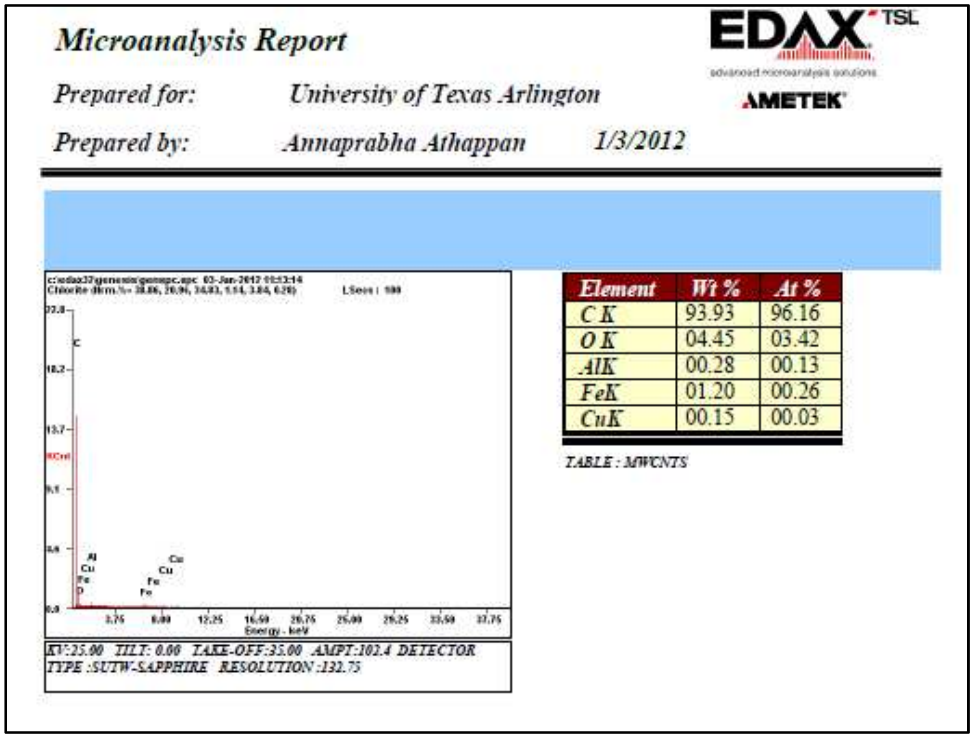

Element	Wt %	At %
C K	93.93	96.16
O K	04.45	03.42
AlK	00.28	00.13
FeK	01.20	00.26
CuK	00.15	00.03

Figure B.17: EDS Results for MWCNTs

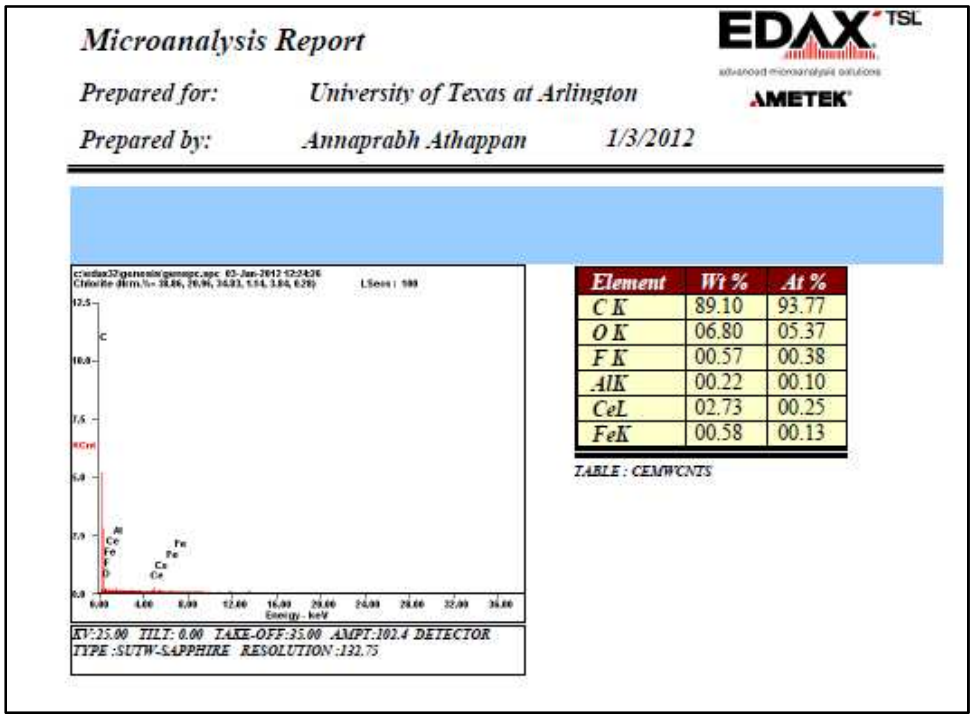

Element	Wt %	At %
C K	89.10	93.77
O K	06.80	05.37
F K	00.57	00.38
AlK	00.22	00.10
CeL	02.73	00.25
FeK	00.58	00.13

Figure B.18: EDS Results for CeMWCNTs

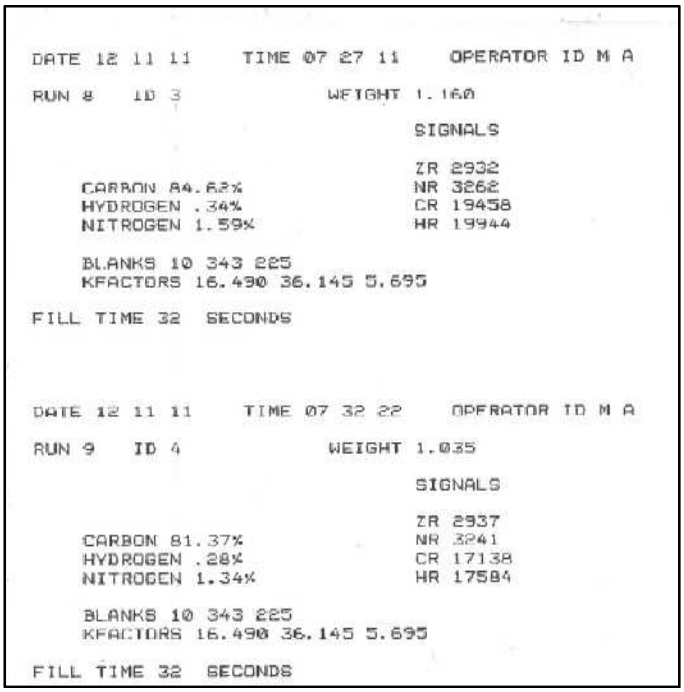

```
DATE 12 11 11     TIME 07 27 11     OPERATOR ID M A

RUN 8    ID 3              WEIGHT 1.160

                                   SIGNALS

                                   ZR 2932
     CARBON 84.62%                 NR 3262
     HYDROGEN .34%                 CR 19458
     NITROGEN 1.59%                HR 19944

     BLANKS 10 343 225
     KFACTORS 16.490 36.145 5.695

FILL TIME 32  SECONDS


DATE 12 11 11     TIME 07 32 22     OPERATOR ID M A

RUN 9    ID 4              WEIGHT 1.035

                                   SIGNALS

                                   ZR 2937
     CARBON 81.37%                 NR 3241
     HYDROGEN .28%                 CR 17138
     NITROGEN 1.34%                HR 17584

     BLANKS 10 343 225
     KFACTORS 16.490 36.145 5.695

FILL TIME 32  SECONDS
```

Figure B.19: CHN Analysis Report for GAC

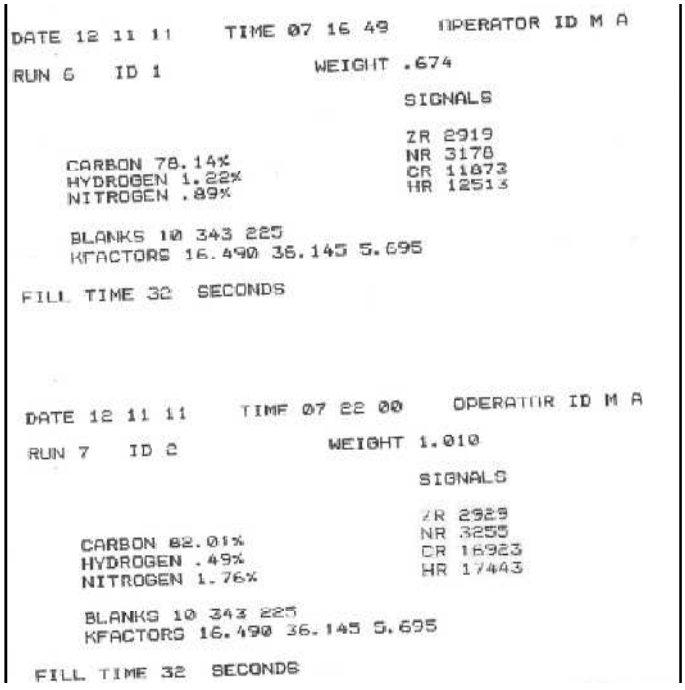

```
DATE 12 11 11     TIME 07 16 49     OPERATOR ID M A

RUN 6    ID 1              WEIGHT .674

                                   SIGNALS

                                   ZR 2919
     CARBON 78.14%                 NR 3178
     HYDROGEN 1.22%                CR 11073
     NITROGEN .89%                 HR 12513

     BLANKS 10 343 225
     KFACTORS 16.490 36.145 5.695

FILL TIME 32  SECONDS


DATE 12 11 11     TIME 07 22 00     OPERATOR ID M A

RUN 7    ID 2              WEIGHT 1.010

                                   SIGNALS

                                   ZR 2929
     CARBON 82.01%                 NR 3255
     HYDROGEN .49%                 CR 16923
     NITROGEN 1.76%                HR 17443

     BLANKS 10 343 225
     KFACTORS 16.490 36.145 5.695

FILL TIME 32  SECONDS
```

Figure B.20: CHN Analysis Report for CeGAC

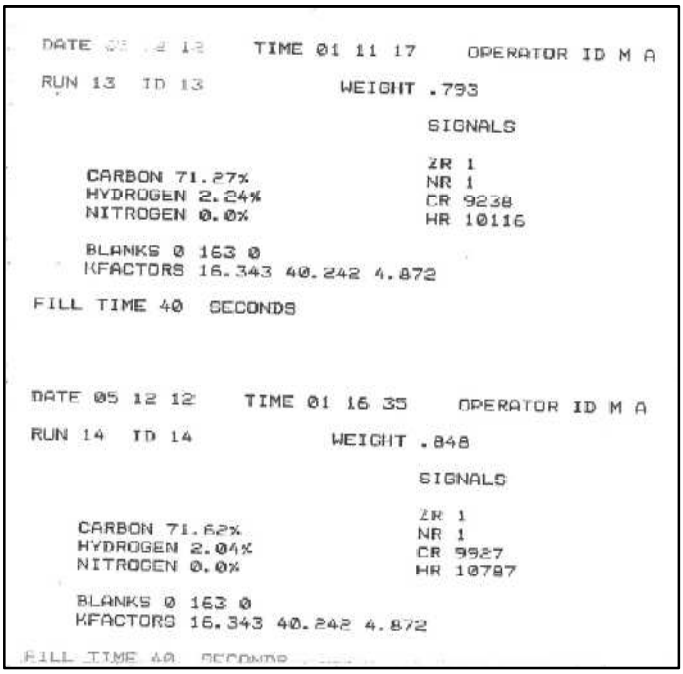

```
DATE 05 12 12     TIME 01 11 17     OPERATOR ID M A
RUN 13  ID 13              WEIGHT .793
                                   SIGNALS
                                   ZR 1
    CARBON 71.27%                  NR 1
    HYDROGEN 2.24%                 CR 9238
    NITROGEN 0.0%                  HR 10116
    BLANKS 0 163 0
    KFACTORS 16.343 40.242 4.872
FILL TIME 40  SECONDS


DATE 05 12 12     TIME 01 16 35     OPERATOR ID M A
RUN 14  ID 14              WEIGHT .848
                                   SIGNALS
                                   ZR 1
    CARBON 71.62%                  NR 1
    HYDROGEN 2.04%                 CR 9927
    NITROGEN 0.0%                  HR 10797
    BLANKS 0 163 0
    KFACTORS 16.343 40.242 4.872
FILL TIME 40  SECONDS
```

Figure B.21: CHN Analysis Report for ACF

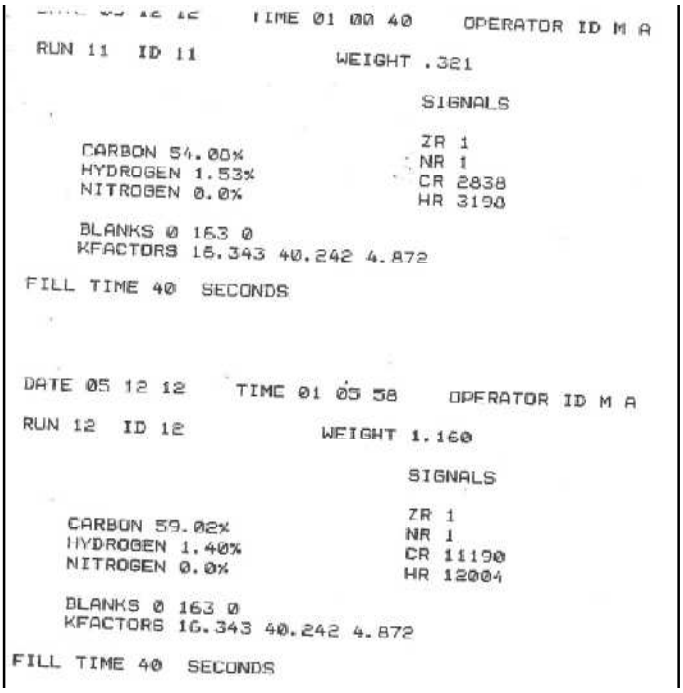

```
                  TIME 01 00 40     OPERATOR ID M A
RUN 11  ID 11              WEIGHT .321
                                   SIGNALS
                                   ZR 1
    CARBON 54.00%                  NR 1
    HYDROGEN 1.53%                 CR 2838
    NITROGEN 0.0%                  HR 3190
    BLANKS 0 163 0
    KFACTORS 16.343 40.242 4.872
FILL TIME 40  SECONDS


DATE 05 12 12     TIME 01 05 58     OPERATOR ID M A
RUN 12  ID 12              WEIGHT 1.160
                                   SIGNALS
                                   ZR 1
    CARBON 59.02%                  NR 1
    HYDROGEN 1.40%                 CR 11190
    NITROGEN 0.0%                  HR 12004
    BLANKS 0 163 0
    KFACTORS 16.343 40.242 4.872
FILL TIME 40  SECONDS
```

Figure B.22: CHN Analysis Report for CeACF

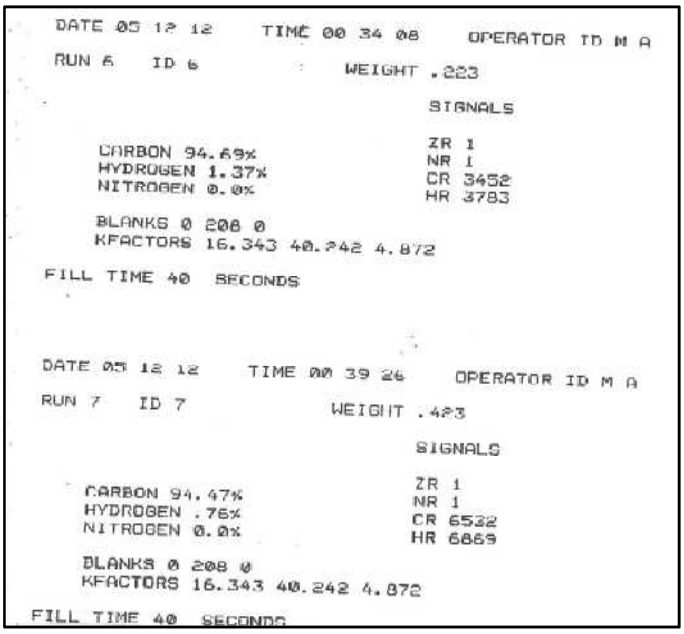

```
DATE 05 12 12     TIME 00 34 08     OPERATOR ID M A

RUN 6    ID 6              WEIGHT .223

                                   SIGNALS

     CARBON 94.69%                 ZR 1
     HYDROGEN 1.37%                NR 1
     NITROGEN 0.0%                 CR 3452
                                   HR 3783

     BLANKS 0 208 0
     KFACTORS 16.343 40.242 4.872

FILL TIME 40  SECONDS


DATE 05 12 12     TIME 00 39 26     OPERATOR ID M A

RUN 7    ID 7              WEIGHT .423

                                   SIGNALS

     CARBON 94.47%                 ZR 1
     HYDROGEN .76%                 NR 1
     NITROGEN 0.0%                 CR 6532
                                   HR 6869

     BLANKS 0 208 0
     KFACTORS 16.343 40.242 4.872

FILL TIME 40  SECONDS
```

Figure B.23: CHN Analysis Report for MWCNTs

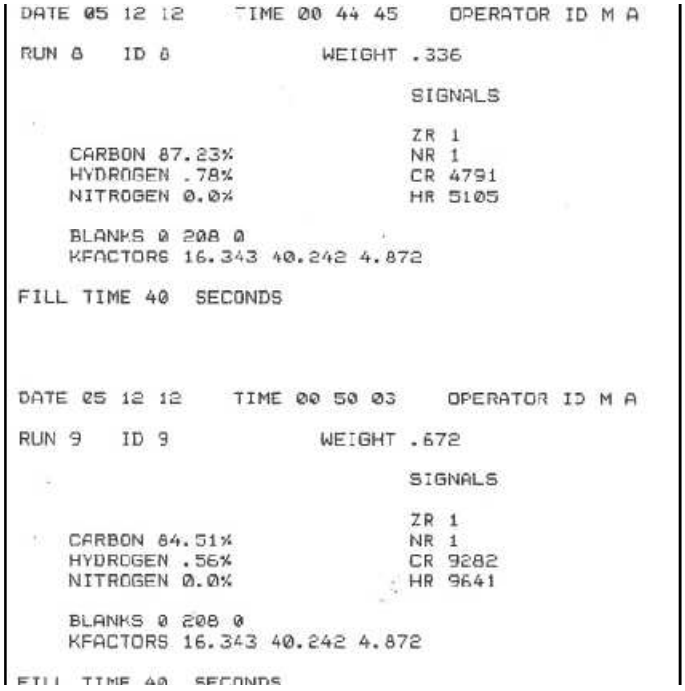

```
DATE 05 12 12     TIME 00 44 45     OPERATOR ID M A

RUN 8    ID 8              WEIGHT .336

                                   SIGNALS

                                   ZR 1
     CARBON 87.23%                 NR 1
     HYDROGEN .78%                 CR 4791
     NITROGEN 0.0%                 HR 5105

     BLANKS 0 208 0
     KFACTORS 16.343 40.242 4.872

FILL TIME 40  SECONDS


DATE 05 12 12     TIME 00 50 03     OPERATOR ID M A

RUN 9    ID 9              WEIGHT .672

                                   SIGNALS

                                   ZR 1
     CARBON 84.51%                 NR 1
     HYDROGEN .56%                 CR 9282
     NITROGEN 0.0%                 HR 9641

     BLANKS 0 208 0
     KFACTORS 16.343 40.242 4.872

FILL TIME 40  SECONDS
```

Figure B.24: CHN Analysis Report for CeMWCNTs

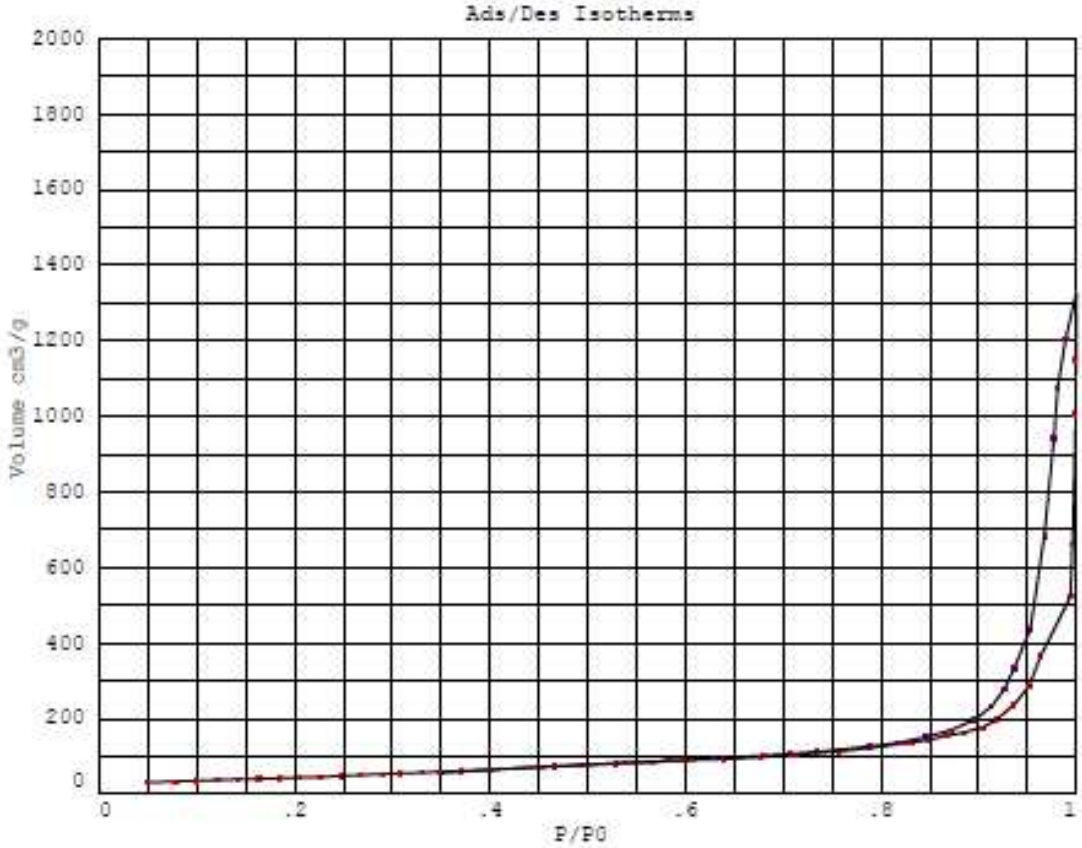

RESULTS

Calculation Method < B.E.T. >

<B.E.T.> Initial-final P/P0 :	.04 - .3
Specific surface calculations	
Monolayer volume (cm3/g) :	39.0948715
Specific surface area (m^2/g) :	170.187759
C value of BET equation :	45.455
Correlation factor :	.9988024
Pore specific volume (cm3/g) :	.36520666
Pore specific volume at P/P0 :	.95
Total Adsorbed volume (cm3/g) :	1326.39078
(Dol./Heal)	
Cumulative area max. (m^2/g) :	180.231628
Pore volume max. (cm3/g) :	.523475349

Figure B.25: BET Analysis Report for MWCNTs

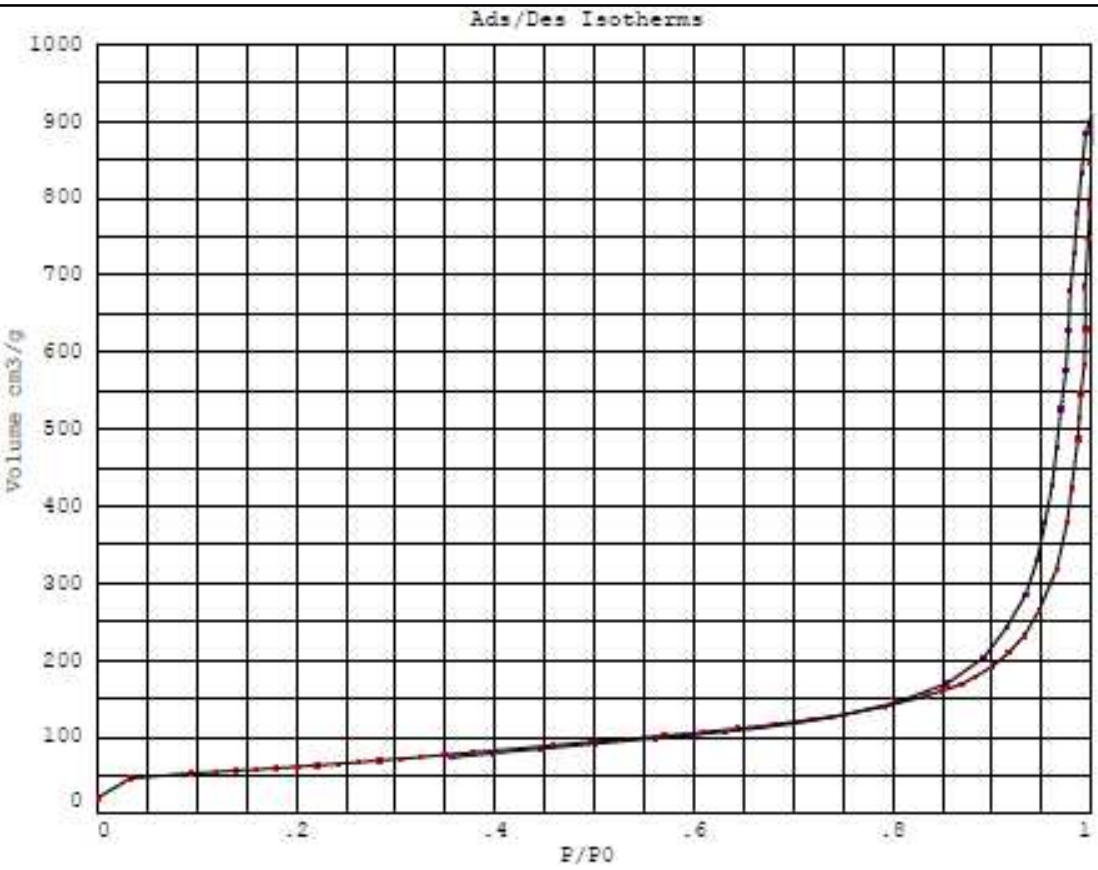

RESULTS

Calculation Method < B.E.T. >

<B.E.T.> Initial-final P/P0 :	.04 - .3
Specific surface calculations	
Monolayer volume (cm3/g) :	50.6397438
Specific surface area (m²/g) :	220.444885
C value of BET equation :	157.0984
Correlation factor :	.9999866
Pore specific volume (cm3/g) :	.40961367
Pore specific volume at P/P0 :	.95
Total Adsorbed volume (cm3/g) :	908.39163
(Dol./Heal)	
Cumulative area max. (m²/g) :	158.422836
Pore volume max. (cm3/g) :	.486813158

Figure B.26: BET Analysis Report for CeMWCNTs

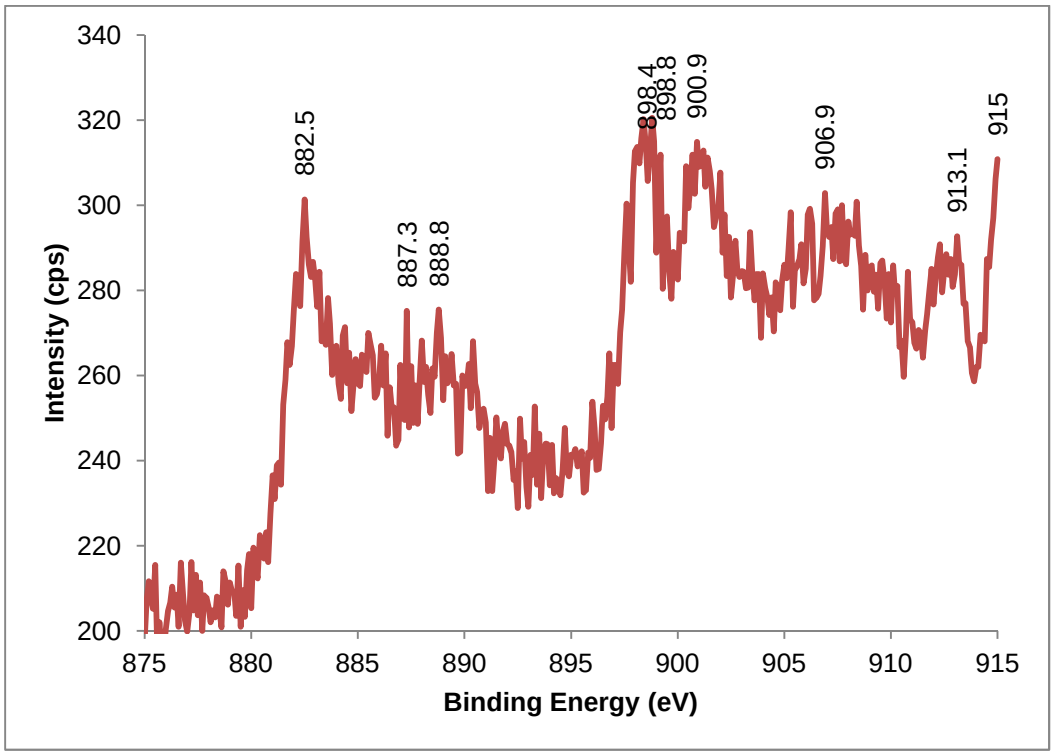

Figure B.26: XPS Results Peak Identification for CeGAC

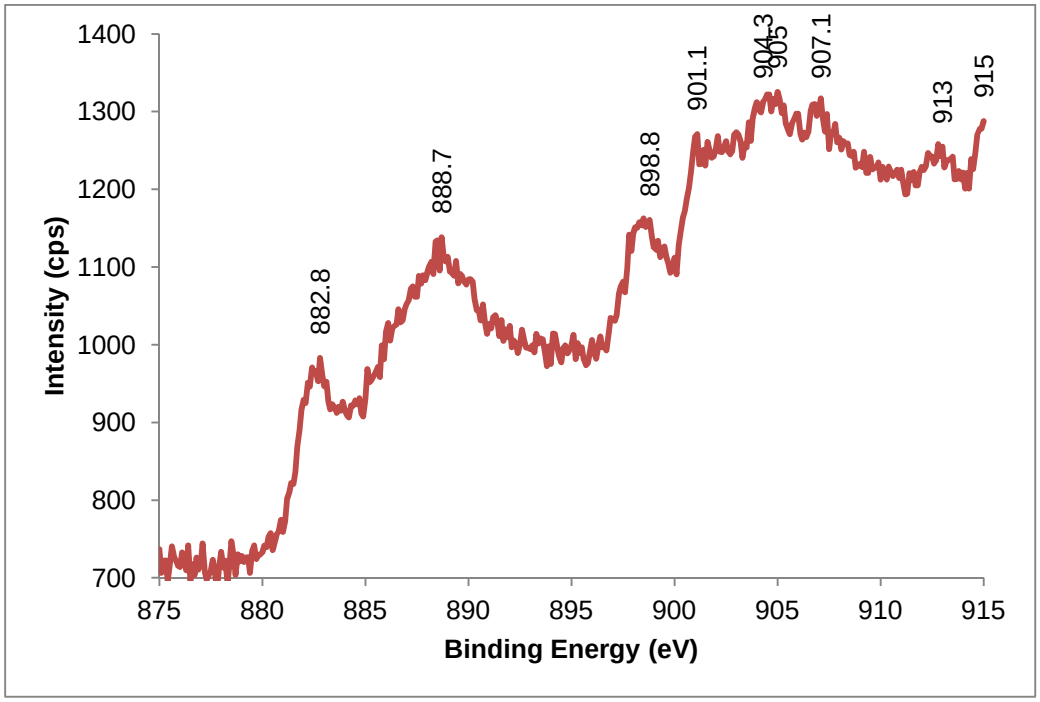

Figure B.27: XPS Results Peak Identification for CeACF

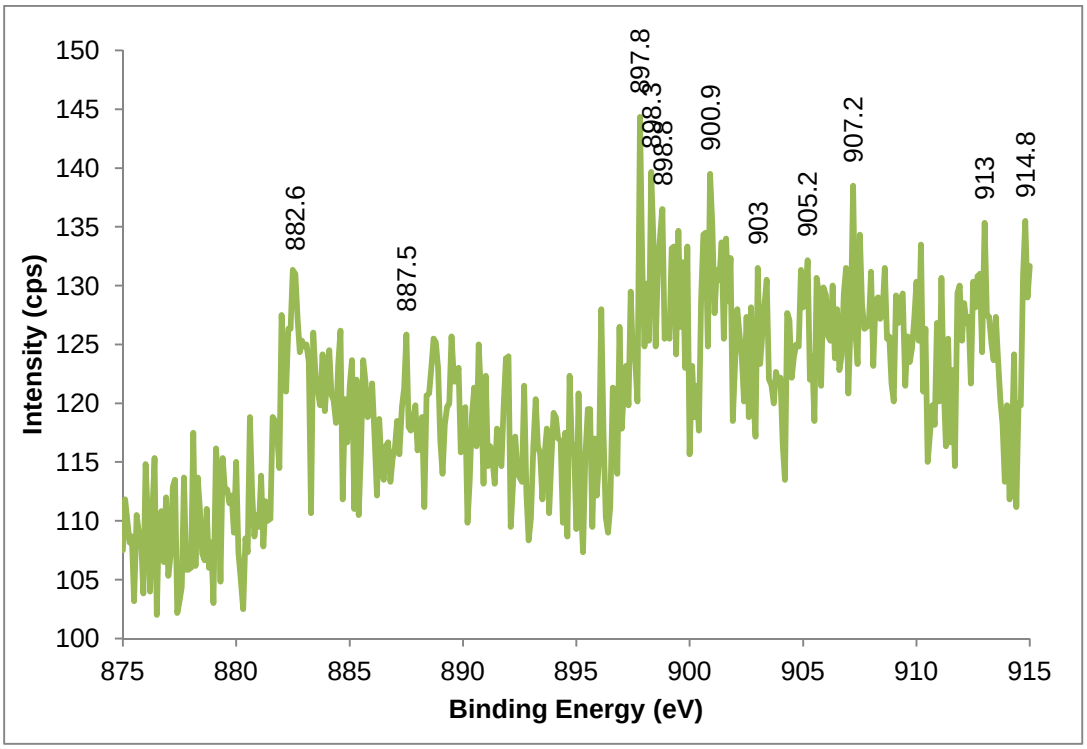

Figure B.28: XPS Results Peak Identification for CeMWCNTs

APPENDIX C

CATALYST ACTIVITY TEST

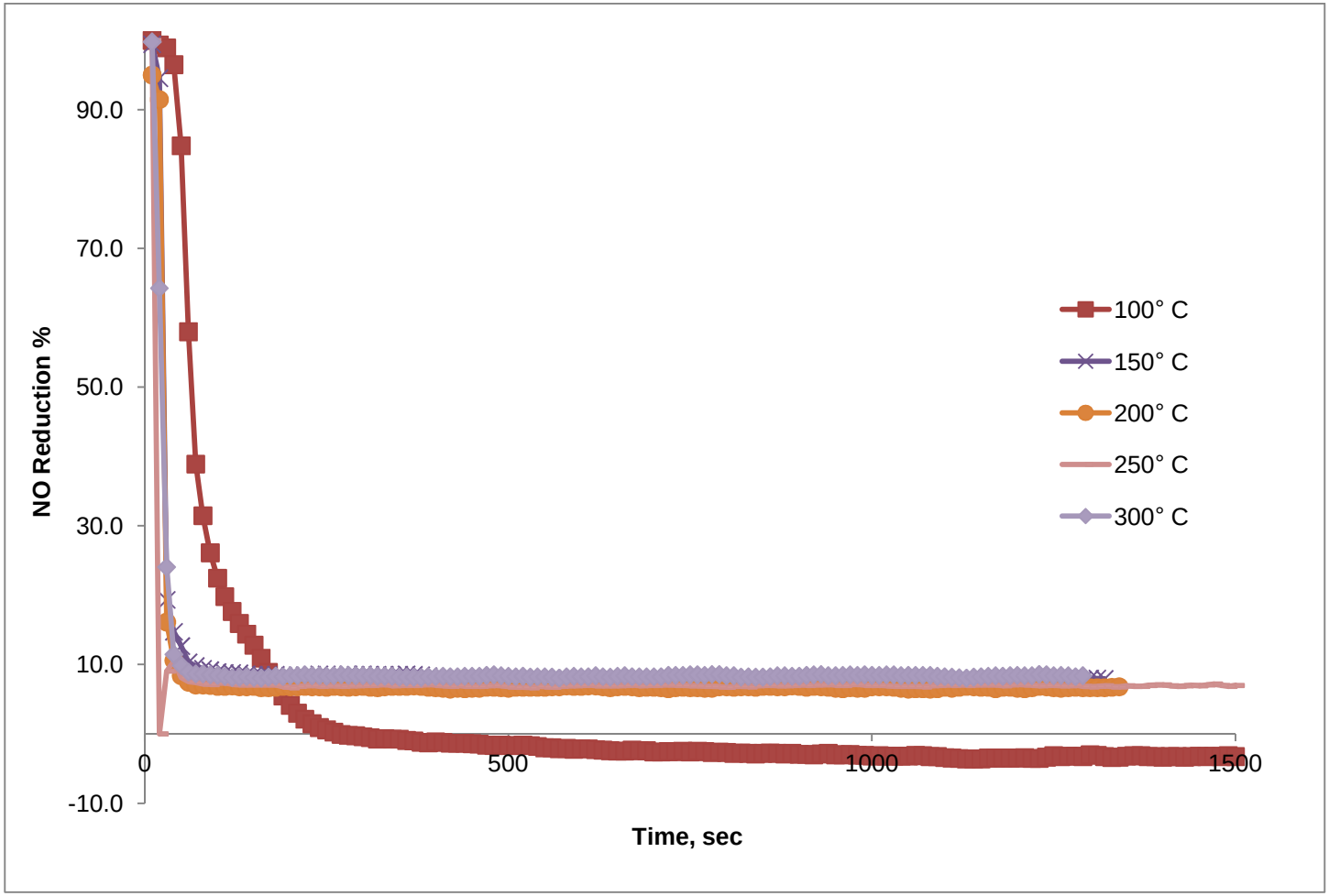

Figure C.1: NO Reduction Percentage for Low NOx GAC

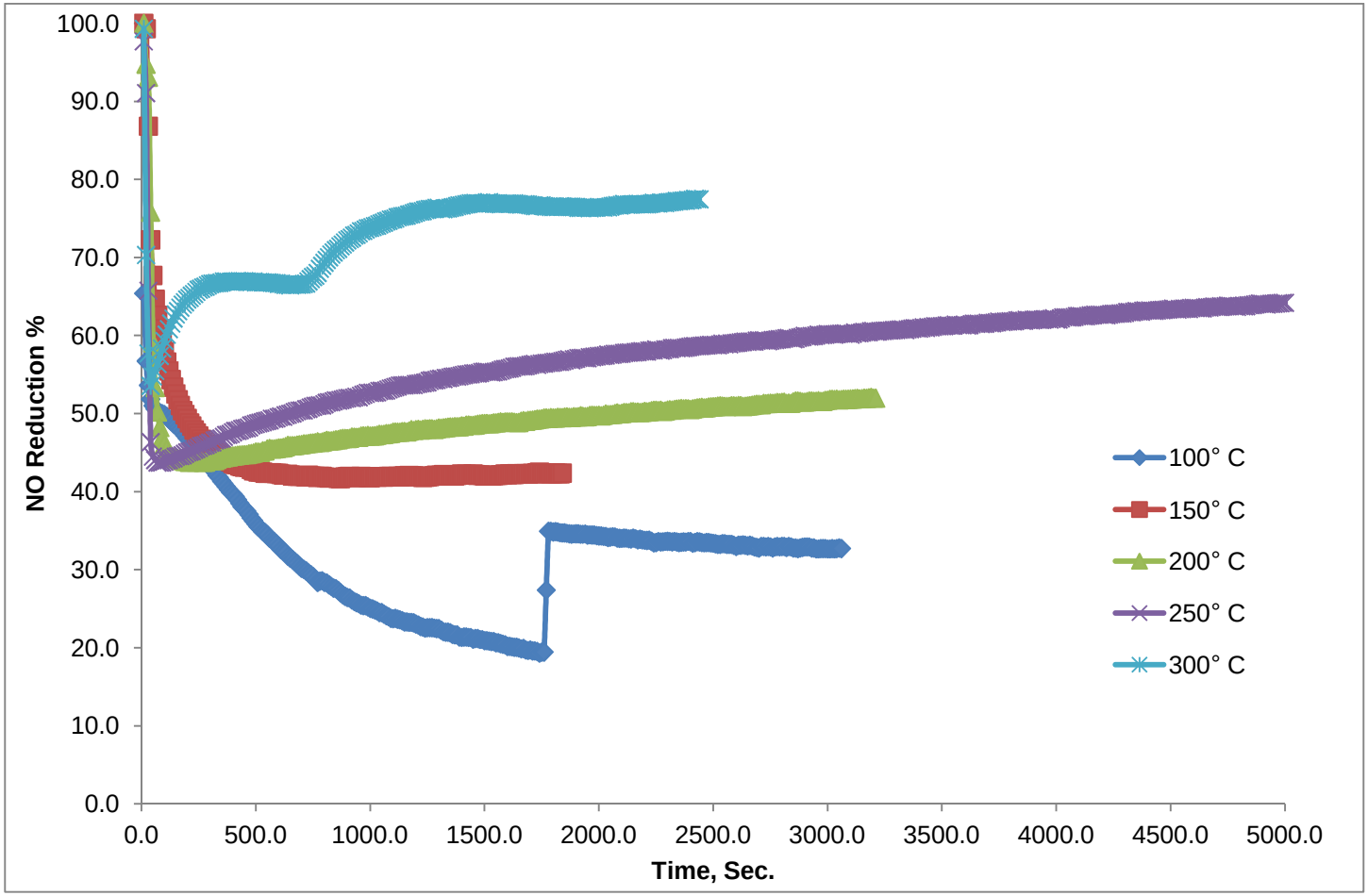

Figure C.2: NO Reduction Percentage for Low NOx CeGAC

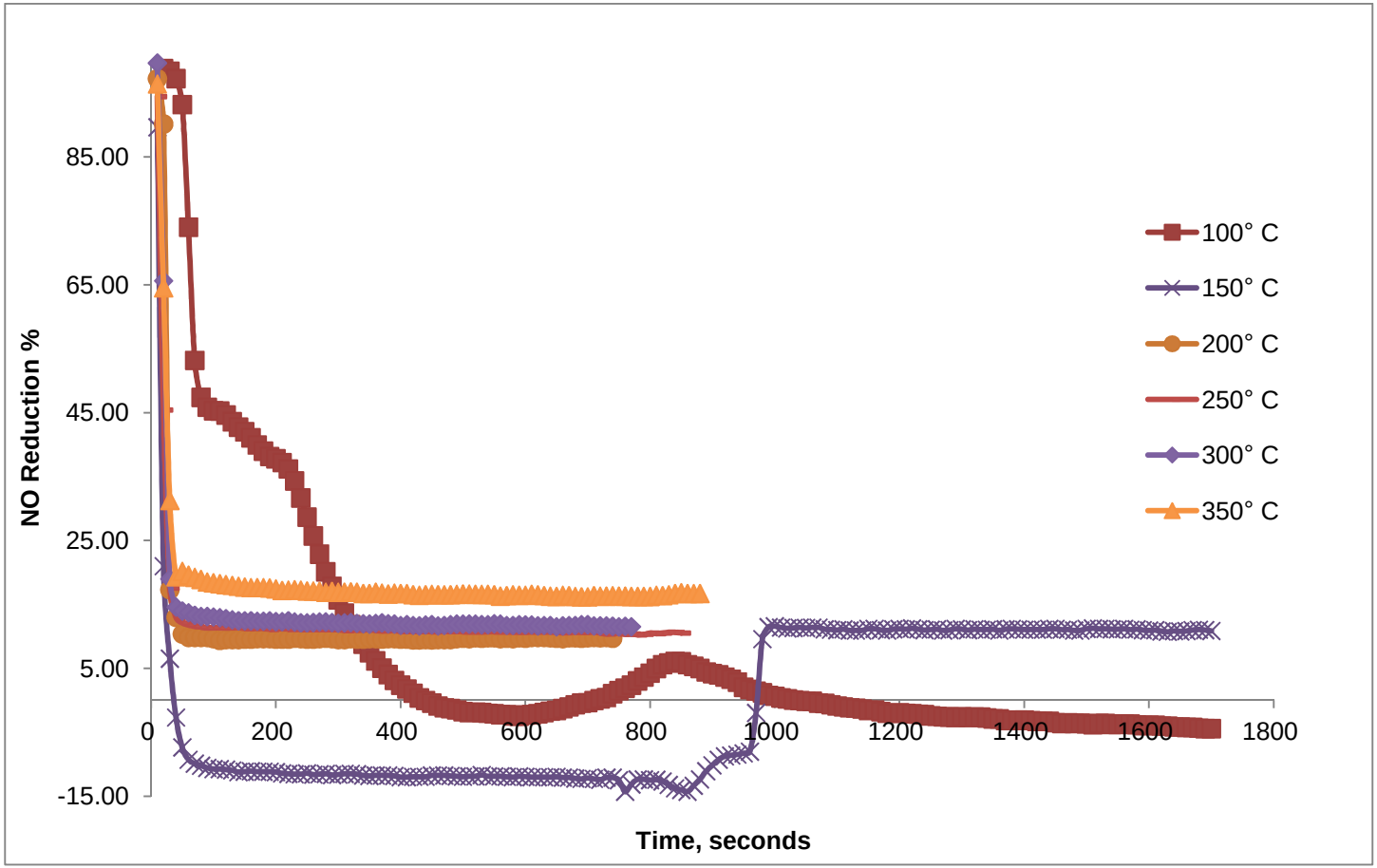

Figure C.3: NO Reduction Percentage for Low NOx ACF

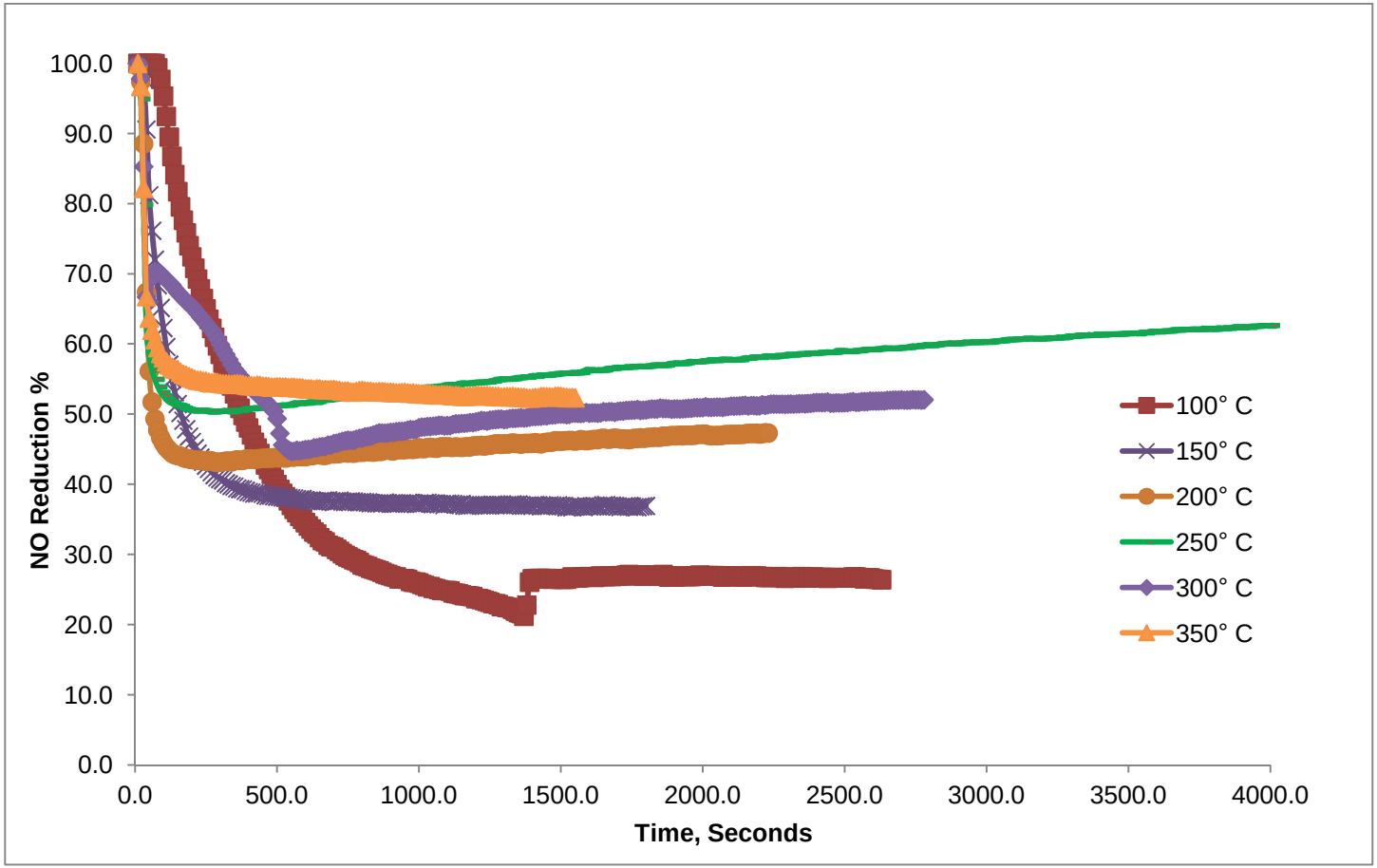

Figure C.4: NO Reduction Percentage for Low NOx CeACF

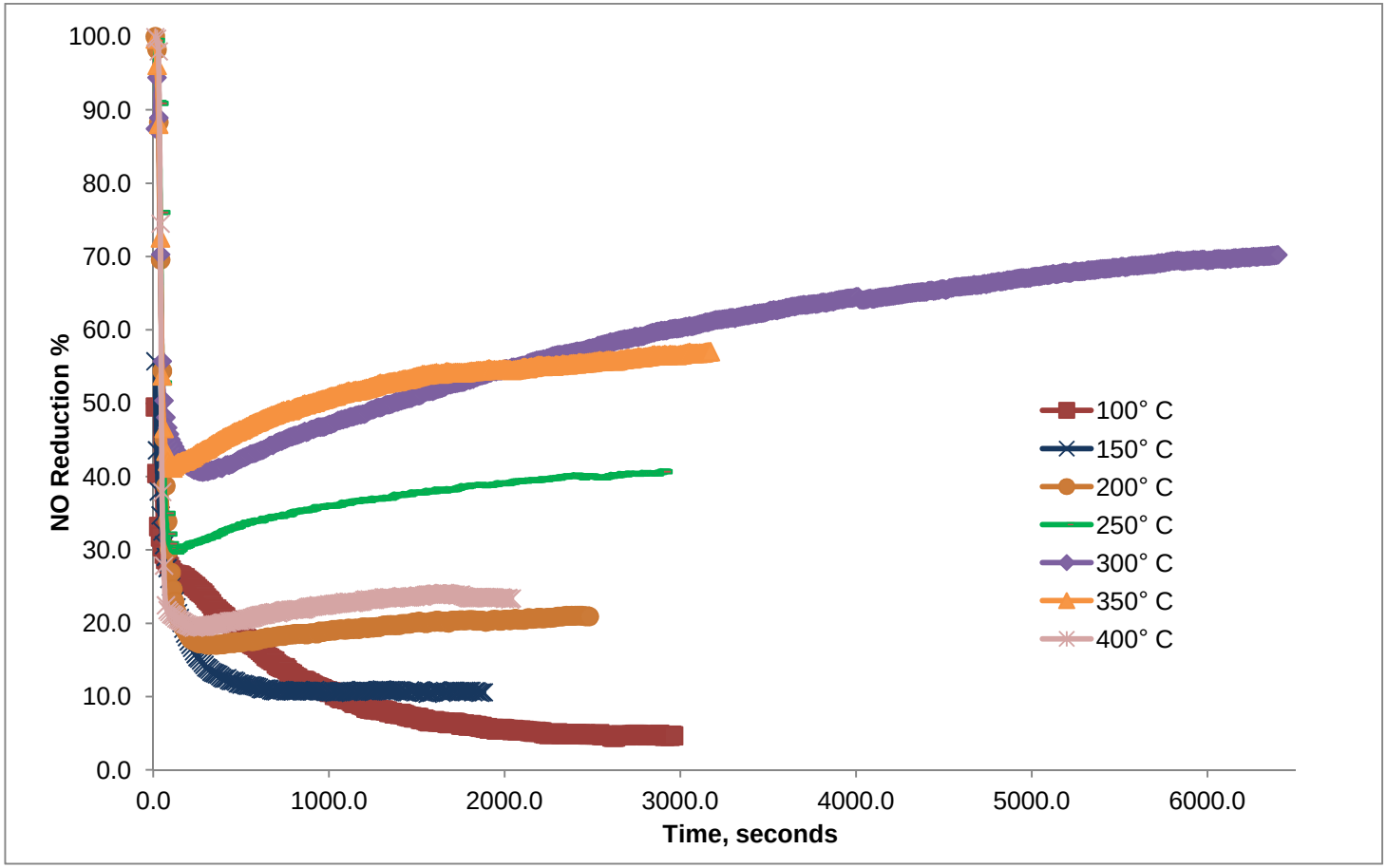

Figure C.5: NO Reduction Percentage for Low NOx CeMWCNTs

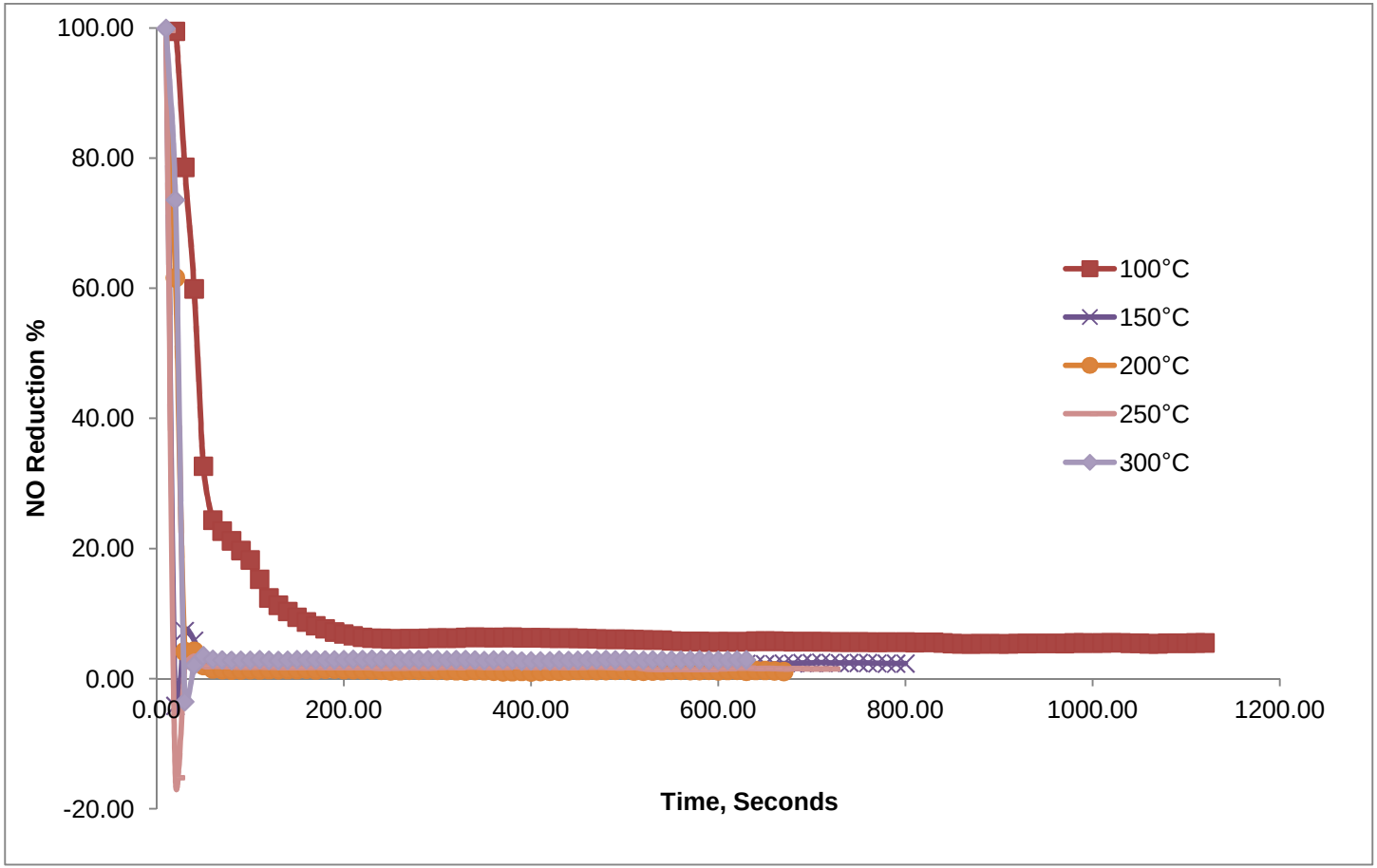

Figure C.6: NO Reduction Percentage for High NOx GAC

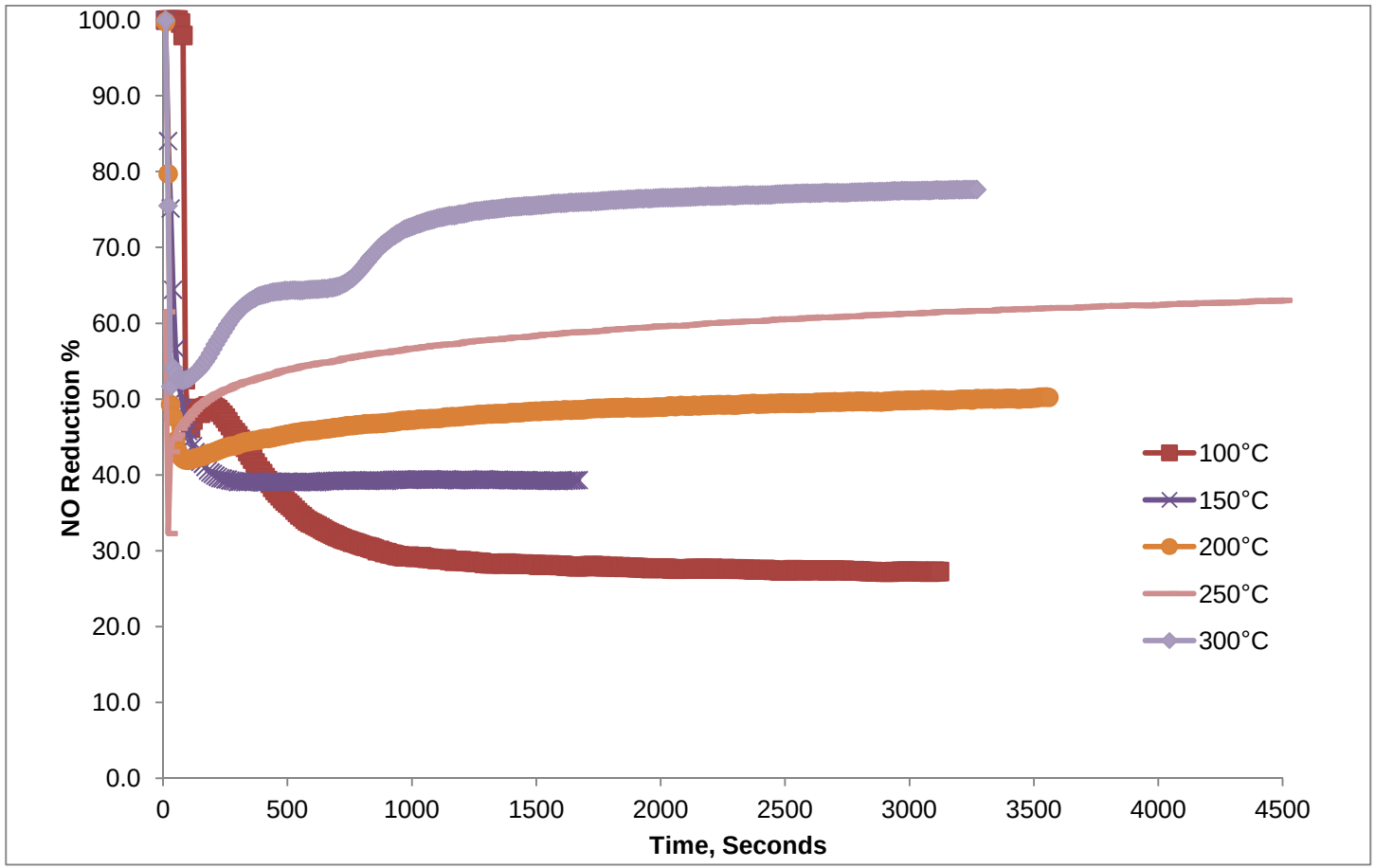

Figure C.7: NO Reduction Percentage for High NOx CeGAC

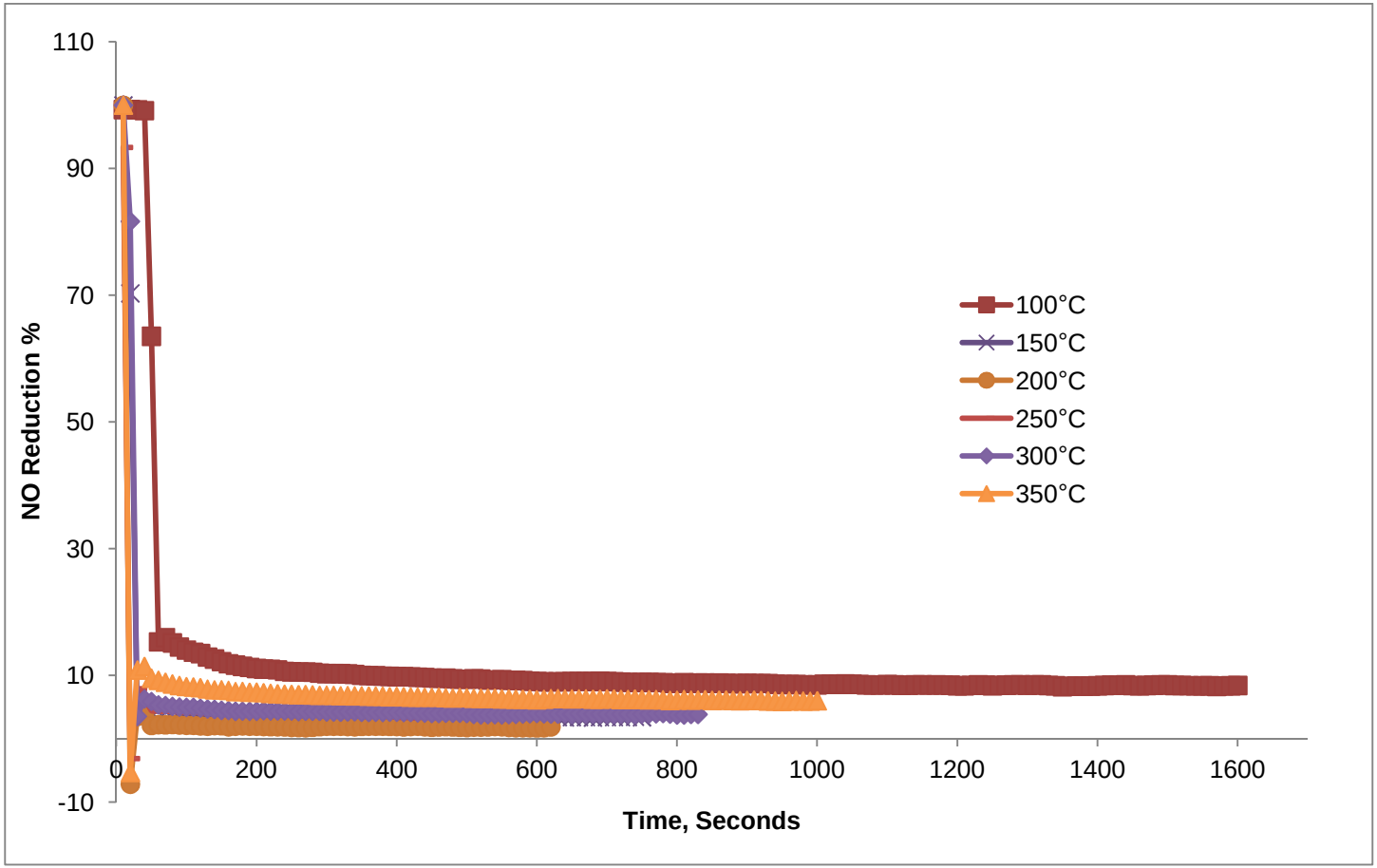

Figure C.8: NO Reduction Percentage for High NOx ACF

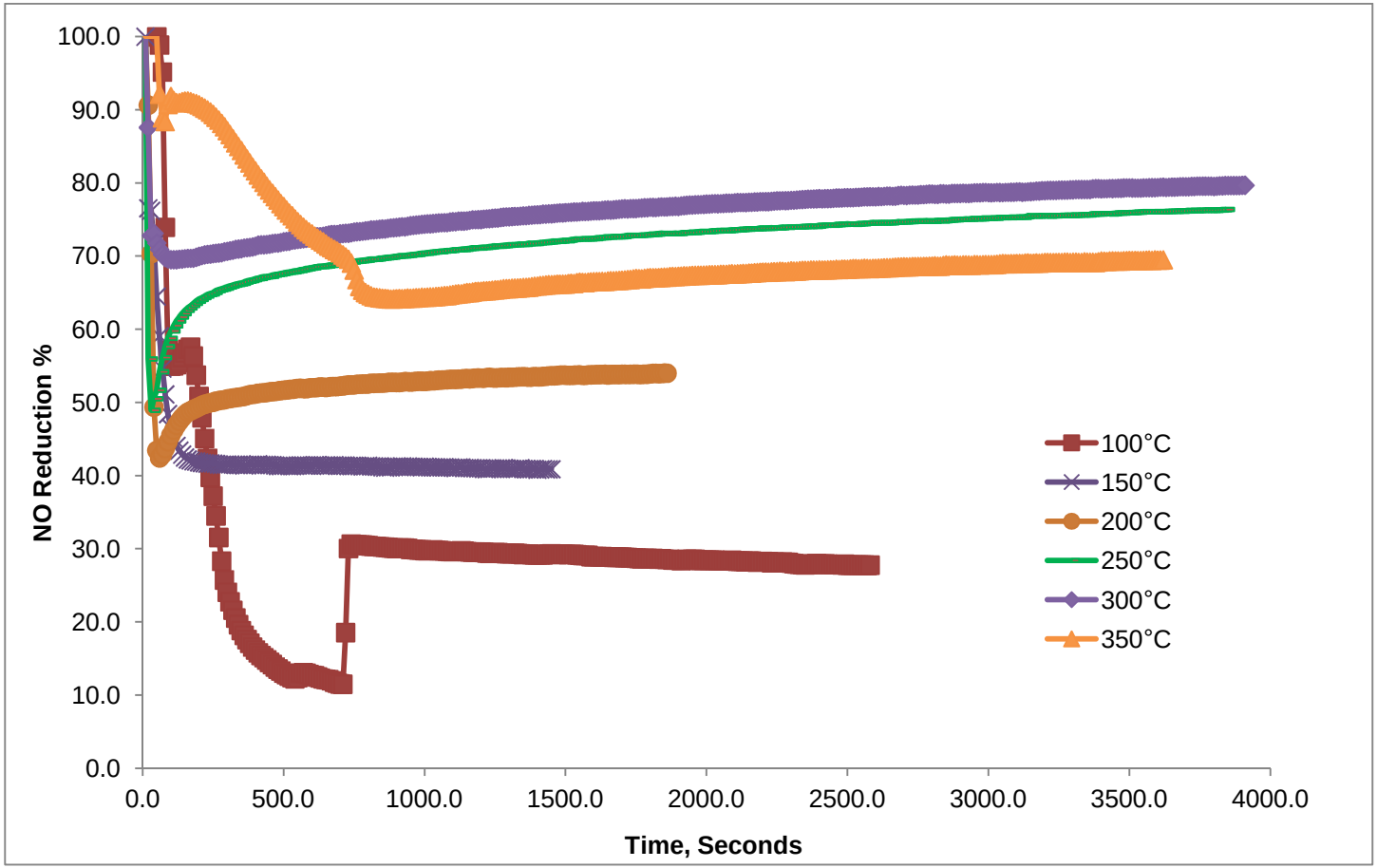

Figure C.9: NO Reduction Percentage for High NOx CeACF

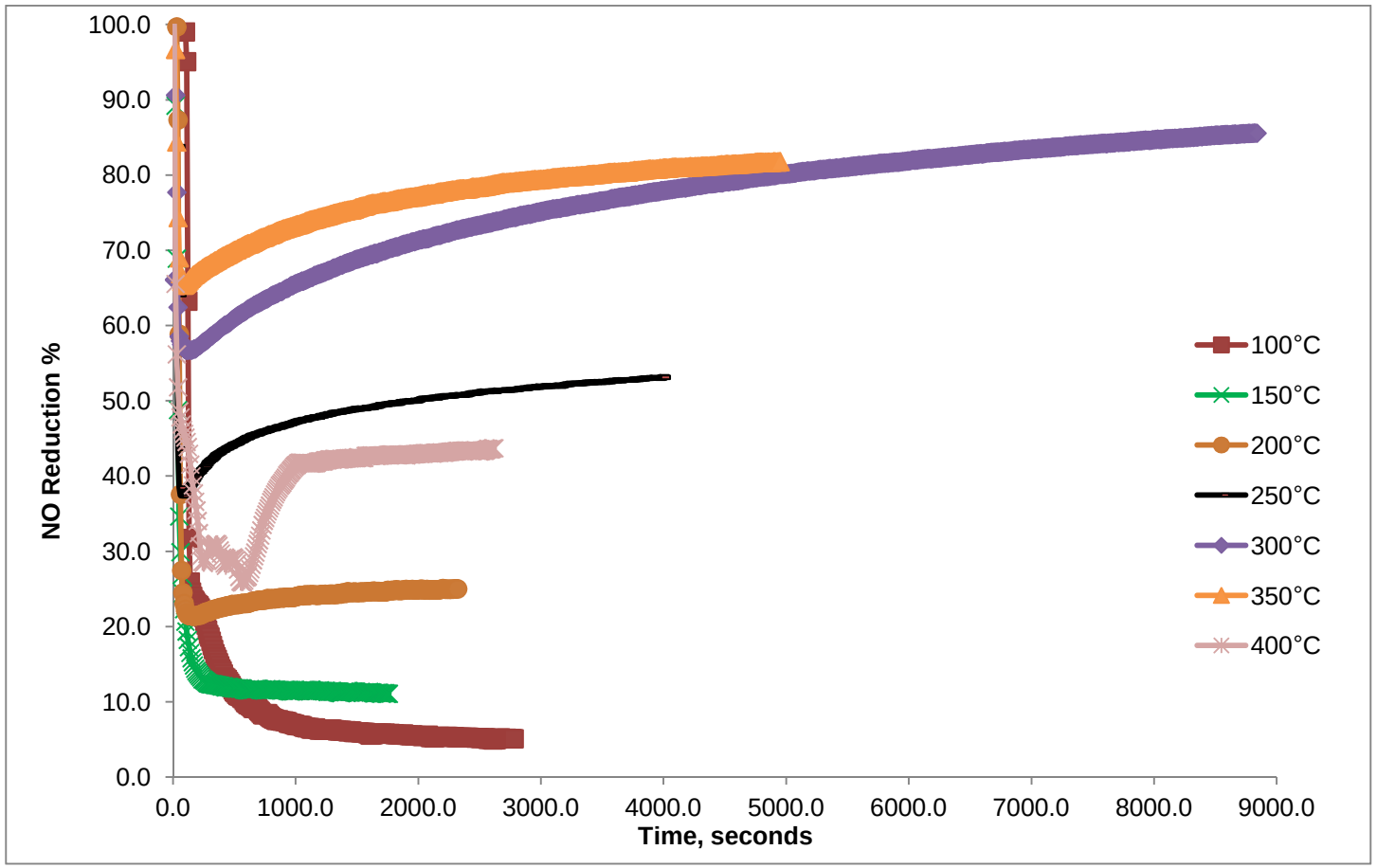

Figure C.10: NO Reduction Percentage for High NOx CeMWCNTs

REFERENCES

Ajayan P. 1999. Nanotubes from carbon. ChemInform 30(39).

Banares MA and Wachs IE. 2002. Molecular structures of supported metal oxide catalysts under different environments. J Raman Spectrosc 33(5):359-80.

Banares MA and Mestl G. Chapter 2 structural characterization of operating catalysts by raman spectroscopy. In: Advances in catalysis. Academic Press. 43 p.

Benfell KE, Beamish BB, Rodgers KA. 1996. Thermogravimetric analytical procedures for characterizing new zealand and eastern australian coals. Thermochimica Acta 286(1):67-
74.

Bhattacharyya S and Das RK. 2001. Catalytic reduction of NOx in gasoline engine exhaust over copper- and nickel-exchanged X–zeolite catalysts. Energy Conversion and Management
42(15-17):2019-27.

Boyano A, Lázaro MJ, Cristiani C, Maldonado-Hodar FJ, Forzatti P, Moliner R. 2009. A comparative study of V2O5/AC and V2O5/Al2O3 catalysts for the selective catalytic reduction of NO by NH3. Chem Eng J 149(1-3):173-82.

Bruggemann TC and Keil FJ. 2008. Theoretical investigation of the mechanism of the selective catalytic reduction of nitric oxide with ammonia on H-form zeolites. The Journal of Physical Chemistry C 112(44):17378-87.

Centi G and Perathoner S. 2007. Chapter 1 introduction: State of the art in the development of catalytic processes for the selective catalytic reduction of NOx into N2. In: Studies in surface science and catalysis. P. Granger and V.I. Pârvulescu, editor. Elsevier. 1 p.

Centi G and Perathoner S. Chapter 1 introduction: State of the art in the development of catalytic processes for the selective catalytic reduction of NOx into N2. In: Studies in surface science and catalysis. Elsevier. 1 p.

Chen X, Gao S, Wang H, Liu Y, Wu Z. 2011. Selective catalytic reduction of NO over carbon nanotubes supported CeO2. Catalysis Communications 14(1):1-5.

Chong M, Cheng D, Liu L, Chen F, Zhan X. 2007. Deactivation of CeO 2 catalyst in the hydrogenation of benzoic acid to benzaldehyde. Catalysis Letters 114(3):198-201.

Colombo M, Nova I, Tronconi E. 2012. A simplified approach to modeling of dual-layer

ammonia slip catalysts. Chemical Engineering Science 75(0):75-83.

Fan X, Qiu F, Yang H, Tian W, Hou T, Zhang X. 2011. Selective catalytic reduction of NOX with ammonia over Mn–Ce–OX/TiO2-carbon nanotube composites. Catalysis Communications 12(14):1298-301.

Faria PCC, Órfão JJM, Pereira MFR. 2008. A novel ceria–activated carbon composite for the catalytic ozonation of carboxylic acids. Catalysis Communications 9(11–12):2121-6.

Gao HO and Niemeier DA. 2008. Using functional data analysis of diurnal ozone and NOx cycles to inform transportation emissions control. Transportation Research Part D: Transport and Environment 13(4):221-38.

Gao X, Liu S, Zhang Y, Luo Z, Cen K. 2011. Physicochemical properties of metal-doped activated carbons and relationship with their performance in the removal of SO2 and NO. J Hazard Mater 188(1-3):58-66.

Garcia-Cortes JM, Illán-Gómez MJ, Linares-Solano A, de Lecea CS. Selective catalytic reduction of NOx with C3H6 under lean-burn conditions on activated carbon-supported metals. In: Studies in surface science and catalysis. Elsevier. 1427 p.

Gomez-Garcia MA, Pitchon V, Kiennemann A. 2005. Pollution by nitrogen oxides: An approach to NOx abatement by using sorbing catalytic materials. Environ Int 31(3):445-67.

Hamlaoui Y, Pedraza F, Remazeilles C, Cohendoz S, Rébéré C, Tifouti L, Creus J. 2009. Cathodic electrodeposition of cerium-based oxides on carbon steel from concentrated cerium nitrate solutions: Part I. electrochemical and analytical characterisation. Mater Chem Phys 113(2–3):650-7.

Heck RM. 1999. Catalytic abatement of nitrogen oxides–stationary applications. Catalysis Today 53(4):519-23.

Huang B, Huang R, Jin D, Ye D. 2007. Low temperature SCR of NO with NH3 over carbon nanotubes supported vanadium oxides. Catalysis Today 126(3-4):279-83.

Huang H, Ye D, Huang B, Wei Z. 2008. Vanadium supported on viscose-based activated carbon fibers modified by oxygen plasma for the SCR of NO. Catalysis Today 139(1–2):100-8.

Kaspar J, Fornasiero P, Graziani M. 1999. Use of CeO2-based oxides in the three-way catalysis. Catalysis Today 50(2):285-98.

Kilbourn BT. 2000. Cerium and cerium compounds. In: Kirk-othmer encyclopedia of chemical technology. John Wiley & Sons, Inc.

Konova P, Arve K, Klingstedt F, Nikolov P, Naydenov A, Kumar N, Murzin DY. 2007. A combination of Ag/alumina and ag modified ZSM-5 to remove NOx and CO during lean conditions. Applied Catalysis B: Environmental 70(1-4):138-45.

Kosacki I, Suzuki T, Anderson HU, Colomban P. 2002. Raman scattering and lattice defects in nanocrystalline CeO2 thin films. Solid State Ionics 149(1–2):99-105.

Larouche F, Smiljanic O, Sun X, Stansfield BL. 2005. Solutal Bénard–Marangoni instability as a

growth mechanism for single-walled carbon nanotubes Carbon 43(5):986.

Li C, Lu P, Zeng G, Wang Q, Li Q, He L, Zhai Y. 2008. Catalytic purification of NO over active carbon fiber-loaded La2O3 catalysts. Huan Jing Ke Xue= Huanjing Kexue/[Bian ji,Zhongguo Ke Xue Yuan Huan Jing Ke Xue Wei Yuan Hui" Huan Jing Ke Xue" Bian Ji WeiYuan Hui 29(11):3280.

Li J, Chen J, Ke R, Luo C, Hao J. 2007. Effects of precursors on the surface mn species and the activities for NO reduction over MnOx/TiO2 catalysts. Catalysis Communications 8(12):1896-900.

Li Q, Yang H, Ma Z, Zhang X. 2012. Selective catalytic reduction of NO with NH3 over CuOX-carbonaceous materials. Catalysis Communications 17(0):8-12.

Li Q, Yang H, Qiu F, Zhang X. 2011. Promotional effects of carbon nanotubes on V2O5/TiO2 for NOX removal. J Hazard Mater 192(2):915-21.

Liu Y, Hayakawa T, Suzuki K, Hamakawa S, Tsunoda T, Ishii T, Kumagai M. 2002. Highly active copper/ceria catalysts for steam reforming of methanol. Applied Catalysis A: General 223(1–2):137-45.

Liu Z, Wang A, Wang X, Zhang T. 2008. Ir–C xerogels synthesized by sol–gel method for NO reduction. Catalysis Today 137(2–4):162-6.

Liu Z and Ihl Woo S. 2006. Recent advances in catalytic DeNOX science and technology. Catalysis Reviews 48(1):43-89.

Lu C and Wey M. 2007. Simultaneous removal of VOC and NO by activated carbon impregnated with transition metal catalysts in combustion flue gas. Fuel Process Technol 88(6):557-67.

Lu P, Li C, Zeng G, He L, Peng D, Cui H, Li S, Zhai Y. 2010. Low temperature selective catalytic reduction of NO by activated carbon fiber loading lanthanum oxide and ceria. Applied Catalysis B: Environmental 96(1–2):157-61.

Maldonado-Hodar F, Moreno-Castilla C, Rivera-Utrilla J, Hanzawa Y, Yamada Y. 2000. Catalytic graphitization of carbon aerogels by transition metals. Langmuir 16(9):4367-73.

Maria Suzana P and Mastelaro VR. 2002. Inhibition of the anatase-rutile phase transformation with addition of CeO2 to CuO-TiO2 system: Raman spectroscopy, X-ray diffraction, and textural studies. Chemistry of Materials 14(6):2514-8.

Matharu J, Cabailh G, Lindsay R, Pang CL, Grinter DC, Skála T, Thornton G. 2011. Reduction of thin-film ceria on pt(111) by supported pd nanoparticles probed with resonant photoemission. Surf Sci 605(11–12):1062-6.

Maunula T, Kintaichi Y, Inaba M, Haneda M, Sato K, Hamada H. 1998. Enhanced activity of in and ga-supported sol-gel alumina catalysts for NO reduction by hydrocarbons in lean conditions. Applied Catalysis B: Environmental 15(3–4):291-304.

Mochida I, Korai Y, Shirahama M, Kawano S, Hada T, Seo Y, Yoshikawa M, Yasutake A. 2000. Removal of SOx and NOx over activated carbon fibers. Carbon 38(2):227-39.

Muller J-, Su DS, Jentoft RE, Kröhnert J, Jentoft FC, Schlögl R. 2005. Morphology-controlled reactivity of carbonaceous materials towards oxidation. Catalysis Today 102–103(0):259-65.

Muzio LJ and Quartucy GC. 1997. Implementing NOx control: Research to application. Progress in Energy and Combustion Science 23(3):233-66.

Nakatsuji T, Yasukawa R, Tabata K, Ueda K, Niwa M. 1999. A highly durable catalytic NOx reduction in the presence of SOx using periodic two steps, an operation in oxidizing conditions and a relatively short operation in reducing conditions. Applied Catalysis B: Environmental 21(2):121-31.

Nejar N and Illán-Gómez MJ. 2007. Potassium–copper and potassium–cobalt catalysts supported on alumina for simultaneous NOx and soot removal from simulated diesel engine exhaust. Applied Catalysis B: Environmental 70(1-4):261-8.

Rathore RS, Srivastava DK, Agarwal AK, Verma N. 2010. Development of surface functionalized activated carbon fiber for control of NO and particulate matter. J Hazard Mater 173(1-3):211-22.

Reinhardt K and Winkler H. 2000. Cerium mischmetal, cerium alloys, and cerium compounds. In: Ullmann's encyclopedia of industrial chemistry. Wiley-VCH Verlag GmbH & Co. KGaA.

Ren X, Chen C, Nagatsu M, Wang X. 2011. Carbon nanotubes as adsorbents in environmental pollution management: A review. Chem Eng J 170(2–3):395-410.

Roy S, Hegde MS, Madras G. 2009. Catalysis for NOx abatement. Appl Energy 86(11):2283-97.

Santillan-Jimenez E, Miljković-Kocić V, Crocker M, Wilson K. 2011. Carbon nanotube-supported metal catalysts for NOx reduction using hydrocarbon reductants. part 1: Catalyst preparation, characterization and NOx reduction characteristics. Applied Catalysis B: Environmental 102(1-2):1-8.

Setiabudi A, Makkee M, Moulijn JA. 2004. The role of NO2 and O2 in the accelerated combustion of soot in diesel exhaust gases. Applied Catalysis B: Environmental 50(3):185-94.

Siokou A, Ntais S, Dracopoulos V, Papaefthimiou S, Leftheriotis G, Yianoulis P. 2006. Substrate related structural, electronic and electrochemical properties of evaporated CeOx ion storage layers. Thin Solid Films 514(1–2):87-96.

Skalska K, Miller JS, Ledakowicz S. 2010. Trends in NOx abatement: A review. Sci Total Environ 408(19):3976-89.

Skarman B, Grandjean D, Benfield RE, Hinz A, Andersson A, Wallenberg LR. 2002. Carbon monoxide oxidation on nanostructured CuOx/CeO2 composite particles characterized by HREM, XPS, XAS, and high-energy diffraction. Journal of Catalysis 211(1):119-33.

Sumathi S, Bhatia S, Lee KT, Mohamed AR. 2010. Cerium impregnated palm shell activated carbon (Ce/PSAC) sorbent for simultaneous removal of SO2 and NO—Process study. Chem Eng J 162(1):51-7.

Tang Q, Huang X, Chen Y, Liu T, Yang Y. 2009. Characterization and catalytic application of highly dispersed manganese oxides supported on activated carbon. Journal of Molecular Catalysis A: Chemical 301(1–2):24-30.

Traa Y, Burger B, Weitkamp J. 1999. Zeolite-based materials for the selective catalytic reduction of NOx with hydrocarbons. Microporous and Mesoporous Materials 30(1):3-41.

Trovarelli A. 1996. Catalytic properties of ceria and CeO2-containing materials. Catalysis Reviews 38(4):439-520.

Wang L, Huang B, Su Y, Zhou G, Wang K, Luo H, Ye D. 2012. Manganese oxides supported on multi-walled carbon nanotubes for selective catalytic reduction of NO with NH3: Catalytic activity and characterization. Chem Eng J 192(0):232-41.

Wang S, Wang W, Zuo J, Qian Y. 2001. Study of the raman spectrum of CeO2 nanometer thin films. Mater Chem Phys 68(1–3):246-8.

Wang Y, Liu Z, Zhan L, Huang Z, Liu Q, Ma J. 2004. Performance of an activated carbon honeycomb supported V2O5 catalyst in simultaneous SO2 and NO removal. Chemical Engineering Science 59(22-23):5283-90.

Warne SSJ. 1991. Proximate analysis of coal, oil shale, low quality fossil fuels and related materials by thermogravimetry. TrAC Trends in Analytical Chemistry 10(6):195-9.

Xu L, McCabe RW, Hammerle RH. 2002. NOx self-inhibition in selective catalytic reduction with urea (ammonia) over a cu-zeolite catalyst in diesel exhaust. Applied Catalysis B: Environmental 39(1):51-63.

Yahiro H and Iwamoto M. 2001. Copper ion-exchanged zeolite catalysts in deNOx reaction. Applied Catalysis A: General 222(1-2):163-81.

Yang J, Zhuang TT, Wei F, Zhou Y, Cao Y, Wu ZY, Zhu JH, Liu C. 2009. Adsorption of nitrogen oxides by the moisture-saturated zeolites in gas stream. J Hazard Mater 162(2-3):866-73.

Yoshikawa M, Yasutake A, Mochida I. 1998. Low-temperature selective catalytic reduction of NOx by metal oxides supported on active carbon fibers. Applied Catalysis A: General 173(2):239-45.

Yun BK and Kim MY. Modeling the selective catalytic reduction of NOx by ammonia over a vanadia-based catalyst from heavy duty diesel exhaust gases. Appl Therm Eng (0).

Zhang F, Wang P, Koberstein J, Khalid S, Chan S. 2004. Cerium oxidation state in ceria nanoparticles studied with X-ray photoelectron spectroscopy and absorption near edge spectroscopy. Surf Sci 563(1–3):74-8.

BIOGRAPHICAL INFORMATION

Annaprabha Athappan, raised in Madurai, India, graduated in 1998 from St. Joseph High Secondary School. She continued her education as an undergraduate in PSNA College of Engineering and Technology, India. She chose civil engineering to become a structural engineer but she became more interested in environmental engineering during her program of work. It motivated her to do undergraduate project on “Necessary Ban on Leaded Petrol”. She pursued her studies as a master’s student at the University of Texas at Arlington at 2005. She was introduced to many environmental issues and control technologies that gave her the interest to do her thesis under the guidance of Dr. Melanie L. Sattler on landfill emissions. She presented a paper based on her master thesis “Adsorption Curve Fits for Landfill VOCs on Bituminous Coal Based and Coconut Shell Based Activated Carbon” at the Air and Waste Management Association National Conference in June 2011. Her professor Dr. Melanie L. Sattler offered her a valuable position as a research assistant for a Texas Commission on Environmental Quality project. She continued her education as a doctoral student at the University of Texas at Arlington at 2009 under the same supervising professor. She has been continuously appointed as a graduate teaching assistant for Dr. Yvette P. Weatherton and offered a STEM scholarship throughout her doctoral program. She successfully completed her doctoral program in December 2012.